Published by
NIGERIAN SOCIETY OF PHYSICAL SCIENCES
Available online @ https://journal.nsps.org.ng/index.php/jnsps

J. Nig. Soc. Phys. Sci. 8 (2026) 3405

Journal of the Nigerian Society of Physical Sciences

Transmission dynamics of dengue–Zika co-infection with antibody-dependent enhancement, cross-immunity, and vaccination: backward bifurcation analysis and data calibration

Thomas U. Onoja[a,*], Benson A. E. Afere[a], Ayodele Gabriel Fasanya[b], Sunday Yomi[c], Bolarinwa Bolaji[a]

[a]*Department of Mathematical Sciences, Prince Abubakar Audu University, Anyigba, Nigeria*
[b]*Department of Science Education, Prince Abubakar Audu University, Anyigba, Nigeria*
[c]*Department of Science Education, Confluence University of Science and Technology, Osara, Nigeria*

Abstract

The co-circulation of dengue virus (DENV) and Zika virus (ZIKV) in *Aedes aegypti*-endemic regions creates a significantly more dangerous epidemiological landscape than either pathogen alone. Yet no existing model simultaneously incorporates antibody-dependent enhancement (ADE), dual Zika transmission routes, synergistic co-infection mortality, dengue vaccination, and calibration against confirmed co-endemic surveillance data. We address this gap by developing a sixteen-compartment deterministic model that captures ADE through susceptibility multipliers ε_1 and ε_2, partial cross-immunity, imperfect dengue vaccination, and both vector-borne and sexual Zika transmission. We derived the disease-free equilibrium and obtained closed-form expressions for the component reproduction numbers $\mathcal{R}_{0d}$ and $\mathcal{R}_{0z}$. The overall reproduction number $\mathcal{R}_0 = \rho(FV^{-1})$, computed as the spectral radius of the 8×8 next-generation matrix, satisfies $\mathcal{R}_0 \geq \max\{\mathcal{R}_{0d}, \mathcal{R}_{0z}\}$, with equality only when the linear cross-infection parameters $\beta_{z3}, \beta_{vd2}, \beta_{vz2}$ are zero. All co-infection effects, including ADE, are confined to the nonlinear regime. This confirms that single-disease models can systematically underestimate epidemic risk during co-circulation. Local asymptotic stability of the disease-free equilibrium when $\mathcal{R}_0 < 1$, uniform persistence when $\mathcal{R}_0 > 1$, and the existence of at least one endemic equilibrium are established. Centre manifold analysis reveals backward bifurcation in both submodels, implying that reducing $\mathcal{R}_0$ below unity is necessary but not sufficient for disease elimination. The model was calibrated using 36 weeks of SINAN surveillance data from Espírito Santo state, Brazil (January–September 2021), yielding key fitted parameters: $b^* = 1.278$ wk^{-1}, $\beta_d^* = 0.749$, $\beta_{z2}^* = 0.161$, $\beta_{vd1}^* = 0.118$, and $\beta_{vz1}^* = 0.252$, with Pearson correlations of $r = 0.594$ (dengue) and $r = 0.739$ (Zika). Sensitivity analysis identifies the mosquito biting rate b and vector mortality μ_v as the dominant intervention targets. Simulations reveal super-linear amplification of co-infections with rising biting rates and a 120-fold suppression of peak dengue incidence when vector mortality doubles. These findings support an integrated control strategy in which sustained vector management is the most cost-effective lever, complemented by improved healthcare access and high-coverage dengue vaccination to mitigate ADE-driven amplification.

DOI: 10.46481/jnsps.2026.3405

Keywords: Dengue–Zika co-infection, Antibody-dependent enhancement, Backward bifurcation, Dengue vaccination, Vector control.

Article History:
Received: 02 April 2026
Received in revised form: 02 July 2026
Accepted for publication: 05 July 2026
Available online: 30 July 2026

Communicated by: B. J. Falaye

1. Introduction

The co-circulation of arboviral pathogens sharing a common mosquito vector has emerged as one of the defining epi-

*Corresponding author Tel. No.: +234-803-962-9410.
Email address: tuonoja@gmail.com (Thomas U. Onoja)

demiological challenges of the twenty-first century. Dengue fever and Zika virus disease are transmitted primarily by *Aedes aegypti*, overlap extensively in their endemic geographic ranges across the tropics and subtropics, belong to the same viral family (*Flaviviridae*), and engage in documented cross-reactive immunological interactions that can amplify the clinical severity of sequential or simultaneous human infection [1, 2]. The simultaneous transmission of both pathogens within a single host population therefore represents a qualitatively more complex and potentially more dangerous epidemic scenario than either disease in isolation. This demands mathematical frameworks capable of representing the coupled transmission dynamics, the mutual immunological interference between the two viruses, and the joint control implications for integrated public health programmes. In the present study, we develop, calibrate, and analyse a deterministic co-infection model using surveillance data from an endemic co-circulation setting, and use it to derive mathematically rigorous and epidemiologically actionable conclusions about the epidemic threshold, the conditions for disease persistence, and the comparative leverage of available interventions.

Dengue virus (DENV) remains one of the fastest-spreading vector-borne diseases. The World Health Organization (WHO) documented the highest annual caseload ever recorded in 2024, with more than 14.6 million reported cases and over 12 000 deaths spanning more than 100 countries [3]. This represents a twelvefold increase relative to 2014 and a near-doubling of the already-historic 2023 global burden of 6.5 million cases and 6 800 deaths [4, 5]. In the Region of the Americas, more than 13 million cases were reported in 2024 alone, and WHO elevated dengue to a Grade 3 emergency in December 2023, its highest emergency classification [6]. Taking a longer perspective, the global incidence of dengue approximately doubled between 1990 and 2021, rising from an estimated 26.5 million to 59.0 million annual cases, while dengue-related deaths climbed from 14 000 to 29 000 over the same three decades [7]. Brazil is consistently the most severely affected country, accounting for approximately half the global annual dengue caseload: in 2023, Brazil reported 3.1 million dengue cases [4], and Espírito Santo state is among the country's highest-burden states owing to its year-round *Aedes aegypti* activity, dense coastal urbanization, and warm humid climate. Despite two licensed vaccines, CYD-TDV (Dengvaxia) and TAK-003 (Qdenga), the latter endorsed by WHO in 2023 for use regardless of prior dengue serostatus [6], no specific antiviral therapy is available, and vector control remains the cornerstone of epidemic prevention.

The global epidemiology of Zika virus (ZIKV) follows a strikingly different trajectory. After decades of near-invisibility following its first isolation from a sentinel rhesus macaque in Uganda in 1947, ZIKV erupted across the Pacific and then swept through the Americas in 2015–2016, compelling WHO to declare a Public Health Emergency of International Concern (PHEIC) in February 2016 [8, 9]. The epidemic was distinguished by the discovery that maternal ZIKV infection causes severe congenital malformations, including microcephaly and other neurodevelopmental deficits, and is associated with Guillain-Barre syndrome in adults [10]. Brazil bore the epicentre, reporting more than 1.5 million suspected ZIKV cases and registering hundreds of laboratory-confirmed congenital Zika-linked microcephaly cases [10]. Although reported incidence declined sharply after 2017 following exhaustion of immunologically naïve populations, ZIKV has not been eliminated: as of December 2023, autochthonous mosquito-borne transmission is documented in 92 countries and territories, sporadic outbreaks continue in Asia, and Brazil still accounts for 97% of cases notified to the Pan American Health Organization in the Americas [11, 12]. Recent sero-prevalence meta-analysis estimates a global ZIKV IgG positivity of 21%, with rates as high as 39.9% in the Americas, indicating that tens of millions of individuals carry prior ZIKV exposure and are immunologically primed for flavivirus cross-reactive interactions with DENV [13]. No licensed vaccine or approved antiviral exists for ZIKV, further underscoring the importance of understanding and controlling transmission dynamics mathematically.

The geographic convergence of DENV and ZIKV in *Aedes* receptive tropical zones means that simultaneous transmission to the same individual population is not a theoretical curiosity but an established clinical and epidemiological reality. Recent ecological modelling estimates that more than 5.66 billion people reside in areas environmentally suitable for both dengue and Zika transmission [2], and prospective surveillance in Brazil has confirmed widespread seasonal co-circulation of DENV, ZIKV, and chikungunya across multiple states [14]. The interaction between the two viruses at the population level has been revealed in a particularly striking way in Brazil, for instance, the emergence of ZIKV in 2015 was followed by an unusual suppression of dengue incidence, which subsequently resurged with a substantially younger age profile, an epidemiological signature consistent with a combination of ZIKV induced cross-protection and disease enhancement that cannot be explained by cross-protection alone [15]. At the individual level, prospective cohort data from Nicaragua have confirmed that prior ZIKV infection significantly increases the risk of symptomatic dengue caused by serotypes 2, 3, and 4, constituting direct human evidence for the cross-reactive immune enhancement that has long been hypothesised [16].

The biological mechanism underlying this immunological interplay is antibody-dependent enhancement (ADE). DENV encompasses four antigenically distinct serotypes (DENV-1 through DENV-4), and secondary infection with a heterologous serotype is the principal risk factor for dengue haemorrhagic fever and dengue shock syndrome, a causal role for ADE now confirmed in longitudinal human cohort studies [17]. Because ZIKV shares approximately 54 to 58% envelope protein sequence identity with DENV, cross-reactive antibodies elicited by primary DENV infection can bind but fail to neutralize ZIKV, instead facilitating viral entry into Fcγ-receptor-bearing myeloid cells and amplifying ZIKV replication in vitro and in vivo [18, 19]. Reciprocal enhancement has been demonstrated: ZIKV immune serum markedly exacerbates DENV infection in human skin, the primary site of vector transmission, through CD32 and CD64 Fcγ receptor engagement, resulting in a 2 to 3 fold increase in the number of cells with viral replication and a tenfold increase in virus genome production [20].

Within host mathematical models have confirmed that ADE is the key determinant of the sharp increase in viral load near peak time in secondary sequential flavivirus infection, while the dynamics of simultaneous co-infection differ from the sequential scenario in ways that population level compartmental models must carefully represent [21]. These findings collectively establish ADE as a mechanistically validated and quantitatively important driver of disease severity in co-endemic dengue–Zika settings that must be explicitly modelled in any framework intended to inform integrated intervention design.

Mathematical modelling has a long and productive history in the epidemiology of arboviral diseases. For dengue, compartmental ordinary differential equation (ODE) models have been employed to derive basic reproduction numbers, establish stability properties, assess vaccine effectiveness, and design vector control strategies across a wide range of endemic settings [22, 23]. Recent systematic reviews covering the period 2010 to 2020 document a rapidly expanding and increasingly sophisticated dengue modelling literature, with growing attention to multi-serotype interactions, fractional order formulations, and data calibrated models [23, 24]. A particularly important structural finding is that dengue models incorporating imperfect vaccination, waning immunity, or sufficiently high vector abundance can exhibit backward bifurcation at the epidemic threshold $\mathcal{R}_0 = 1$ [25–27]. Under backward bifurcation, a stable endemic equilibrium coexists with the stable disease-free equilibrium for $\mathcal{R}_0 < 1$. This implies that reducing the basic reproduction number below unity is a necessary but not sufficient condition for disease elimination because the system can sustain endemic transmission even after the threshold has nominally been crossed, depending on the magnitude of intervention relative to the size of the existing epidemic [26, 28]. This has far reaching implications for public health policy, particularly for vaccination programmes, as it implies that gradual relaxation of intervention near the epidemic threshold risks triggering a sudden resurgence to high endemic prevalence, a mathematical phenomenon now widely recognized in dengue modelling [24, 27].

For Zika, the dual transmission mechanism (mosquito-borne and direct human-to-human through sexual, blood-borne, and congenital routes) introduces a structural complexity absent from all other arboviral frameworks [29, 30]. Multiple modelling studies have confirmed that the vector-borne route overwhelmingly dominates ZIKV transmission in endemic settings, with direct sexual transmission contributing less than 5% of epidemic potential in most scenarios [29, 31], although its relative contribution is elevated when mosquito density is very low or when transmission networks are asymmetric. The consequence for the basic reproduction number is significant: $\mathcal{R}_{0_z}$ takes a quadratic form in which the direct transmission term interacts with the vector borne cycle, elevating the Zika threshold above the purely vector borne baseline in any setting where sexual transmission is non negligible, a property with direct implications for the conditions under which backward bifurcation occurs in the Zika submodel.

Despite the extensive single disease literature, models that simultaneously capture the coupled transmission dynamics of dengue and Zika are markedly fewer and often employ simplified formulations that do not fully represent the immunological interactions between the two pathogens. Early co-infection frameworks [32] laid important groundwork, establishing conditions for coexistence and identifying the role of partial cross immunity, but typically omit several mechanisms now known to be epidemiologically significant: ADE of secondary infection, synergistic mortality from simultaneous co-infection, a vaccination pathway for dengue recovered individuals, and dual transmission routes for Zika. More recent contributions have incorporated some of these features. Jose *et al.* [33] performed backward bifurcation analysis of a dengue–Zika co-infection model with sub-compartments for both pathogens and demonstrated that each submodel independently exhibits backward bifurcation, a finding with important threshold control implications. Omame *et al.* [34] extended the co-infection paradigm to a four-pathogen setting including COVID-19 and chikungunya, with optimal control analysis, while Wang and Zhao [32] analysed a dengue vaccine co-infection model incorporating ADE at the population level. Also, Ayuba *et al.* [35] examined the stability and sensitivity of a dengue–malaria co-infection model in an endemic setting, identifying key parameters governing co-infection persistence that are structurally analogous to those identified in the present study. A recent scoping review of 137 Zika modelling studies identified only thirteen that considered co-infection or co-circulation with other pathogens, confirming that the dengue–Zika co-infection modelling literature remains sparse relative to its single disease counterparts [22]. Recent dengue modelling with vaccination and transovarial transmission has further demonstrated the role of vector dynamics in shaping long-term epidemic outcomes [36].

Beyond co-infection frameworks, the single-disease dengue modelling literature has continued to expand in epidemiologically important directions that directly inform the present work. Abidemi and Peter [37] developed a host–vector dengue model incorporating asymptomatic, isolation, and vigilant compartments. They demonstrated through Lyapunov analysis that increasing isolation rates for both symptomatic and asymptomatic individuals substantially reduces dengue burden. Their finding that the model exhibits backward bifurcation in the presence of immunity loss reinforces a structural conclusion shared by the dengue sub-model presented here. The same authors subsequently extended this framework to an optimal control formulation [38], identifying personal protection combined with treatment as the most cost-effective strategy in resource-limited settings. This result has direct relevance to the co-endemic Brazilian context modelled in the present study. Oguntolu *et al.* [36] developed a deterministic compartmental model incorporating vaccination and transovarial transmission. They analysed its dynamics via the basic reproduction number and bifurcation theory, validated the model using real dengue case data from Brazil, and extended it to assess time-dependent control strategies through optimal control theory. Herdicho *et al.* [39] incorporated individual awareness dynamics into a dengue transmission model calibrated to East Java surveillance data, showing that awareness-driven behavioural change can achieve globally asymptotically stable endemic equilibria when the reproduction

number exceeds unity. They further demonstrated through optimal control analysis that awareness-based and treatment-based interventions are complementary levers of comparable magnitude. These recent contributions collectively reinforce the sensitivity hierarchy identified in our study and provide further justification for the integrated intervention framework we recommend.

A key gap in the existing co-infection literature is the absence of models that simultaneously: (i) explicitly represent ADE through modification of secondary infection susceptibility rates; (ii) incorporate synergistic co-infection mortality and a within-system dengue vaccination pathway; (iii) include dual transmission routes for Zika; (iv) establish the full next-generation matrix and prove analytically that $\mathcal{R}_0 \geq \max\{\mathcal{R}_{0d}, \mathcal{R}_{0z}\}$; (v) conduct backward bifurcation analysis for both submodels under the centre manifold theorem; and (vi) calibrate the model against confirmed co-endemic surveillance data with simultaneous dengue and Zika reporting. The absence of a model satisfying all six criteria is not merely a theoretical shortcoming. In practice, it means that public health authorities in co-endemic settings such as Espírito Santo state, Brazil, cannot reliably quantify how much more stringent the intervention threshold is during co-circulation compared to the single disease setting, nor can they identify the parameter combinations at which the system is most sensitive to ADE mediated amplification.

The present study addresses these gaps by developing, analyzing, and calibrating a sixteen-compartment deterministic ODE model for the co-transmission dynamics of dengue fever and Zika virus disease. Thirteen human epidemiological compartments stratify the population by infection status with respect to both pathogens and their co-infection, incorporating: antibody-dependent enhancement through modified susceptibility multipliers ε_1 and ε_2 acting on secondary infection forces; synergistic co-infection mortality through $\varepsilon_3 \geq 1$; partial and asymmetric cross-immunity through η_d and η_z; a dengue vaccine offering imperfect but meaningful protection; and both vector-borne and direct transmission routes for ZIKV. Three mosquito vector compartments complete the host–vector system. The model is calibrated against thirty-six weeks of SINAN dengue and Zika surveillance data from Espírito Santo state, Brazil (January–September 2021), using the Trust Region Reflective optimization algorithm with an eight-point multi-start strategy to minimise the risk of convergence to local minima.

The principal mathematical and epidemiological contributions of this work are as follows. First, positivity and boundedness of solutions and the positive invariance of the biologically feasible region are established rigorously. Second, the disease-free equilibrium is derived in closed form and the component reproduction numbers $\mathcal{R}_{0d}$ and $\mathcal{R}_{0z}$ are computed analytically from their respective next-generation sub-matrices; these are shown to take structurally distinct forms reflecting the presence of dual transmission routes for ZIKV. Third, the full model basic reproduction number $\mathcal{R}_0 = \rho(FV^{-1})$ is computed as the spectral radius of the complete 8×8 next-generation matrix and shown to satisfy $\mathcal{R}_0 \geq \max\{\mathcal{R}_{0d}, \mathcal{R}_{0z}\}$; local asymptotic stability of the disease-free equilibrium is established for $\mathcal{R}_0 < 1$ and its instability demonstrated for $\mathcal{R}_0 > 1$ [40]. Fourth, persistence theory is applied to establish the existence of at least one endemic equilibrium when $\mathcal{R}_0 > 1$. Fifth, the centre manifold theorem [41] is used to show that both the dengue-only and Zika-only submodels exhibit backward bifurcation at their respective thresholds, with the conditions driving this phenomenon identified analytically. Sixth, normalised forward sensitivity analysis reveals a consistent hierarchy of intervention leverage across both disease sub-systems. Seventh, comprehensive numerical simulations and joint surface–contour analysis of $\mathcal{R}_0$ over key two-dimensional parameter spaces quantify the additional epidemic risk introduced by co-circulation and demonstrate the cross-disease coupling effects unique to the co-infection formulation.

Table 1: Description of state variables.

Variable	Description
$S_h(t)$	Susceptible individuals
$E_d(t)$	Individuals exposed to dengue virus
$I_d(t)$	Individuals infected with dengue virus
$T_d(t)$	Individuals under treatment for dengue
$R_d(t)$	Individuals recovered from dengue
$V_d(t)$	Individuals vaccinated against dengue
$E_z(t)$	Individuals exposed to Zika virus
$I_z(t)$	Individuals infected with Zika virus
$T_z(t)$	Individuals under treatment for Zika
$R_z(t)$	Individuals recovered from Zika
$E_{dz}(t)$	Individuals exposed to both dengue and Zika
$I_{dz}(t)$	Individuals co-infected with dengue and Zika
$T_{dz}(t)$	Individuals under treatment for co-infection
$S_v(t)$	Susceptible mosquito vectors
$I_{vd}(t)$	Mosquito vectors infected with dengue virus
$I_{vz}(t)$	Mosquito vectors infected with Zika virus

The remainder of this paper is organised as follows. Section 2 presents the model formulation, biological assumptions, and governing system of differential equations. Section 3 provides the mathematical analysis covering the disease-free equilibrium, reproduction numbers, local asymptotic stability, persistence, endemic equilibrium existence, and backward bifurcation. Section 4 describes the data-fitting methodology, reports the calibrated parameter estimates, and presents the sensitivity analysis. Section 5 presents numerical simulations and joint surface–contour analysis. Section 6 concludes with public health implications and directions for future research.

2. Model formulation

The model stratifies the human population into thirteen epidemiological compartments based on infection status: susceptible individuals (S_h), those exposed to dengue (E_d), dengue-infected (I_d), dengue-treated (T_d), dengue-recovered (R_d), dengue-vaccinated (V_d), those exposed to Zika (E_z), Zika-infected (I_z), Zika-treated (T_z), Zika-recovered (R_z), individuals exposed to both viruses (E_{dz}), co-infected (I_{dz}), and those under treatment for co-infection (T_{dz}). The mosquito vector pop-

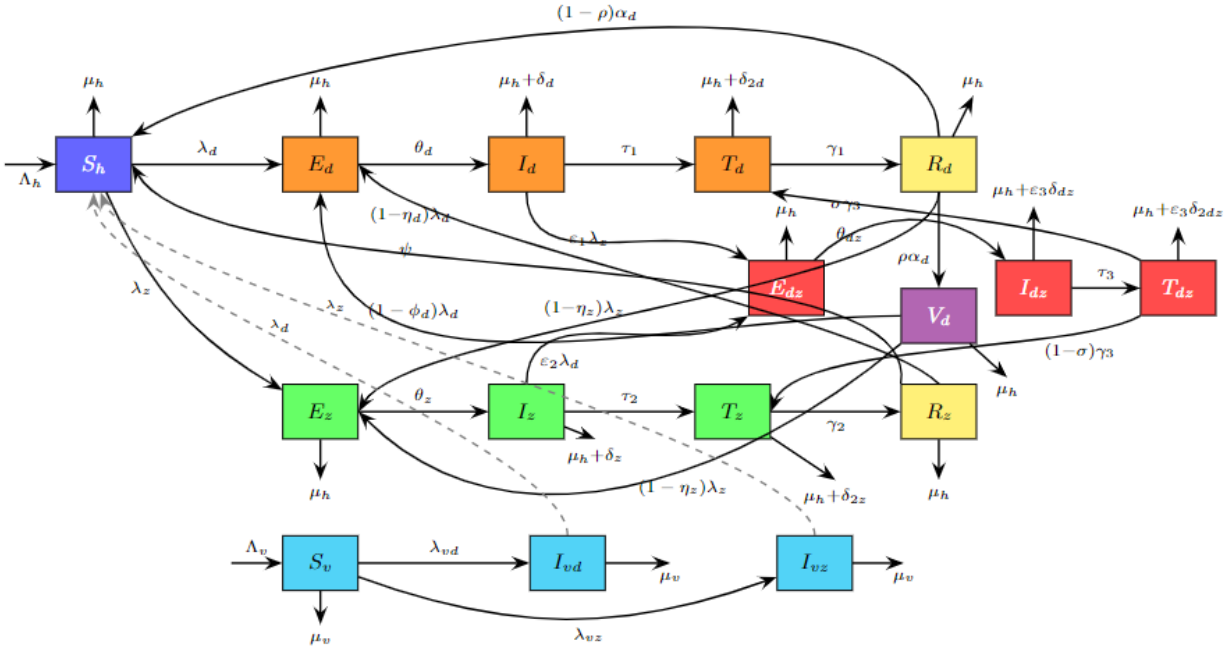

Figure 1: Schematic diagram.

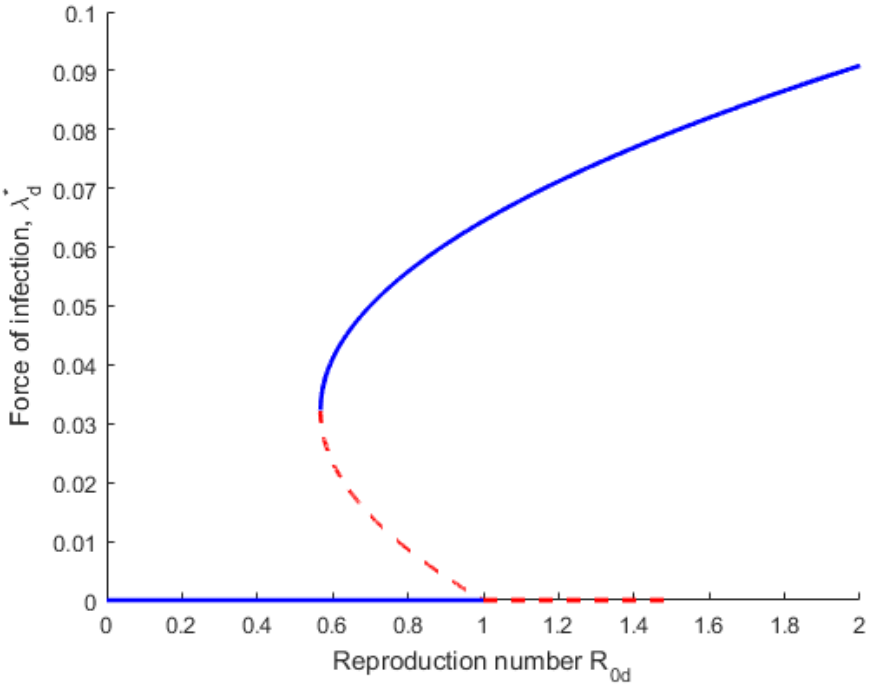

Figure 2: Backward bifurcation diagram for the dengue only submodel, illustrating the coexistence of a stable endemic equilibrium (blue, solid) and an unstable endemic equilibrium (red, dashed) with the stable disease free equilibrium for $\mathcal{R}_{0d} < 1$. Parameter values are chosen to satisfy the backward bifurcation condition $a > 0$ (low vaccine efficacy ϕ_d, vector abundance ξ below the critical threshold) as established analytically in Theorem 10; see Table 4 for fitted values.

ulation is divided into three classes: susceptible vectors (S_v), dengue-infected vectors (I_{vd}), and Zika-infected vectors (I_{vz}).

The state variables and model parameters are summarized in Tables 1 and 2, respectively.

Susceptible class (S_h): The susceptible human population increases through constant recruitment at rate Λ_h and from wan-

Table 2: Description of parameters.

Parameter	Description
Λ_h	Recruitment rate into human population
Λ_v	Recruitment rate of mosquito vectors
μ_h	Natural death rate of humans
μ_v	Natural death rate of mosquito vectors
N_h	Total human population size
b	Mosquito biting rate
β_d	Transmission probability from dengue-infected vector to human
β_{z1}	Direct human-to-human transmission rate for Zika
β_{z2}	Transmission probability from Zika-infected vector to human
β_{z3}	Direct transmission rate from co-infected humans (Zika)
β_{vd1}	Transmission probability from dengue-infected human to vector
β_{vd2}	Transmission probability from co-infected human to vector (dengue)
β_{vz1}	Transmission probability from Zika-infected human to vector
β_{vz2}	Transmission probability from co-infected human to vector (Zika)
θ_d	Progression rate from dengue-exposed to dengue-infected
θ_z	Progression rate from Zika-exposed to Zika-infected
θ_{dz}	Progression rate from co-infection exposed to co-infected
τ_1	Treatment-seeking rate for dengue-infected individuals
τ_2	Treatment-seeking rate for Zika-infected individuals
τ_3	Treatment-seeking rate for co-infected individuals
γ_1	Recovery rate under treatment for dengue
γ_2	Recovery rate under treatment for Zika
γ_3	Recovery rate under treatment for co-infection
σ	Fraction recovering from Zika during co-infection treatment
δ_d	Disease-induced death rate (dengue-infected class)
δ_{2d}	Disease-induced death rate (dengue-treated class), $\delta_{2d} < \delta_d$
δ_z	Disease-induced death rate (Zika-infected class)
δ_{2z}	Disease-induced death rate (Zika-treated class), $\delta_{2z} < \delta_z$
δ_{dz}	Disease-induced death rate (co-infected class)
δ_{2dz}	Disease-induced death rate (co-infection treated class)
ε_3	Synergistic mortality factor for co-infection, $\varepsilon_3 \geq 1$
α_d	Waning rate of dengue immunity
ψ	Waning rate of Zika immunity
ρ	Fraction of dengue-recovered individuals receiving vaccination
ϕ_d	Vaccine efficacy against dengue infection, $0 \leq \phi_d \leq 1$
η_d	Cross-immunity protection factor $0 \leq \eta_d \leq 1$
η_z	Cross-immunity protection factor $0 \leq \eta_z \leq 1$
ε_1	Modification factor for Zika acquisition by dengue-infected individuals
ε_2	Modification factor for dengue acquisition by Zika-infected individuals

ing immunity. Dengue-recovered individuals return to susceptibility at rate $(1-\rho)\alpha_d R_d$, while Zika-recovered individuals return at rate ψR_z. This compartment decreases through acquisition of dengue infection (force of infection λ_d), Zika infection (force of infection λ_z), and natural mortality at rate μ_h.

Dengue-exposed class (E_d): Individuals enter this compartment through three pathways: susceptible individuals exposed to dengue at rate $\lambda_d S_h$, vaccinated individuals with reduced susceptibility exposed at rate $(1-\phi_d)\lambda_d V_d$, and Zika-recovered individuals with partial cross-immunity exposed at rate $(1-\eta_d)\lambda_d R_z$. Exposed individuals progress to infectiousness at rate θ_d and exit through natural death at rate μ_h.

Dengue-infected class (I_d): This compartment receives individuals from the exposed class at rate $\theta_d E_d$. Co-infection occurs when dengue-infected individuals acquire Zika at the modified rate $\varepsilon_1\lambda_z I_d$, where ε_1 captures altered susceptibility. The compartment decreases through treatment-seeking at rate τ_1, disease-induced mortality at rate δ_d, and natural death at rate μ_h.

Dengue-treated class (T_d): Individuals enter treatment from the infected class at rate $\tau_1 I_d$ and from the co-infection treatment class when they recover from Zika while still under dengue treatment at rate $\sigma\gamma_3 T_{dz}$. The compartment decreases through recovery at rate γ_1, disease-induced death at rate δ_{2d} (where $\delta_{2d} < \delta_d$), and natural mortality.

Dengue-recovered class (R_d): Individuals recover from

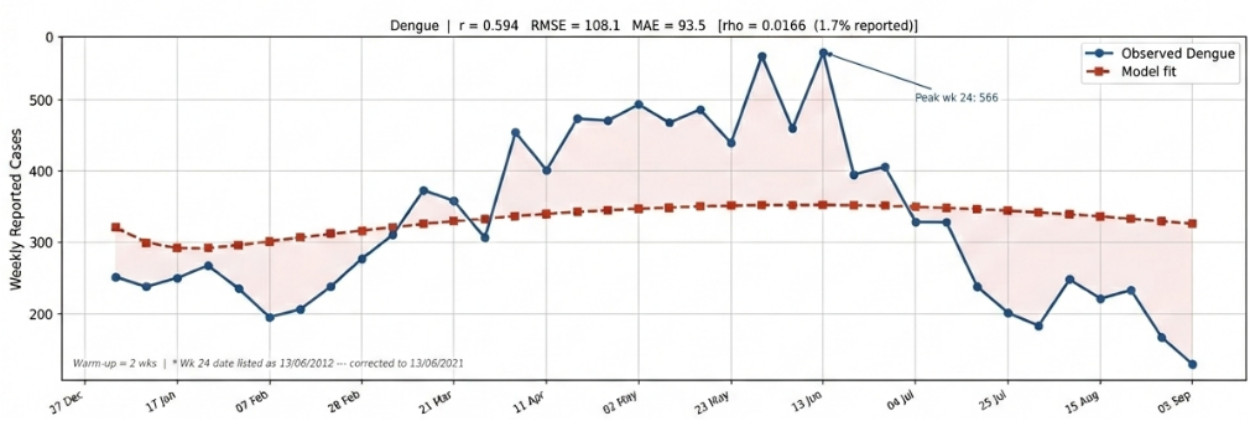

(a) Dengue fit

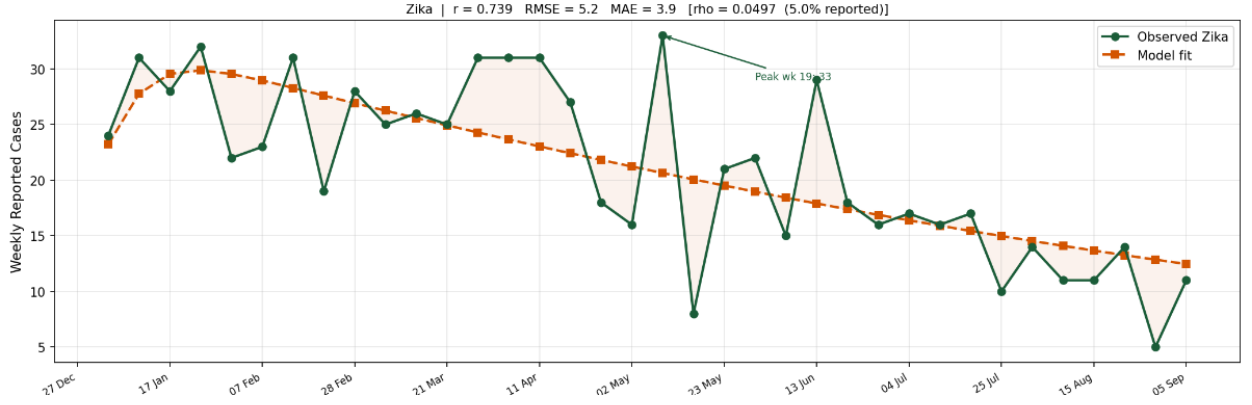

(b) Zika Fit

Figure 3: Dengue–Zika Data Fitting Espírito Santo, Brazil (Jan.–Sept. 2021, 36 Weeks) $\Lambda_v = 4000000$/wk [Mosquito:Human= 2.0:1].

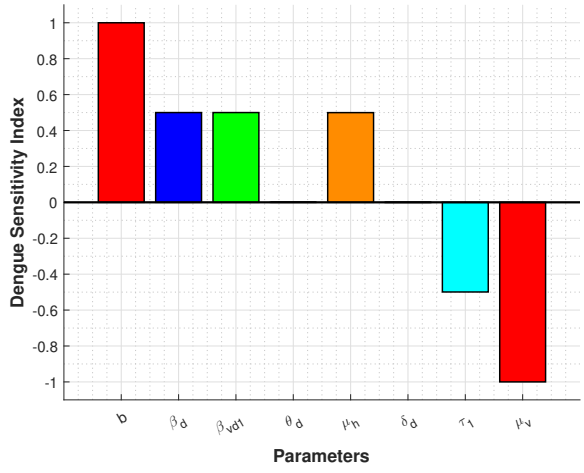

(a) Dengue sub-system ($\mathcal{R}_{0d}$).

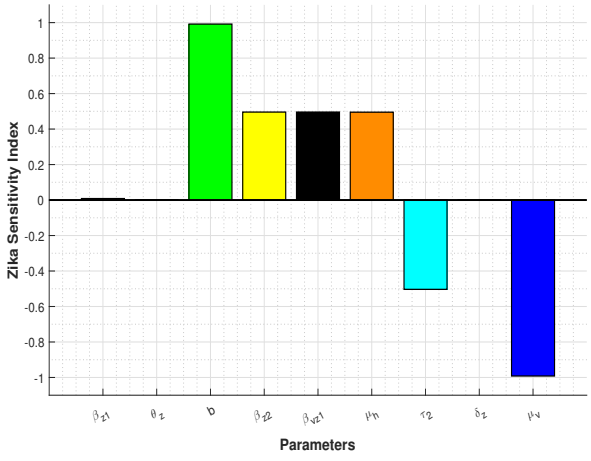

(b) Zika sub-system ($\mathcal{R}_{0z}$).

Figure 4: Normalised forward sensitivity indices of the basic reproduction numbers for the dengue and Zika sub-systems (see Table 6 for exact values). Bars above the horizontal axis increase $\mathcal{R}_0$; bars below suppress it.

dengue treatment at rate $\gamma_1 T_d$. This compartment decreases when recovered individuals lose immunity and return to susceptibility at rate α_d, when they acquire Zika with partial cross-protection at rate $(1-\eta_z)\lambda_z R_d$, and through natural death. A

Table 3: Data from Espírito Santo State in Brazil for Dengue and Zika cases in 2021 [42]

Week	Zika virus	Dengue fever
3/01/2021	24	251
10/01/2021	31	238
17/01/2021	28	250
24/01/2021	32	267
31/01/2021	22	235
7/02/2021	23	195
14/02/2021	31	206
21/02/2021	19	238
28/02/2021	28	277
7/03/2021	25	310
14/03/2021	26	373
21/03/2021	25	358
28/03/2021	31	306
4/04/2021	31	454
11/04/2021	31	401
18/04/2021	27	473
25/04/2021	18	471
2/05/2021	16	493
9/05/2021	33	468
16/05/2021	8	486
23/05/2021	21	439
30/05/2021	22	561
6/06/2021	15	460
13/06/2021	29	566
20/06/2021	18	395
27/06/2021	16	406
4/07/2021	17	328
11/07/2021	16	328
18/07/2021	17	238
25/07/2021	10	201
1/08/2021	14	183
8/08/2021	11	248
15/08/2021	11	221
22/08/2021	14	233
29/08/2021	5	167
5/09/2021	11	129

Table 4: Parameter values for the dengue–Zika co-infection model.

Parameter	Value	Status	Reference
N_h	4,000,000	Fixed	[43]
Λ_h	$\mu_h \times N_h$	Fixed	[25]
μ_h	$1/(70 \times 52)$ wk^{-1}	Fixed	[44]
Λ_v	4,000,000 wk^{-1}	Fixed	[45, 46]
μ_v	0.5 wk^{-1}	Fixed	[47]
b	1.278 wk^{-1} (0.18 day^{-1})	Fitted	–
β_d	0.749	Fitted	–
β_{z1}	0.0047 wk^{-1}	Fitted	–
β_{z2}	0.161	Fitted	–
β_{z3}	0.001 wk^{-1}	Fitted	–
β_{vd1}	0.118	Fitted	–
β_{vd2}	0.496	Fitted	–
β_{vz1}	0.252	Fitted	–
β_{vz2}	0.061	Fitted	–
θ_d	1.0 wk^{-1}	Fixed	[25, 48]
θ_z	1.0 wk^{-1}	Fixed	[10, 29]
θ_{dz}	1.0 wk^{-1}	Estimated	[25]
τ_1	0.5 wk^{-1}	Fixed	[49, 50]
τ_2	0.3 wk^{-1}	Fixed	[10]
τ_3	0.5 wk^{-1}	Fixed	[51]
γ_1	0.5 wk^{-1}	Fixed	[49, 51]
γ_2	0.5 wk^{-1}	Fixed	[10, 29]
γ_3	0.5 wk^{-1}	Fixed	[51]
σ	0.5	Fixed	[25]
δ_d	5×10^{-4} wk^{-1}	Fixed	[49, 51]
δ_{2d}	2×10^{-4} wk^{-1}	Fixed	[49]
δ_z	2×10^{-4} wk^{-1}	Fixed	[10]
δ_{2z}	1×10^{-4} wk^{-1}	Fixed	[10]
δ_{dz}	1×10^{-3} wk^{-1}	Fixed	[52]
δ_{2dz}	5×10^{-4} wk^{-1}	Fixed	[51, 52]
ε_3	1.5	Fixed	[52]
α_d	$1/(52 \times 2)$ wk^{-1}	Fixed	[53]
ψ	$1/52$ wk^{-1}	Fixed	[54]
η_d	0.3	Fixed	[1]
η_z	0.3	Fixed	[1]
ε_1	1.2	Fixed	[52]
ε_2	1.2	Fixed	[1]
ρ	0.1	Fixed	[55]
ϕ_d	0.70	Fixed	[56]

Table 5: Initial conditions and observation/reporting parameters

Parameter	Value	Status
(a) Initial Conditions		
I_{d0}	1,975	Fitted
I_{z0}	14.1	Fitted
f_{Ivd0}	0.50%	Fitted
f_{Ivz0}	0.036%	Fitted
Warm-up	2 weeks	Fitted
(b) Observation / Reporting Parameters		
κ_d	0.0166 (1.7%)	Fitted
κ_z	0.0497 (5.0%)	Fitted

fraction ρ of recovered individuals receive vaccination upon recovery.

Dengue-vaccinated class (V_d): This compartment comprises dengue-recovered individuals who receive vaccination at rate $\rho\alpha_d R_d$. Vaccinated individuals can still acquire dengue with reduced susceptibility at rate $(1-\phi_d)\lambda_d V_d$ and Zika at reduced rate $(1-\eta_z)\lambda_z V_d$. The compartment experiences natural mortality at rate μ_h.

Zika-exposed class (E_z): Individuals enter through exposure of susceptible ($\lambda_z S_h$), dengue-vaccinated with reduced susceptibility ($(1-\eta_z)\lambda_z V_d$), and dengue-recovered individuals with cross-immunity ($(1-\eta_z)\lambda_z R_d$). Progression to infectiousness occurs at rate θ_z, with natural death at rate μ_h.

Zika-infected class (I_z): This compartment increases at rate $\theta_z E_z$ and decreases when co-infection with dengue occurs at modified rate $\varepsilon_2\lambda_d I_z$, through treatment-seeking at rate τ_2, disease-induced death at rate δ_z, and natural mortality.

Zika-treated class (T_z): Individuals enter from the infected class at rate $\tau_2 I_z$ and from co-infection treatment when recovering from dengue at rate $(1-\sigma)\gamma_3 T_{dz}$. The class decreases

Table 6: Normalised forward sensitivity indices of the basic reproduction numbers with respect to model parameters for the dengue and Zika sub-systems, evaluated at the fitted baseline parameter set ($\mathcal{R}_{0d} \approx 1.074$, $\mathcal{R}_{0z} \approx 0.947$). Positive indices indicate parameters that increase $\mathcal{R}_0$; negative indices indicate suppressive parameters.

Parameter	Description	$\Upsilon_p^{\mathcal{R}_{0d}}$	$\Upsilon_p^{\mathcal{R}_{0z}}$
b	Mosquito biting rate	+1.0000	+0.9917
β_d	Dengue vector-to-human transmission probability	+0.5000	—
β_{vd1}	Dengue human-to-vector transmission probability	+0.5000	—
β_{z1}	Direct (sexual) Zika transmission rate	—	+0.0083
β_{z2}	Zika vector-to-human transmission probability	—	+0.4958
β_{vz1}	Zika human-to-vector transmission probability	—	+0.4958
θ_d	Dengue exposed-to-infected progression rate	+0.0001	—
θ_z	Zika exposed-to-infected progression rate	—	+0.0001
τ_1	Dengue treatment-seeking rate	−0.4992	—
τ_2	Zika treatment-seeking rate	—	−0.5034
δ_d	Dengue disease-induced mortality rate	−0.0005	—
δ_z	Zika disease-induced mortality rate	—	−0.0003
μ_h	Natural human mortality rate	+0.4996	+0.4952
μ_v	Natural mosquito mortality rate	−1.0000	−0.9917

through recovery at rate γ_2, disease-induced mortality at rate δ_{2z} (with $\delta_{2z} < \delta_z$), and natural death.

Zika-recovered class (R_z): Zika-treated individuals recover at rate $\gamma_2 T_z$. The compartment loses individuals when immunity wanes at rate ψ, when secondary dengue infection occurs with partial cross-immunity at rate $(1 - \eta_d)\lambda_d R_z$, and through natural death.

Co-infection exposed class (E_{dz}): This compartment represents individuals simultaneously exposed to both viruses, receiving inflow from dengue-infected individuals acquiring Zika ($\varepsilon_1 \lambda_z I_d$) and Zika-infected individuals acquiring dengue ($\varepsilon_2 \lambda_d I_z$). Individuals progress to active co-infection at rate θ_{dz} and exit through natural mortality.

Co-infected class (I_{dz}): Individuals develop active co-infection at rate $\theta_{dz} E_{dz}$. This compartment experiences enhanced disease-induced mortality at rate $\varepsilon_3 \delta_{dz}$, where $\varepsilon_3 \geq 1$ represents the synergistic effect of co-infection on disease severity. Treatment is sought at rate τ_3, with additional exits through natural death.

Co-infection treated class (T_{dz}): This compartment receives co-infected individuals at rate $\tau_3 I_{dz}$. Individuals exit either through recovery at rate γ_3 (where a fraction σ recovers from Zika only and moves to dengue treatment, while fraction $1 - \sigma$ recovers from dengue only and moves to Zika treatment), through enhanced disease-induced death at rate $\varepsilon_3 \delta_{2dz}$, or natural mortality.

Susceptible vectors (S_v): The mosquito population is recruited at constant rate Λ_v and decreases through acquisition of dengue infection (force of infection λ_{vd}), Zika infection (λ_{vz}), and natural vector mortality at rate μ_v.

Dengue-infected vectors (I_{vd}): Vectors become infected at rate $\lambda_{vd} S_v$ through contact with dengue-infected (I_d) and co-infected (I_{dz}) humans, where transmission depends on biting rate b and transmission probabilities. The compartment decreases only through vector mortality at rate μ_v.

Zika-infected vectors (I_{vz}): Similarly, susceptible vectors acquire Zika at rate $\lambda_{vz} S_v$ from contact with Zika-infected and co-infected humans, exiting only through natural death.

The forces of infection governing disease transmission are:

$$\lambda_d = \frac{b\beta_d I_{vd}}{N_h}, \qquad \lambda_z = \frac{(\beta_{z1} I_z + \beta_{z3} I_{dz}) + b\beta_{z2} I_{vz}}{N_h}, \tag{1}$$

$$\lambda_{vd} = \frac{b(\beta_{vd1} I_d + \beta_{vd2} I_{dz})}{N_h}, \quad \lambda_{vz} = \frac{b(\beta_{vz1} I_z + \beta_{vz2} I_{dz})}{N_h}, \tag{2}$$

where N_h represents the total human population, b is the mosquito biting rate, and the β parameters represent transmission probabilities for different infection routes. Notably, Zika transmission includes both vector-borne ($b\beta_{z2} I_{vz}$) and direct human-to-human transmission ($\beta_{z1} I_z + \beta_{z3} I_{dz}$), reflecting sexual and other non-vector transmission routes documented for Zika virus.

2.1. Model assumptions

The following are the major assumptions underlying the formulation of the dengue–Zika co-infection model:

- The human population is homogeneous with respect to mixing, contact rates, and exposure to mosquitoes, except for stratification by infection/vaccination status.
- Recruitment into the human population occurs at a constant rate Λ_h and all individuals are born susceptible (no vertical transmission of either virus is included).
- Natural death occurs at constant per-capita rate μ_h in every human compartment; disease-induced mortality is additional and virus-specific.
- Mosquito population dynamics are modelled with constant recruitment Λ_v and natural mortality μ_v; infected

mosquitoes remain infectious for life (no recovery or latency in vectors) [25, 45].

- Transmission is frequency-dependent (forces of infection are divided by total human population N_h) [25, 57].
- Dengue confers temporary immunity that wanes at rate α_d; a fraction ρ of dengue-recovered individuals move into a partially protected vaccinated state (V_d) [26, 27, 53].
- There is a dengue vaccine offering partial protection against dengue infection (efficacy ϕ_d) but no (or limited) cross-protection against Zika (η_z) [25, 55, 56].
- Asymmetric cross-immunity or antibody-dependent enhancement (ADE) is captured through reduced/increased susceptibility parameters η_d (protection against Zika after dengue) and η_z (protection against dengue after Zika), with $0 < \eta_d, \eta_z \leq 1$ [1, 16, 17].
- Secondary infection risk is enhanced in some individuals: $\varepsilon_1 > 1$ increases Zika susceptibility during acute dengue, and $\varepsilon_2 > 1$ increases dengue susceptibility during acute Zika (possible ADE mechanism) [18, 21].
- Co-infection leads to modified disease severity, captured by the multiplier $\varepsilon_3 \geq 1$ on disease-induced death rates in co-infected compartments [32, 33, 52].
- Zika virus can be transmitted by two routes: vector-borne (mosquito-to-human) and direct human-to-human (sexual, congenital, or close contact), represented by the non-vector terms $\beta_{z1} I_z$ and $\beta_{z3} I_{dz}$ in the force of infection λ_z [29–31].
- Treatment reduces disease-induced mortality ($\delta_{2d} < \delta_d$, $\delta_{2z} < \delta_z$, $\varepsilon_3 \delta_{2dz} < \varepsilon_3 \delta_{dz}$) but does not eliminate infectivity [26, 49].
- Co-infected individuals under treatment can recover from one virus before the other; the splitting parameter σ determines the proportion that recovers from Zika first (σ) versus dengue first ($1 - \sigma$) [33, 34].
- No births from infected mothers produce congenitally infected infants, and no vertical transmission to mosquitoes is included [29, 58, 59].
- Environmental and seasonal forcing (temperature, rainfall, vector breeding) are not explicitly modelled; parameters are assumed constant [23, 24, 45].

Arising from the model formulation described above, following the model assumptions and the flow diagram in Figure 1, the governing system of differential equations is:

$$
\begin{aligned}
\frac{dS_h}{dt} &= \Lambda_h - (\lambda_d + \lambda_z) S_h - \mu_h S_h + (1-\rho)\alpha_d R_d + \psi R_z, \\
\frac{dE_d}{dt} &= \lambda_d S_h + (1-\phi_d)\lambda_d V_d + (1-\eta_d)\lambda_d R_z - (\theta_d + \mu_h) E_d, \\
\frac{dI_d}{dt} &= \theta_d E_d - \varepsilon_1 \lambda_z I_d - (\tau_1 + \delta_d + \mu_h) I_d, \\
\frac{dT_d}{dt} &= \tau_1 I_d + \sigma\gamma_3 T_{dz} - (\gamma_1 + \delta_{2d} + \mu_h) T_d, \\
\frac{dR_d}{dt} &= \gamma_1 T_d - (\alpha_d + \mu_h) R_d - (1-\eta_z)\lambda_z R_d, \\
\frac{dV_d}{dt} &= \rho\alpha_d R_d - (1-\phi_d)\lambda_d V_d - \mu_h V_d - (1-\eta_z)\lambda_z V_d, \\
\frac{dE_z}{dt} &= \lambda_z S_h + (1-\eta_z)\lambda_z V_d + (1-\eta_z)\lambda_z R_d - (\theta_z + \mu_h) E_z, \\
\frac{dI_z}{dt} &= \theta_z E_z - \varepsilon_2 \lambda_d I_z - (\tau_2 + \delta_z + \mu_h) I_z, \\
\frac{dT_z}{dt} &= \tau_2 I_z + (1-\sigma)\gamma_3 T_{dz} - (\gamma_2 + \delta_{2z} + \mu_h) T_z, \\
\frac{dR_z}{dt} &= \gamma_2 T_z - (\psi + \mu_h) R_z - (1-\eta_d)\lambda_d R_z, \\
\frac{dE_{dz}}{dt} &= \varepsilon_1 \lambda_z I_d + \varepsilon_2 \lambda_d I_z - (\theta_{dz} + \mu_h) E_{dz}, \\
\frac{dI_{dz}}{dt} &= \theta_{dz} E_{dz} - (\tau_3 + \varepsilon_3 \delta_{dz} + \mu_h) I_{dz}, \\
\frac{dT_{dz}}{dt} &= \tau_3 I_{dz} - (\gamma_3 + \varepsilon_3 \delta_{2dz} + \mu_h) T_{dz}, \\
\frac{dS_v}{dt} &= \Lambda_v - (\lambda_{vd} + \lambda_{vz}) S_v - \mu_v S_v, \\
\frac{dI_{vd}}{dt} &= \lambda_{vd} S_v - \mu_v I_{vd}, \\
\frac{dI_{vz}}{dt} &= \lambda_{vz} S_v - \mu_v I_{vz},
\end{aligned}
\tag{3}
$$

with forces of infection

$$
\lambda_d = \frac{b\beta_d I_{vd}}{N_h}, \quad \lambda_z = \frac{\beta_{z1} I_z + \beta_{z3} I_{dz} + b\beta_{z2} I_{vz}}{N_h},
$$

$$
\lambda_{vd} = \frac{b(\beta_{vd1} I_d + \beta_{vd2} I_{dz})}{N_h}, \quad \lambda_{vz} = \frac{b(\beta_{vz1} I_z + \beta_{vz2} I_{dz})}{N_h}.
$$

3. Model analysis

As is standard practice in the mathematical modelling of infectious diseases, we begin by analyzing the basic properties of the proposed model. These properties provide essential insights into the model's structural integrity, biological relevance, and mathematical consistency.

3.1. Positivity of solutions for the dengue–Zika co-infection model

For the dengue-Zika co-infection model to be epidemiologically meaningful, all state variables must remain non-negative for all time $t > 0$, assuming non-negative initial conditions. This ensures that populations (human and vector compartments) do not become negative, which would be biologically meaningless.

Theorem 1. *Let the initial data for the dengue–Zika co-infection model be:*

$$
S_h(0) > 0,\ E_d(0) > 0,\ I_d(0) > 0,\ T_d(0) > 0,\ R_d(0) > 0,
$$

$$V_d(0) > 0,\ E_z(0) > 0,\ I_z(0) > 0,\ T_z(0) > 0,\ R_z(0) > 0,$$
$$E_{dz}(0) > 0,\ I_{dz}(0) > 0,\ T_{dz}(0) > 0,\ S_v(0) > 0,$$
$$I_{vd}(0) > 0,\ I_{vz}(0) > 0.$$

Then all solutions remain positive for all time $t > 0$.

Proof. Let

$$t_1 = \sup\{t \in [0,t] : S_h, E_d, I_d, T_d, R_d, V_d > 0, \\ E_z, I_z, T_z, R_z, E_{dz} > 0, \\ I_{dz}, T_{dz}, S_v, I_{vd}, I_{vz} > 0\}.$$

Thus, $t_1 > 0$. We will show that each compartment remains non-negative.

The model is positively invariant in the feasible region $D = D_h \times D_v \subset \mathbb{R}_+^{16}$, where

$$D_h = \left\{(S_h, E_d, I_d, T_d, R_d, V_d, E_z, I_z, T_z, R_z, E_{dz}, I_{dz}, T_{dz}) \in \mathbb{R}_+^{13} \right. \\ \left. : N_h \le \frac{\Lambda_h}{\mu_h}\right\},$$
$$D_v = \{(S_v, I_{vd}, I_{vz}) \in \mathbb{R}_+^3 : N_v \le \frac{\Lambda_v}{\mu_v}\},$$

with total human population $N_h = S_h + E_d + I_d + T_d + R_d + V_d + E_z + I_z + T_z + R_z + E_{dz} + I_{dz} + T_{dz}$ and total vector population $N_v = S_v + I_{vd} + I_{vz}$.

Adding the human equations yields

$$\frac{dN_h}{dt} = \Lambda_h - \mu_h N_h - \delta_d I_d - \delta_{2d} T_d - \delta_z I_z \\ - \delta_{2z} T_z - \varepsilon_3 \delta_{dz} I_{dz} - \delta_{2dz} T_{dz} \\ \le \Lambda_h - \mu_h N_h.$$

so $N_h(t) \le \max\left(N_h(0), \frac{\Lambda_h}{\mu_h}\right)$.

Similarly for vectors:

$$\frac{dN_v}{dt} = \Lambda_v - \mu_v N_v, \quad \text{so } N_v(t) \le \max\left(N_v(0), \frac{\Lambda_v}{\mu_v}\right).$$

Assuming bounded disease-induced deaths, D is attracting and positively invariant. ■

3.2. Invariant region

The dengue-Zika co-infection model is epidemiologically meaningful if its solutions remain non-negative and bounded for all $t > 0$, as established in the positivity proof. Here, we determine the positively invariant region that attracts all solutions, ensuring the model is mathematically and epidemiologically well-posed.

Lemma 2. *The solutions of the dengue-Zika co-infection model are feasible for all time $t > 0$ within the invariant region $D = D_h \times D_v \subset \mathbb{R}_+^{16}$ and attract all solutions in $\mathbb{R}_+^{16}$, given by:*

$$D_h = \left\{(S_h, E_d, I_d, T_d, R_d, V_d, E_z, I_z, T_z, R_z, E_{dz}, I_{dz}, T_{dz}) \right. \\ \left. \in \mathbb{R}_+^{13} : N_h \le \frac{\Lambda_h}{\mu_h}\right\},$$

$$D_v = \left\{(S_v, I_{vd}, I_{vz}) \in \mathbb{R}_+^3 : N_v \le \frac{\Lambda_v}{\mu_v}\right\},$$

where $N_h = S_h + E_d + I_d + T_d + R_d + V_d + E_z + I_z + T_z + R_z + E_{dz} + I_{dz} + T_{dz}$ is the total human population and $N_v = S_v + I_{vd} + I_{vz}$ is the total vector population.

Proof. First, consider the total human population $N_h(t)$. Differentiating and substituting the model equations yields:

$$\frac{dN_h}{dt} = \Lambda_h - \mu_h N_h - (\delta_d I_d + \delta_{2d} T_d + \delta_z I_z \\ + \delta_{2z} T_z + \varepsilon_3 \delta_{dz} I_{dz} + \varepsilon_3 \delta_{2dz} T_{dz}).$$

Since the disease-induced death terms are non-negative ($\delta_d I_d + \delta_{2d} T_d + \delta_z I_z + \delta_{2z} T_z + \varepsilon_3 \delta_{dz} I_{dz} + \varepsilon_3 \delta_{2dz} T_{dz} \ge 0$), it follows that:

$$\frac{dN_h}{dt} \le \Lambda_h - \mu_h N_h.$$

Thus, whenever $N_h > \frac{\Lambda_h}{\mu_h}$, $\frac{dN_h}{dt} < 0$. Solving this differential inequality:

$$\frac{d}{dt}\left(N_h e^{\mu_h t}\right) \le \Lambda_h e^{\mu_h t}.$$

Integrating both sides from 0 to t:

$$N_h(t)e^{\mu_h t} - N_h(0) \le \frac{\Lambda_h}{\mu_h}(e^{\mu_h t} - 1),$$

$$N_h(t) \le N_h(0)e^{-\mu_h t} + \frac{\Lambda_h}{\mu_h}(1 - e^{-\mu_h t}).$$

Hence, $N_h(t) \le \max\left(N_h(0), \frac{\Lambda_h}{\mu_h}\right)$ for all $t > 0$. Applying Birkhoff and Rota's theorem on differential inequalities, as $t \to \infty$:

$$\limsup_{t\to\infty} N_h(t) \le \frac{\Lambda_h}{\mu_h}.$$

From the positivity proof, all compartments are non-negative ($N_h(t) \ge 0$) for $t > 0$.

Therefore, if $N_h(0) \le \frac{\Lambda_h}{\mu_h}$, then $N_h(t) \le \frac{\Lambda_h}{\mu_h}$ for all $t > 0$, making D_h positively invariant.

Now, for the total vector population $N_v(t)$:

$$\frac{dN_v}{dt} = \Lambda_v - \mu_v N_v.$$

(This is exact, with no disease-induced deaths in vectors.) Solving directly:

$$N_v(t) = N_v(0)e^{-\mu_v t} + \frac{\Lambda_v}{\mu_v}(1 - e^{-\mu_v t}).$$

Thus, $N_v(t) \le \max\left(N_v(0), \frac{\Lambda_v}{\mu_v}\right)$, and as $t \to \infty$, $N_v(t) \to \frac{\Lambda_v}{\mu_v}$. If $N_v(0) \le \frac{\Lambda_v}{\mu_v}$, then $N_v(t) \le \frac{\Lambda_v}{\mu_v}$ for all $t > 0$, making D_v positively invariant.

The region $D = D_h \times D_v$ is thus positively invariant and attracts all non-negative solutions (initial conditions outside D approach it asymptotically). The dengue-Zika co-infection model is both epidemiologically and mathematically well-posed in D. Hence, it is appropriate to examine the dynamics of the model in the region D. ■

3.3. Disease-free equilibrium

The disease-free equilibrium (DFE) is the steady state where there is no disease in the population, i.e., all disease-related compartments are zero.

At the DFE, denoted by ζ_0, we have:

- No exposed, infected, or treated individuals for dengue, Zika, or co-infection.
- Only the susceptible humans $S_h^0 = \frac{\Lambda_h}{\mu_h}$ and susceptible vectors $S_v^0 = \frac{\Lambda_v}{\mu_v}$ remain positive. All infected, treated, recovered, and vaccinated compartments are zero.

Consider the first equation of (3), S_h. at equilibrium:

$$\frac{dS_h}{dt} = \Lambda_h - (\lambda_d + \lambda_z)S_h - \mu_h S_h + (1-\rho)\alpha_d R_d + \psi R_z = 0$$

Since $\lambda_d = 0$, $\lambda_z = 0$, and $R_d^* = 0$:

$$\Lambda_h - \mu_h S_h^* = 0$$

Therefore:

$$S_h^* = \frac{\Lambda_h}{\mu_h}$$

For S_v^*: From the equation for S_v at equilibrium:

$$\frac{dS_v}{dt} = 0 \Rightarrow \Lambda_v - (\lambda_{vd} + \lambda_{vz})S_v - \mu_v S_v = 0$$

Since $\lambda_{vd} = 0$ and $\lambda_{vz} = 0$:

$$\Lambda_v - \mu_v S_v^0 = 0$$

Therefore:

$$S_v^* = \frac{\Lambda_v}{\mu_v}$$

The disease-free equilibrium of the dengue–Zika co-infection model is:

$$\zeta_* = (S_h^*, E_d^*, I_d^*, T_d^*, R_d^*, V_d^*, E_z^*, I_z^*, T_z^*, R_z^*, E_{dz}^*, I_{dz}^*, T_{dz}^*, S_v^*, I_{vd}^*, I_{vz}^*).$$

where

$$\zeta_0 = \left(\frac{\Lambda_h}{\mu_h}, 0,0,0,0,0,0,0,0,0,0,0,0, \frac{\Lambda_v}{\mu_v}, 0, 0\right) \tag{4}$$

3.4. Basic reproduction number

The basic reproduction number, $\mathcal{R}_0$, is computed using the next generation operator method [40, 60]. This approach partitions the model into infected and non-infected compartments and analyzes the production of new infections.

The infected compartments are:

$$\mathbf{x} = (E_d,\ I_d,\ E_z,\ I_z,\ E_{dz},\ I_{dz},\ I_{vd},\ I_{vz})^T \tag{5}$$

where the first six components represent infected human states and the last two represent infected mosquito vectors. All other compartments (S_h, T_d, T_z, T_{dz}, R_d, R_z, V_d, S_v) are non-infected states.

At the disease-free equilibrium (DFE) (4), we have:

$$S_h^0 = N_h^0 = \frac{\Lambda_h}{\mu_h}, \quad \text{(all humans are susceptible)}$$

$$S_v^0 = \frac{\Lambda_v}{\mu_v}, \quad \text{(all mosquitoes are susceptible)}$$

$$E_d = I_d = E_z = I_z = E_{dz} = I_{dz} = I_{vd} = I_{vz} = 0.$$

We define the equilibrium vector-to-host ratio

$$\xi = \frac{S_v^0}{N_h^0} = \frac{\Lambda_v \mu_h}{\Lambda_h \mu_v}.$$

The vector of new infection terms is:

$$\mathcal{F} = \begin{pmatrix} \frac{b\beta_d I_{vd}}{N_h} S_h \\ 0 \\ \frac{(\beta_{z1} I_z + \beta_{z3} I_{dz}) + b\beta_{z2} I_{vz}}{N_h} S_h \\ 0 \\ \varepsilon_1 \frac{(\beta_{z1} I_z + \beta_{z3} I_{dz}) + b\beta_{z2} I_{vz}}{N_h} I_d + \varepsilon_2 \frac{b\beta_d I_{vd}}{N_h} I_z \\ 0 \\ \frac{b(\beta_{vd1} I_d + \beta_{vd2} I_{dz})}{N_h} S_v \\ \frac{b(\beta_{vz1} I_z + \beta_{vz2} I_{dz})}{N_h} S_v \end{pmatrix}.$$

Taking the Jacobian of $\mathcal{F}$ with respect to the infected compartments and evaluating at the DFE (where $S_h^* = N_h^*$ and $S_v^* = \Lambda_v/\mu_v$), we obtain the matrix F:

$$F = \begin{pmatrix} 0 & 0 & 0 & 0 & 0 & 0 & b\beta_d & 0 \\ 0 & 0 & 0 & 0 & 0 & 0 & 0 & 0 \\ 0 & 0 & 0 & \beta_{z1} & 0 & \beta_{z3} & 0 & b\beta_{z2} \\ 0 & 0 & 0 & 0 & 0 & 0 & 0 & 0 \\ 0 & 0 & 0 & 0 & 0 & 0 & 0 & 0 \\ 0 & 0 & 0 & 0 & 0 & 0 & 0 & 0 \\ 0 & b\beta_{vd1}\xi & 0 & 0 & 0 & b\beta_{vd2}\xi & 0 & 0 \\ 0 & 0 & 0 & b\beta_{vz1}\xi & 0 & b\beta_{vz2}\xi & 0 & 0 \end{pmatrix}.$$

The matrix V represents the rates of transfer of individuals out of infected compartments due to disease progression, treatment, recovery, and death. The vector of transition terms is:

$$\mathcal{V} = \begin{pmatrix} (\theta_d + \mu_h)E_d \\ -\theta_d E_d + (\tau_1 + \delta_d + \mu_h)I_d \\ (\theta_z + \mu_h)E_z \\ -\theta_z E_z + (\tau_2 + \delta_z + \mu_h)I_z \\ -\varepsilon_1 \lambda_z I_d - \varepsilon_2 \lambda_d I_z + (\theta_{dz} + \mu_h)E_{dz} \\ -\theta_{dz} E_{dz} + (\tau_3 + \varepsilon_3 \delta_{dz} + \mu_h)I_{dz} \\ \mu_v I_{vd} \\ \mu_v I_{vz} \end{pmatrix}.$$

At the DFE, where $\lambda_d = \lambda_z = 0$, taking the Jacobian yields:

$$V = \begin{pmatrix} m_1 & 0 & 0 & 0 & 0 & 0 & 0 & 0 \\ -\theta_d & m_2 & 0 & 0 & 0 & 0 & 0 & 0 \\ 0 & 0 & m_3 & 0 & 0 & 0 & 0 & 0 \\ 0 & 0 & -\theta_z & m_4 & 0 & 0 & 0 & 0 \\ 0 & 0 & 0 & 0 & m_5 & 0 & 0 & 0 \\ 0 & 0 & 0 & 0 & -\theta_{dz} & m_6 & 0 & 0 \\ 0 & 0 & 0 & 0 & 0 & 0 & \mu_v & 0 \\ 0 & 0 & 0 & 0 & 0 & 0 & 0 & \mu_v \end{pmatrix},$$

where for notational convenience we define:

$$m_1 = \theta_d + \mu_h, \quad m_2 = \tau_1 + \delta_d + \mu_h,$$
$$m_3 = \theta_z + \mu_h, \quad m_4 = \tau_2 + \delta_z + \mu_h,$$
$$m_5 = \theta_{dz} + \mu_h, \quad m_6 = \tau_3 + \varepsilon_3\delta_{dz} + \mu_h.$$

The block-diagonal structure of V reflects the independence of the dengue, Zika, and co-infection progression pathways at the DFE. The inverse of V is therefore:

$$V^{-1} = \begin{pmatrix} \frac{1}{m_1} & 0 & 0 & 0 & 0 & 0 & 0 & 0 \\ \frac{\theta_d}{m_1 m_2} & \frac{1}{m_2} & 0 & 0 & 0 & 0 & 0 & 0 \\ 0 & 0 & \frac{1}{m_3} & 0 & 0 & 0 & 0 & 0 \\ 0 & 0 & \frac{\theta_z}{m_3 m_4} & \frac{1}{m_4} & 0 & 0 & 0 & 0 \\ 0 & 0 & 0 & 0 & \frac{1}{m_5} & 0 & 0 & 0 \\ 0 & 0 & 0 & 0 & \frac{\theta_{dz}}{m_5 m_6} & \frac{1}{m_6} & 0 & 0 \\ 0 & 0 & 0 & 0 & 0 & 0 & \frac{1}{\mu_v} & 0 \\ 0 & 0 & 0 & 0 & 0 & 0 & 0 & \frac{1}{\mu_v} \end{pmatrix}.$$

The next generation matrix is $K = FV^{-1}$, and the basic reproduction number is defined as its spectral radius:

$$\mathcal{R}_0 = \rho(FV^{-1}). \tag{6}$$

To derive analytically tractable expressions for the component reproduction numbers, we formally decouple the dengue and Zika subsystems by setting all co-infection-related states and parameters to zero.

3.4.1. Dengue-only subsystem

Setting all Zika-related compartments to zero, the infected compartments reduce to (E_d, I_d, I_{vd}), yielding the 3×3 submatrices:

$$F_d = \begin{pmatrix} 0 & 0 & b\beta_d \\ 0 & 0 & 0 \\ 0 & b\beta_{vd1} & 0 \end{pmatrix}, \qquad V_d = \begin{pmatrix} m_1 & 0 & 0 \\ -\theta_d & m_2 & 0 \\ 0 & 0 & \mu_v \end{pmatrix}$$

with inverse:

$$V_d^{-1} = \begin{pmatrix} \frac{1}{m_1} & 0 & 0 \\ \frac{\theta_d}{m_1 m_2} & \frac{1}{m_2} & 0 \\ 0 & 0 & \frac{1}{\mu_v} \end{pmatrix}.$$

The next generation sub-matrix is:

$$K_d = F_d V_d^{-1} = \begin{pmatrix} 0 & 0 & \frac{b\beta_d}{\mu_v} \\ 0 & 0 & 0 \\ \frac{b\beta_{vd1}\theta_d\xi}{m_1 m_2} & \frac{b\beta_{vd1}\xi}{m_2} & 0 \end{pmatrix}.$$

The characteristic equation $\det(\lambda I - K_d) = 0$ yields one non-trivial eigenvalue satisfying:

$$\lambda^2 = \frac{b^2\beta_d\beta_{vd1}\theta_d\,\xi}{m_1 m_2 \mu_v}. \tag{7}$$

Therefore, the dengue reproduction number is:

$$\mathcal{R}_{0d} = \sqrt{\frac{b^2\beta_d\beta_{vd1}\theta_d\,\xi}{m_1 m_2 \mu_v}} \tag{8}$$

The square-root structure of $\mathcal{R}_{0d}$ reflects the two-stage vector-borne transmission cycle: human-to-mosquito followed by mosquito-to-human.

3.4.2. Zika-only subsystem

Setting all dengue-related compartments to zero, the infected compartments reduce to (E_z, I_z, I_{vz}), yielding:

$$F_z = \begin{pmatrix} 0 & \beta_{z1} & b\beta_{z2} \\ 0 & 0 & 0 \\ 0 & b\beta_{vz1} & 0 \end{pmatrix}, \qquad V_z = \begin{pmatrix} m_3 & 0 & 0 \\ -\theta_z & m_4 & 0 \\ 0 & 0 & \mu_v \end{pmatrix}$$

with inverse:

$$V_z^{-1} = \begin{pmatrix} \frac{1}{m_3} & 0 & 0 \\ \frac{\theta_z}{m_3 m_4} & \frac{1}{m_4} & 0 \\ 0 & 0 & \frac{1}{\mu_v} \end{pmatrix}$$

The next generation sub-matrix is:

$$K_z = F_z V_z^{-1} = \begin{pmatrix} \frac{\beta_{z1}\theta_z}{m_3 m_4} & \frac{\beta_{z1}}{m_4} & \frac{b\beta_{z2}}{\mu_v} \\ 0 & 0 & 0 \\ \frac{b\beta_{vz1}\theta_z\xi}{m_3 m_4} & \frac{b\beta_{vz1}\xi}{m_4} & 0 \end{pmatrix}.$$

The characteristic equation $\det(\lambda I - K_z) = 0$ expands to:

$$\lambda^3 - \frac{\beta_{z1}\theta_z}{m_3 m_4}\lambda^2 - \frac{b^2\beta_{z2}\beta_{vz1}\theta_z\,\xi}{m_3 m_4 \mu_v}\lambda = 0.$$

Factoring out the trivial eigenvalue $\lambda = 0$ yields the quadratic:

$$\lambda^2 - \frac{\beta_{z1}\theta_z}{m_3 m_4}\lambda - \frac{b^2\beta_{z2}\beta_{vz1}\theta_z\,\xi}{m_3 m_4 \mu_v} = 0. \tag{9}$$

Applying the quadratic formula and retaining the positive root:

$$\mathcal{R}_{0z} = \rho(K_z) = \frac{\beta_{z1}\theta_z}{2\,m_3 m_4} + \sqrt{\left(\frac{\beta_{z1}\theta_z}{2\,m_3 m_4}\right)^2 + \frac{b^2\beta_{z2}\beta_{vz1}\theta_z\,\xi}{m_3 m_4 \mu_v}}. \tag{10}$$

3.4.3. The overall basic reproduction number

The overall basic reproduction number satisfies

$$\mathcal{R}_0 \geq \max\{\mathcal{R}_{0d}, \mathcal{R}_{0z}\}, \tag{11}$$

with equality only when the linear cross-infection parameters β_{z3}, β_{vd2}, β_{vz2} are zero. All co-infection effects, including both linear coupling and ADE, belong entirely to the nonlinear regime. This justifies the use of centre manifold analysis to study backward bifurcation and endemic equilibria.

Remark 1. The composite structure of $\mathcal{R}_0$ reflects dengue vector-borne transmission, Zika transmission via both sexual and vector routes, and linear co-infection transmission pathways (β_{z3}, β_{vd2}, β_{vz2}). Nonlinear effects due to ADE are captured separately in the bifurcation analysis.

3.5. Local asymptotic stability of the disease-free equilibrium

Theorem 3. *Let ξ_0 denote the disease-free equilibrium (DFE) (4) of the dengue–Zika co-infection model. Then ξ_0 is locally asymptotically stable if $\mathcal{R}_0 < 1$ and unstable if $\mathcal{R}_0 > 1$, where*

$$\mathcal{R}_0 = \rho(FV^{-1}) \geq \max\{\mathcal{R}_{0d}, \mathcal{R}_{0z}\},$$

with

$$\mathcal{R}_{0d} = \sqrt{\frac{b^2\beta_d\beta_{vd1}\theta_d\,\xi}{m_1 m_2 \mu_v}},$$

$$\mathcal{R}_{0z} = \frac{\beta_{z1}\theta_z}{2\,m_3 m_4} + \sqrt{\left(\frac{\beta_{z1}\theta_z}{2\,m_3 m_4}\right)^2 + \frac{b^2\beta_{z2}\beta_{vz1}\theta_z\,\xi}{m_3 m_4 \mu_v}},$$

and $\xi = \frac{\Lambda_v\mu_h}{\Lambda_h\mu_v}$ is the equilibrium vector-to-host ratio. Here $m_1 = \theta_d + \mu_h$, $m_2 = \tau_1 + \delta_d + \mu_h$, $m_3 = \theta_z + \mu_h$, and $m_4 = \tau_2 + \delta_z + \mu_h$.

Proof. We establish local stability of the disease-free equilibrium using the next-generation matrix method of van den Driessche and Watmough [40].

Disease-free equilibrium. At the DFE, all infected compartments vanish:

$$E_d = I_d = T_d = R_d = E_z = I_z = T_z = R_z = E_{dz} = I_{dz} = T_{dz} = I_{vd} = I_{vz} = 0,$$

with

$$S_h^0 = N_h^0 = \frac{\Lambda_h}{\mu_h}, \qquad S_v^0 = \frac{\Lambda_v}{\mu_v}.$$

We define the equilibrium vector-to-host ratio

$$\xi = \frac{S_v^0}{N_h^0} = \frac{\Lambda_v\mu_h}{\Lambda_h\mu_v}.$$

Linearized Infected Subsystem. We consider the infected state vector

$$\mathbf{x} = (E_d,\ I_d,\ E_z,\ I_z,\ E_{dz},\ I_{dz},\ I_{vd},\ I_{vz})^T.$$

The linearized infected subsystem near ξ_0 takes the form

$$\frac{d\mathbf{x}}{dt} = (F - V)\mathbf{x},$$

where F contains the rates of new infections and V contains transitions, recovery, treatment, and death.

Evaluating the Jacobian of $\mathcal{F}$ with respect to $\mathbf{x}$ at the DFE yields the matrix

$$F = \begin{pmatrix} 0 & 0 & 0 & 0 & 0 & 0 & b\beta_d & 0 \\ 0 & 0 & 0 & 0 & 0 & 0 & 0 & 0 \\ 0 & 0 & 0 & \beta_{z1} & 0 & \beta_{z3} & 0 & b\beta_{z2} \\ 0 & 0 & 0 & 0 & 0 & 0 & 0 & 0 \\ 0 & 0 & 0 & 0 & 0 & 0 & 0 & 0 \\ 0 & 0 & 0 & 0 & 0 & 0 & 0 & 0 \\ 0 & b\beta_{vd1}\xi & 0 & 0 & 0 & b\beta_{vd2}\xi & 0 & 0 \\ 0 & 0 & 0 & b\beta_{vz1}\xi & 0 & b\beta_{vz2}\xi & 0 & 0 \end{pmatrix}. \tag{12}$$

The transition matrix V (evaluated at the DFE) is block-diagonal as previously defined, with positive diagonal entries, and is invertible. The next-generation matrix is $K = FV^{-1}$, and the basic reproduction number is

$$\mathcal{R}_0 = \rho(K) = \rho(FV^{-1}).$$

The component reproduction numbers $\mathcal{R}_{0d}$ and $\mathcal{R}_{0z}$ are obtained by decoupling the subsystems and are given in the theorem statement. By properties of the spectral radius of nonnegative matrices,

$$\mathcal{R}_0 \geq \max\{\mathcal{R}_{0d}, \mathcal{R}_{0z}\},$$

with equality only when the linear cross-infection parameters $\beta_{z3}, \beta_{vd2}, \beta_{vz2}$ are zero. All co-infection effects, including ADE, are confined to the nonlinear regime. The ADE parameters ε_1 and ε_2 do not appear in F because the corresponding terms in $\mathcal{F}$ are nonlinear and vanish upon linearization at the DFE. Therefore, while co-infection and ADE can amplify disease burden in the nonlinear regime (as revealed by the centre manifold analysis), they do not increase the linear invasion threshold $\mathcal{R}_0$.

By the theorem of van den Driessche and Watmough [40], the disease-free equilibrium ξ_0 is locally asymptotically stable if $\mathcal{R}_0 < 1$ and unstable if $\mathcal{R}_0 > 1$. ■

3.6. Existence of endemic equilibrium

In this section, we establish the existence of an endemic equilibrium when the basic reproduction number exceeds unity. To do this, we employ persistence theory to demonstrate that the disease remains endemic whenever $\mathcal{R}_0 > 1$.

3.6.1. Preliminaries and definitions

We begin by establishing the necessary framework for persistence analysis.

Definition 4 (Positively Invariant Set)**.** A set $\Gamma \subset \mathbb{R}^{16}$ is positively invariant for the system if every solution starting in Γ remains in Γ for all future time.

Definition 5 (Omega Limit Set)**.** For a trajectory $\phi(t, \mathbf{x}_0)$ starting at $\mathbf{x}_0$, the omega limit set $\omega(\mathbf{x}_0)$ is the set of all accumulation points of the trajectory as $t \to \infty$.

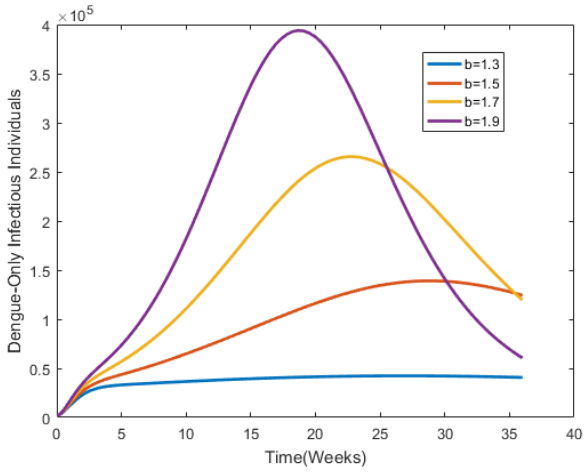

(a) Effects of mosquito biting rate on the dengue infectious population.

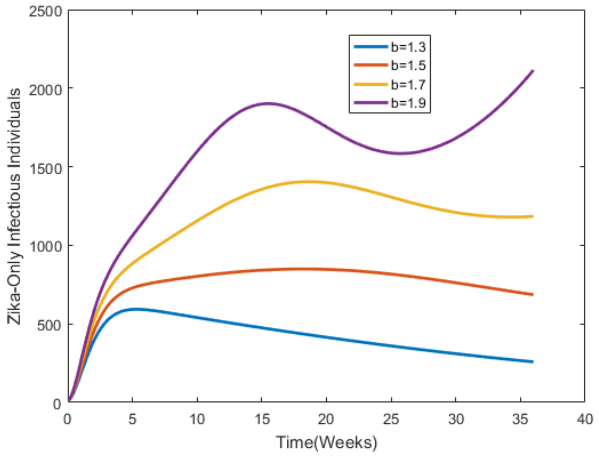

(b) Effects of mosquito biting rate on Zika Infectious Population.

Figure 5: Effects of Mosquito biting rates on infectious classes of Dengue and Zika submodels.

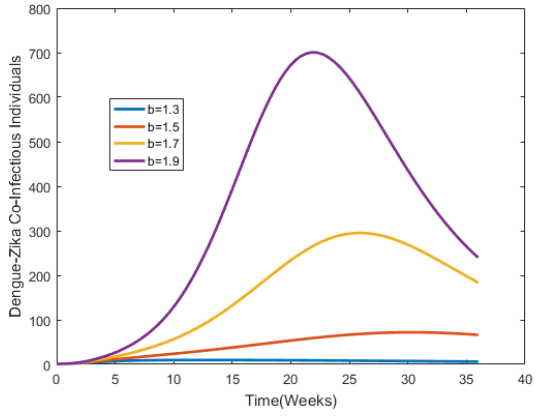

Figure 6: Effects of mosquito biting rate on the dengue–Zika co-infectious class

Definition 6 (Uniform Persistence)**.** The system is said to be *uniformly persistent* with respect to the infected compartments if there exists a constant $\epsilon > 0$ such that for any initial condition with at least one infected compartment positive, we have

$$\liminf_{t\to\infty} E_d(t) \geq \epsilon, \quad \liminf_{t\to\infty} I_d(t) \geq \epsilon, \quad \ldots, \quad \liminf_{t\to\infty} I_{vz}(t) \geq \epsilon.$$

In other words, once infection is introduced, all infected compartments remain bounded away from zero.

3.6.2. *Feasible region and invariance*

Consider the biologically feasible region:

$$\Omega = \left\{(S_h, E_d, \ldots, I_{vz}) \in \mathbb{R}_+^{16} : N_h \leq \frac{\Lambda_h}{\mu_h}, \quad N_v \leq \frac{\Lambda_v}{\mu_v}\right\}, \quad (13)$$

where $N_h = S_h + E_d + I_d + T_d + R_d + V_d + E_z + I_z + T_z + R_z + E_{dz} + I_{dz} + T_{dz}$ and $N_v = S_v + I_{vd} + I_{vz}$.

Lemma 7 (Positive Invariance and Boundedness)**.** *The region Ω is positively invariant for the model system, and all solutions starting in Ω are bounded.*

Proof. For the human population, summing all human compartment equations yields:

$$\frac{dN_h}{dt} = \Lambda_h - \mu_h N_h - \delta_d I_d - \delta_{2d} T_d - \delta_z I_z - \delta_{2z} T_z - \varepsilon_3 \delta_{dz} I_{dz} - \varepsilon_3 \delta_{2dz} T_{dz}. \quad (14)$$

Since all disease-induced death terms are non-negative, we have:

$$\frac{dN_h}{dt} \leq \Lambda_h - \mu_h N_h.$$

By standard comparison theorems, this implies:

$$N_h(t) \leq N_h(0)e^{-\mu_h t} + \frac{\Lambda_h}{\mu_h}(1 - e^{-\mu_h t}) \to \frac{\Lambda_h}{\mu_h} \quad \text{as } t \to \infty.$$

Thus, N_h is ultimately bounded by $\frac{\Lambda_h}{\mu_h}$.

Similarly, for the vector population:

$$\frac{dN_v}{dt} = \Lambda_v - \mu_v N_v, \quad (15)$$

which gives:

$$N_v(t) \leq N_v(0)e^{-\mu_v t} + \frac{\Lambda_v}{\mu_v}(1 - e^{-\mu_v t}) \to \frac{\Lambda_v}{\mu_v} \quad \text{as } t \to \infty.$$

Since all state variables are non-negative (verified by checking that no variable can become negative once positive) and the total populations are bounded, Ω is positively invariant and compact. ■

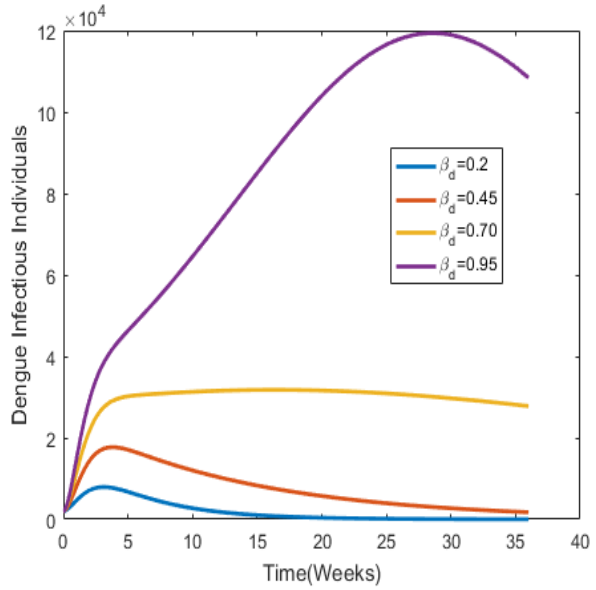

(a) Effects of β_d on the dengue infectious population.

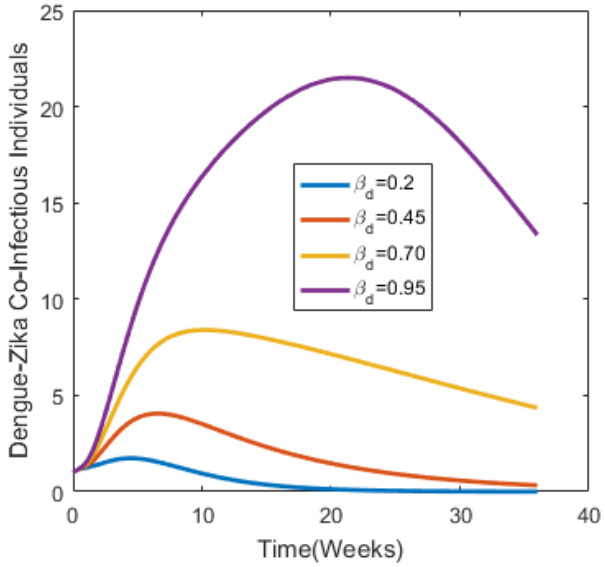

(b) Effects of β_d on dengue–Zika co-infectious Dynamic.

Figure 7: Effects of dengue vector-to-human transmission probability on infectious classes of Dengue and dengue–Zika co-infectious classes.

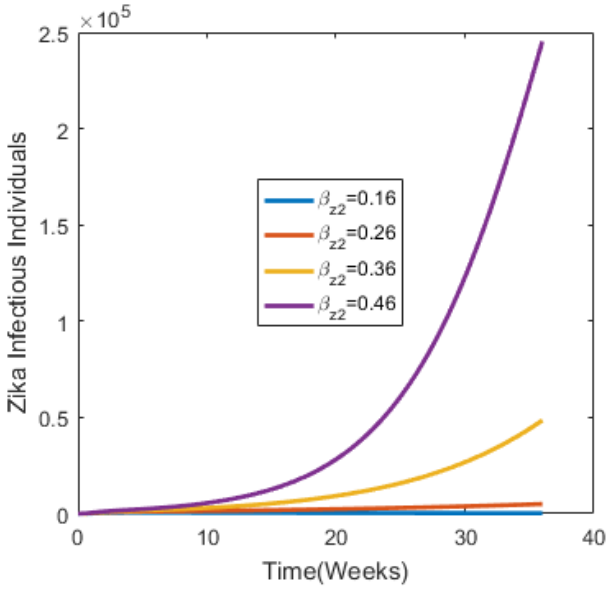

(a) Effects of β_{z2} on the Zika infectious population.

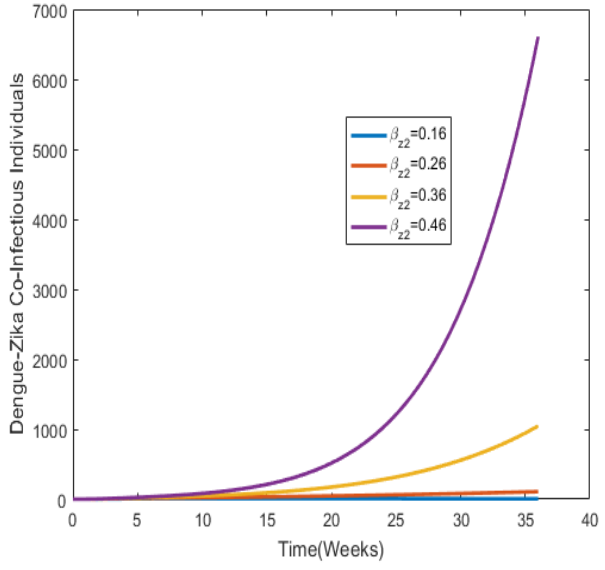

(b) Effects of $\beta_z 2$ on dengue–Zika co-infectious population.

Figure 8: Effects of Zika vector-to-human transmission probability on infectious classes of Zika and dengue–Zika co-infectious classes.

3.6.3. Structure of the boundary equilibrium

Define the disease-free boundary as:

$$\partial\Omega_0 = \{(S_h, E_d, \ldots, I_{vz}) \in \Omega : E_d = I_d = E_z = I_z = E_{dz} = I_{dz} = I_{vd} = I_{vz} = 0\}. \quad (16)$$

The unique equilibrium on $\partial\Omega_0$ is the disease-free equilibrium:

$$\xi_0 = \left(\frac{\Lambda_h}{\mu_h}, 0, \ldots, 0, \frac{\Lambda_v}{\mu_v}, 0, 0\right). \quad (17)$$

3.6.4. Instability of the disease-free equilibrium when $\mathcal{R}_0 > 1$

From Theorem 3 (Local Asymptotic Stability of DFE), we have established that ξ_0 is unstable when $\mathcal{R}_0 > 1$. Specifically, the Jacobian matrix evaluated at ξ_0 has at least one eigenvalue

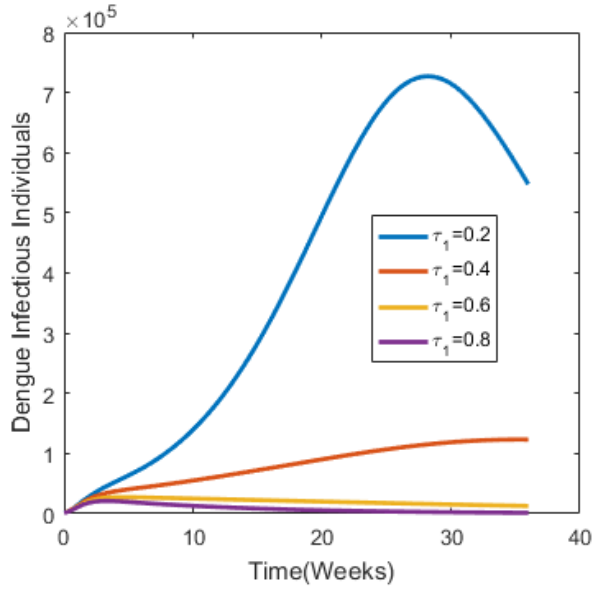

(a) Effects of τ_1 on the dengue infectious population.

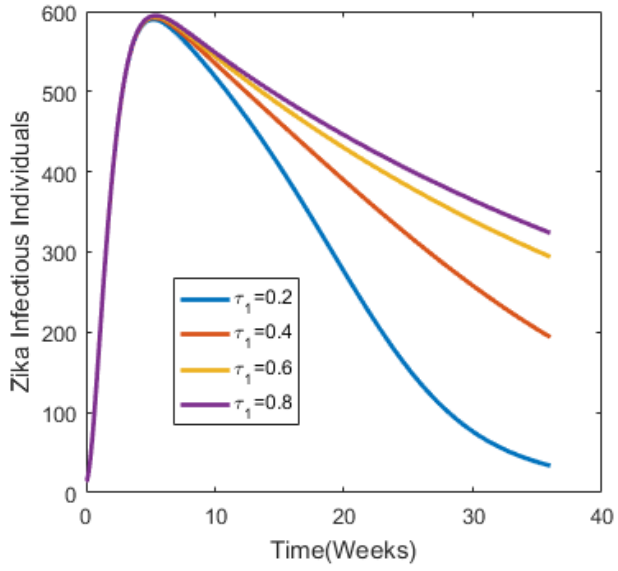

(b) Effects of τ_1 on Zika Infectious population.

Figure 9: Effects of dengue treatment-seeking rate τ_1 on Dengue and Zika infectious dynamics.

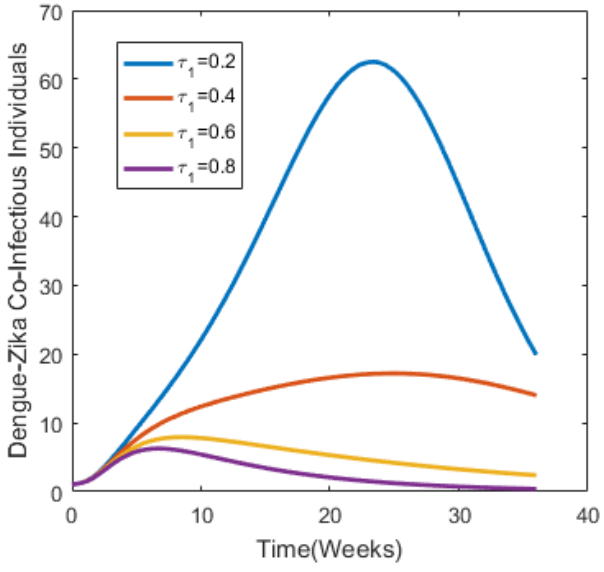

(a) Effects of τ_1 on the dengue–Zika co-infectious population.

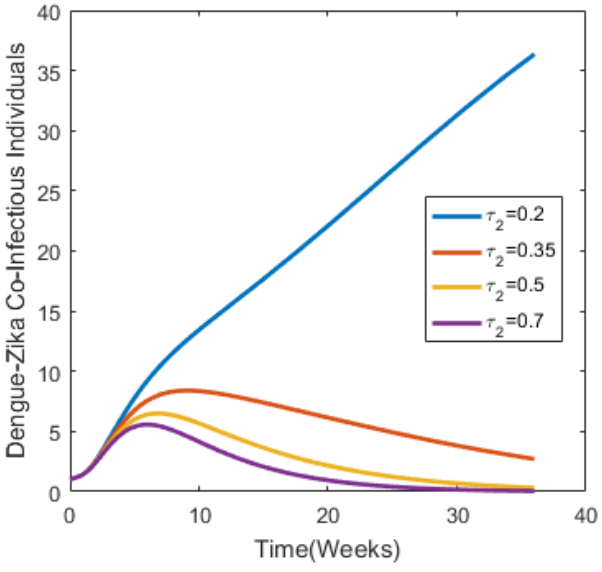

(b) Effects of τ_2 on dengue–Zika co-infectious population.

Figure 10: Effects of dengue and Zika treatment-seeking rates τ_1 and τ_2 on dengue–Zika co-infectious dynamics.

with positive real part.

Lemma 8 (Repelling Property of DFE)**.** *When $\mathcal{R}_0 > 1$, the disease-free equilibrium ξ_0 is a repelling equilibrium on the boundary $\partial\Omega_0$. That is, there exists a neighborhood U of ξ_0 such that trajectories starting in $U \cap \Omega \setminus \partial\Omega_0$ (i.e., with small but positive infection) move away from ξ_0.*

Proof. Since $\mathcal{R}_0 > 1$ implies instability of ξ_0 with respect to the infected subsystem, the stable manifold of ξ_0 lies entirely within $\partial\Omega_0$. Any trajectory starting with positive infection (i.e., in the interior of Ω) cannot converge to ξ_0 but must instead move away from it along the unstable manifold. ■

3.6.5. Uniform persistence

We now invoke a standard result from persistence theory.

Theorem 9 (Uniform persistence of infection)**.** *If $\mathcal{R}_0 > 1$, then the dengue–Zika co-infection model is uniformly persistent with respect to the infected compartments. That is, there exists $\epsilon > 0$ such that for any initial condition with at least one infected*

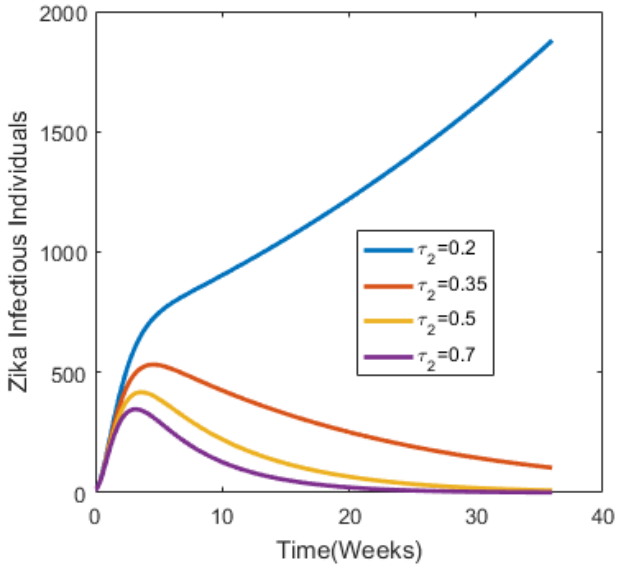

(a) Effects of τ_2 on the Zika infectious population.

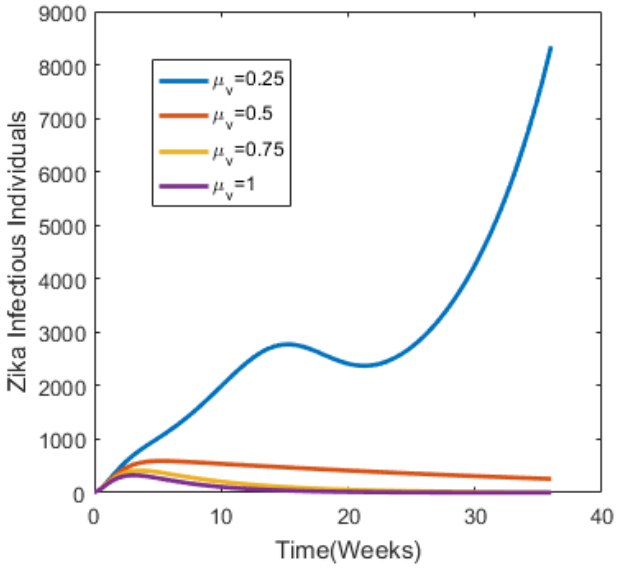

(b) Effects of μ_v on Zika Infectious population.

Figure 11: Effects of τ_2 and Mosquito Mortality μ_v on Zika Infectious dynamics.

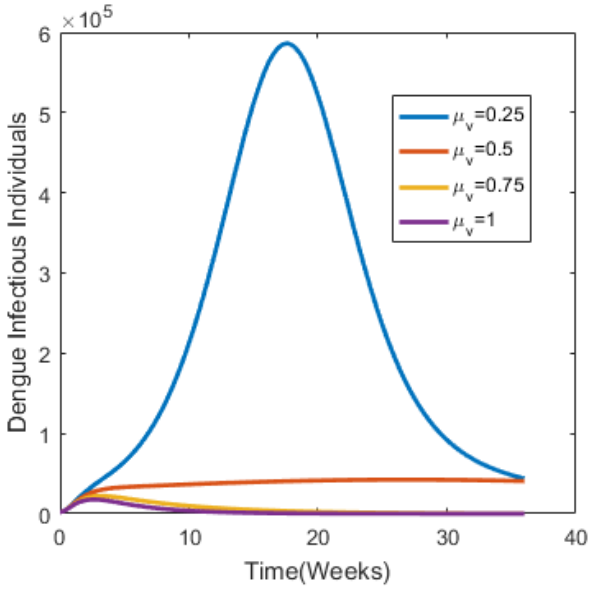

(a) Effects of μ_v on the dengue infectious population.

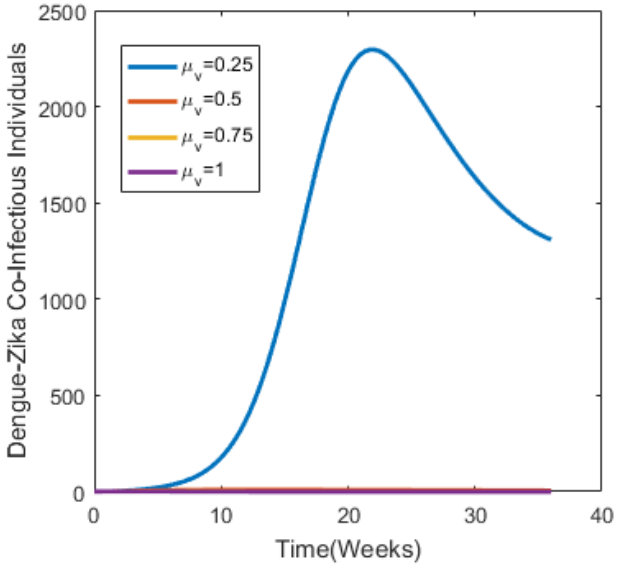

(b) Effects of μ_v on dengue–Zika co-infectious population.

Figure 12: Effects of mosquito mortality rate μ_v on Dengue and dengue–Zika co-infectious dynamics.

compartment positive, we have:

$$\liminf_{t\to\infty} E_d(t) \geq \epsilon, \quad \liminf_{t\to\infty} I_d(t) \geq \epsilon,$$
$$\liminf_{t\to\infty} E_z(t) \geq \epsilon, \quad \liminf_{t\to\infty} I_z(t) \geq \epsilon, \tag{18}$$

and similarly for E_{dz}, I_{dz}, I_{vd}, and I_{vz}.

Proof. We apply the persistence framework developed by Thieme [61] and Castillo-Chavez *et al.* [62].

The system satisfies the following key conditions:

(P1) Compactness: By Lemma 7, the feasible region Ω is compact and positively invariant.

(P2) Persistence Function: Define the persistence function:

$$\rho(\mathbf{x}) = \min\{E_d, I_d, E_z, I_z, E_{dz}, I_{dz}, I_{vd}, I_{vz}\}.$$

This function is positive in the interior of Ω and zero on the disease-free boundary $\partial\Omega_0$.

(P3) Acyclicity on Boundary: The chain recurrent set on $\partial\Omega_0$ consists of the single equilibrium ξ_0. To see this, note that on $\partial\Omega_0$, all infection dynamics are absent, and the system re-

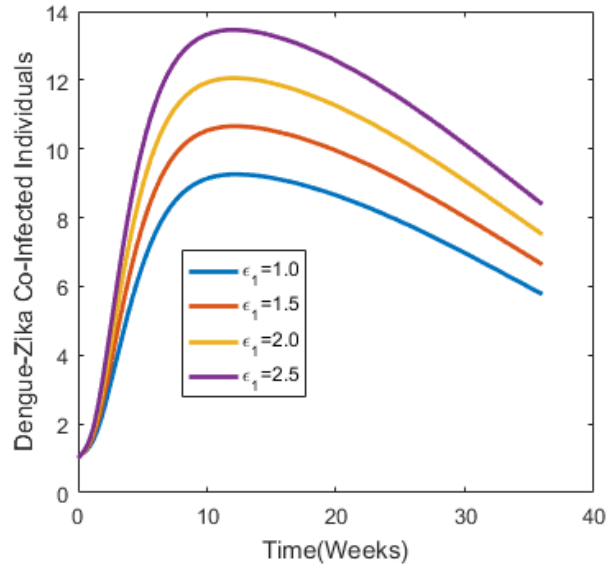

(a) Effects of ε_1 on the dengue–Zika co-infectious population.

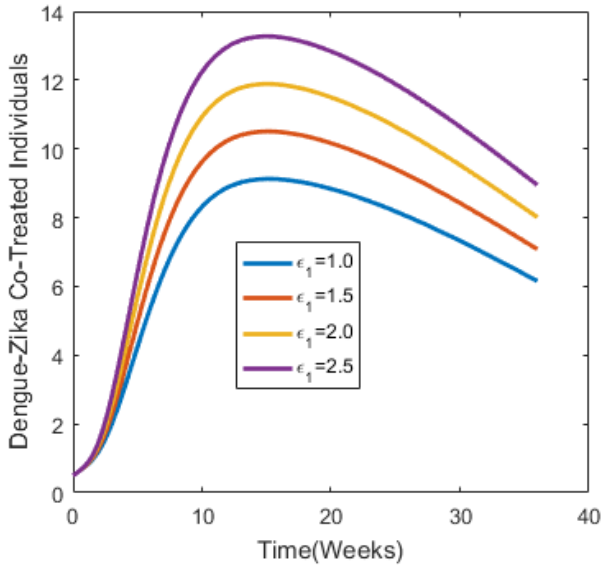

(b) Effects of ε_1 on dengue–Zika Co-Treated population.

Figure 13: Effects of ε_1 on Co-Infection dynamics.

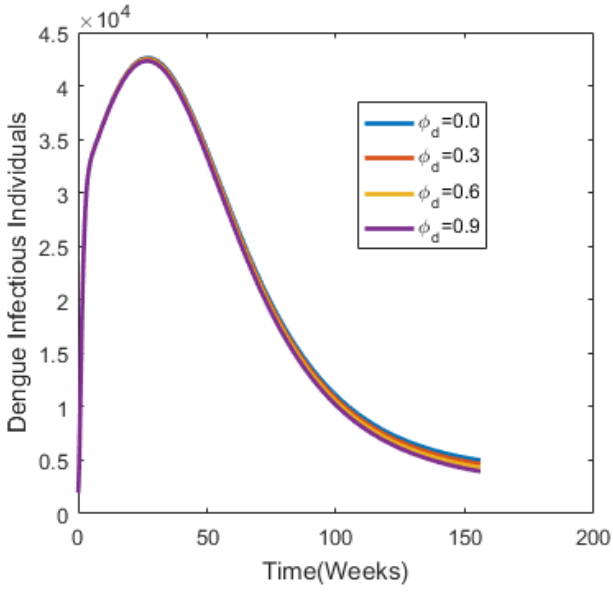

(a) Effects of ϕ_d on the dengue infectious population.

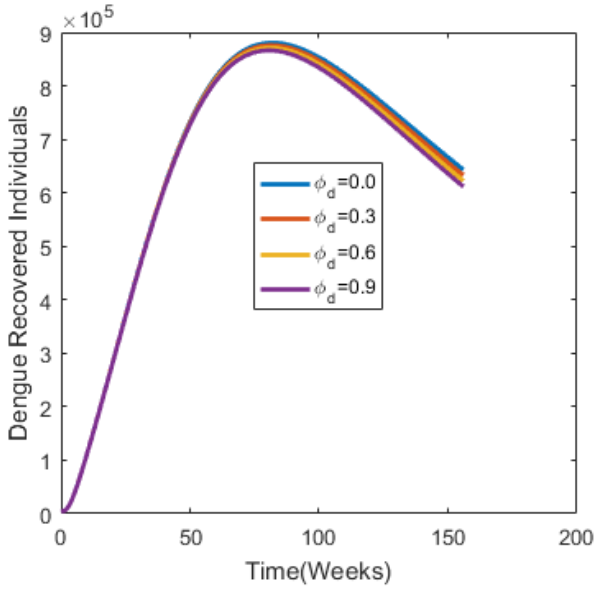

(b) Effects of ϕ_d on Dengue Recovered population.

Figure 14: Effects of Vaccine efficacy ϕ_d on Dengue Infection dynamics.

duces to:

$$\frac{dS_h}{dt} = \Lambda_h - \mu_h S_h + (\text{terms from } R_d, R_z \text{ which decay to zero}), \tag{19}$$

$$\frac{dS_v}{dt} = \Lambda_v - \mu_v S_v. \tag{20}$$

These equations converge to the unique equilibrium $\left(\frac{\Lambda_h}{\mu_h}, \frac{\Lambda_v}{\mu_v}\right)$ on the boundary, confirming acyclicity.

(P4) Instability of Boundary Equilibrium: By Lemma 8, when $\mathcal{R}_0 > 1$, the DFE is unstable with respect to perturbations introducing infection. The stable manifold $W^s(\xi_0)$ of ξ_0 is contained entirely in $\partial\Omega_0$.

By the uniform persistence theorem [61, Theorem 4.3], conditions (P1)–(P4) guarantee that the system is uniformly persistent. Specifically, there exists $\epsilon > 0$ (depending on the parameters but independent of initial conditions) such that all solutions starting with positive infection satisfy: $\liminf_{t\to\infty} E_d(t) \geq \epsilon$, and similarly for all other infected compartments. ■

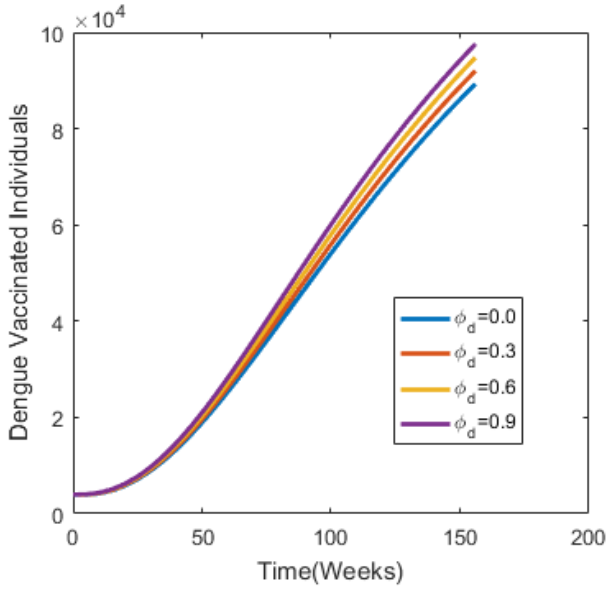

(a) Effects of ϕ_d on the dengue-vaccinated population.

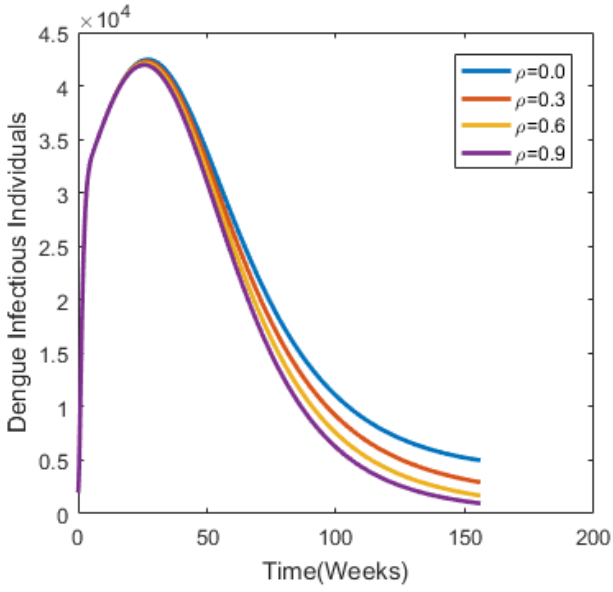

(b) Effects of ρ on Dengue Infectious population.

Figure 15: Effects of vaccine efficacy ϕ_d and vaccination coverage ρ on Dengue Vaccinated and Infectious Population.

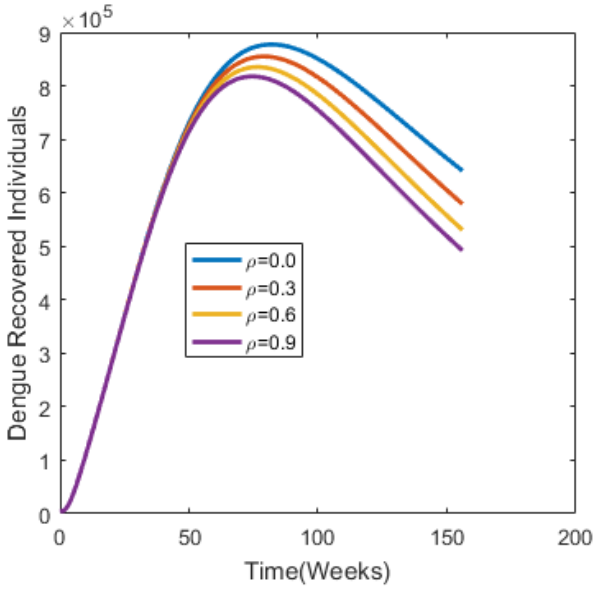

(a) Effects of ρ on the dengue-recovered population.

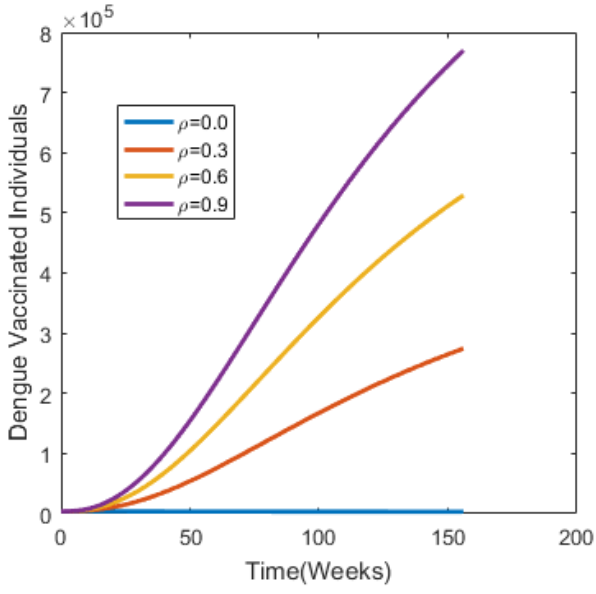

(b) Effects of ρ on Dengue Vaccinated population.

Figure 16: Effects of Vaccination coverage ρ on Dengue dynamics.

3.6.6. Persistence and existence of endemic states

We now establish that whenever $\mathcal{R}_0 > 1$, the disease-free equilibrium (DFE) loses stability and the infection persists in the population in the sense of uniform persistence.

Positivity and Invariance.

Let $\Omega \subset \mathbb{R}^{16}_+$ denote the biologically feasible region determined by nonnegative initial data and the population bounds established previously. Standard comparison arguments show that all solutions with initial conditions in Ω remain nonnegative for all $t > 0$. Moreover, the total human and vector populations remain uniformly bounded. Hence Ω is positively invariant and absorbing.

Define the infection-free boundary set

$$\partial\Omega_0 = \{x \in \Omega : E_d = I_d = E_z = I_z = E_{dz} = I_{dz} = I_{vd} = I_{vz} = 0\}.$$

This set is invariant under the flow, since in the absence of infected individuals no infection terms are generated. The DFE ξ_0 is the unique equilibrium contained in $\partial\Omega_0$.

Instability of the DFE.

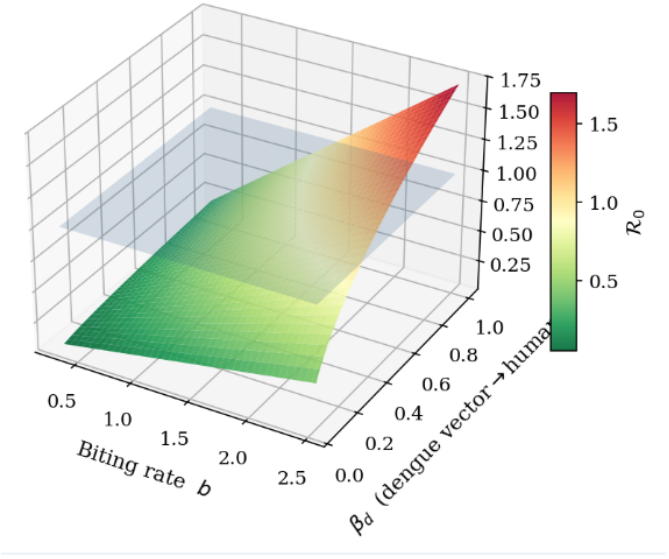

(a) Surface R_{0d} Vs b and β_d.

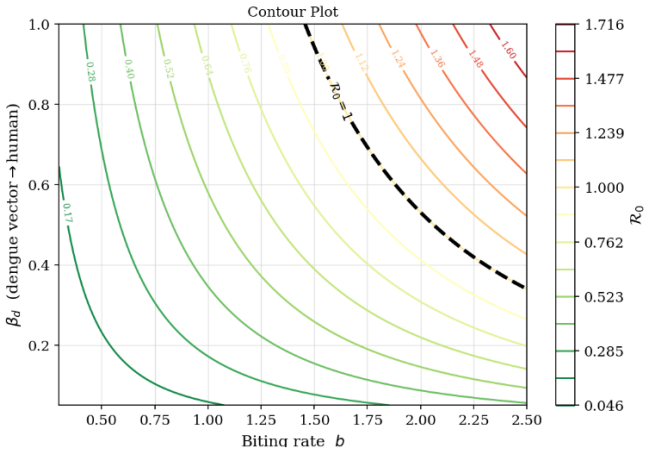

(b) Contour R_{0d} Vs b and β_d.

Figure 17: Contour plot of the dengue reproduction number $\mathcal{R}_{0d}$ as a function of the mosquito biting rate b and the dengue vector-to-human transmission probability β_d.

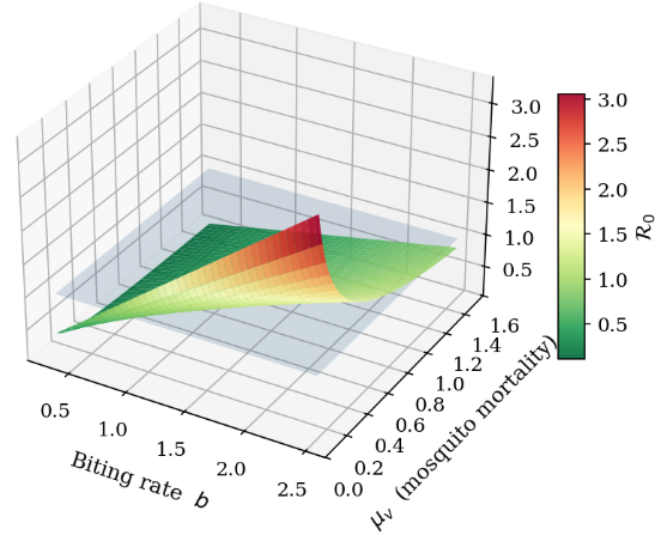

(a) Surface R_{0d} Vs b and μ_v.

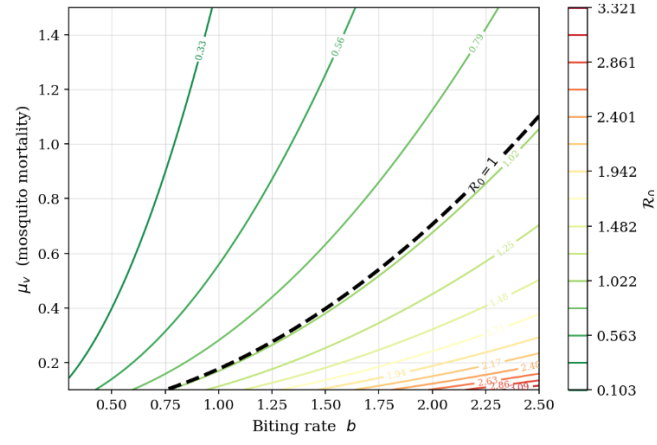

(b) Contour R_{0d} Vs b and μ_v.

Figure 18: Dengue Reproduction Number $\mathcal{R}_{0d}$ as a function of mosquito biting rate b and mosquito mortality μ_v.

From the previous section, the Jacobian matrix evaluated at ξ_0 admits a block decomposition separating infected and uninfected variables. By the theorem of van den Driessche and Watmough, the DFE is locally asymptotically stable if $\mathcal{R}_0 < 1$ and unstable if $\mathcal{R}_0 > 1$.

In particular, when $\mathcal{R}_0 > 1$, the linearized dynamics restricted to the infected subsystem possesses a positive eigenvalue. Since the boundary $\partial\Omega_0$ contains no equilibria other than ξ_0, trajectories initiated sufficiently close to the DFE with at least one infected component positive cannot converge to ξ_0. Consequently, the DFE acts as a repeller for solutions originating in the interior of Ω.

Uniform Persistence.

We now show that the infection persists whenever $\mathcal{R}_0 > 1$. Let

$$\Omega_0 = \Omega \setminus \partial\Omega_0$$

denote the interior region in which at least one infected component is positive.

The semiflow generated by the system is point dissipative and admits a compact global attractor in Ω. Since the only invariant set on $\partial\Omega_0$ is the unstable equilibrium ξ_0, classical persistence results for dissipative systems (see, e.g., Thieme, 2003)

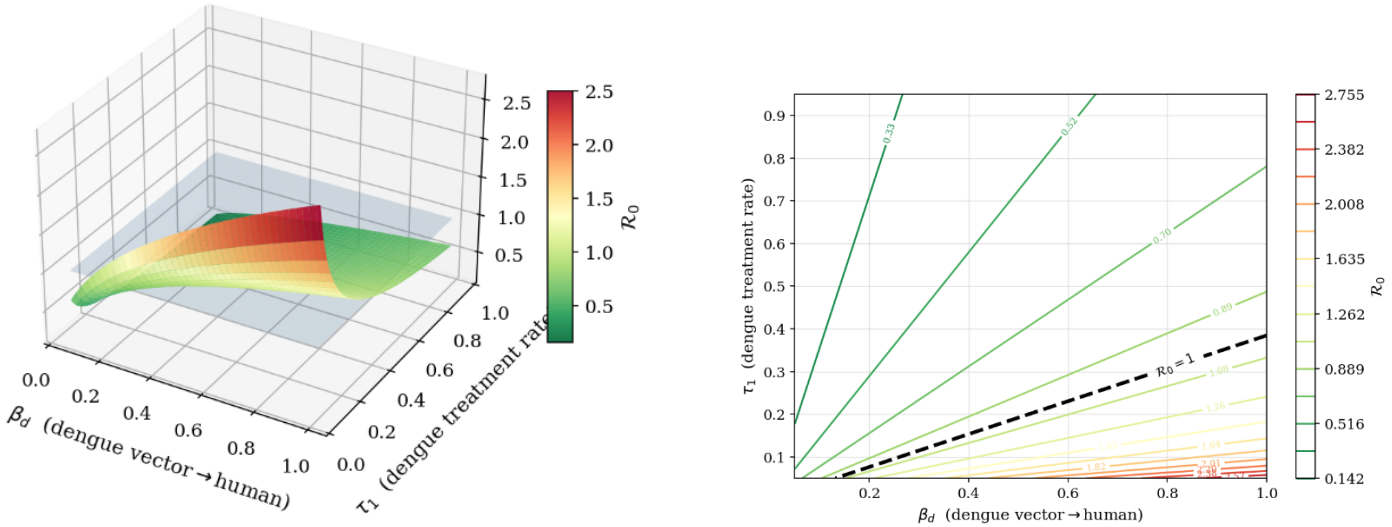

(a) Surface R_{0d} Vs β_d and τ_1.

(b) Contour R_{0d} Vs β_d and τ_1.

Figure 19: Dengue Reproduction Number R_{0d} Vs β_d and τ_1.

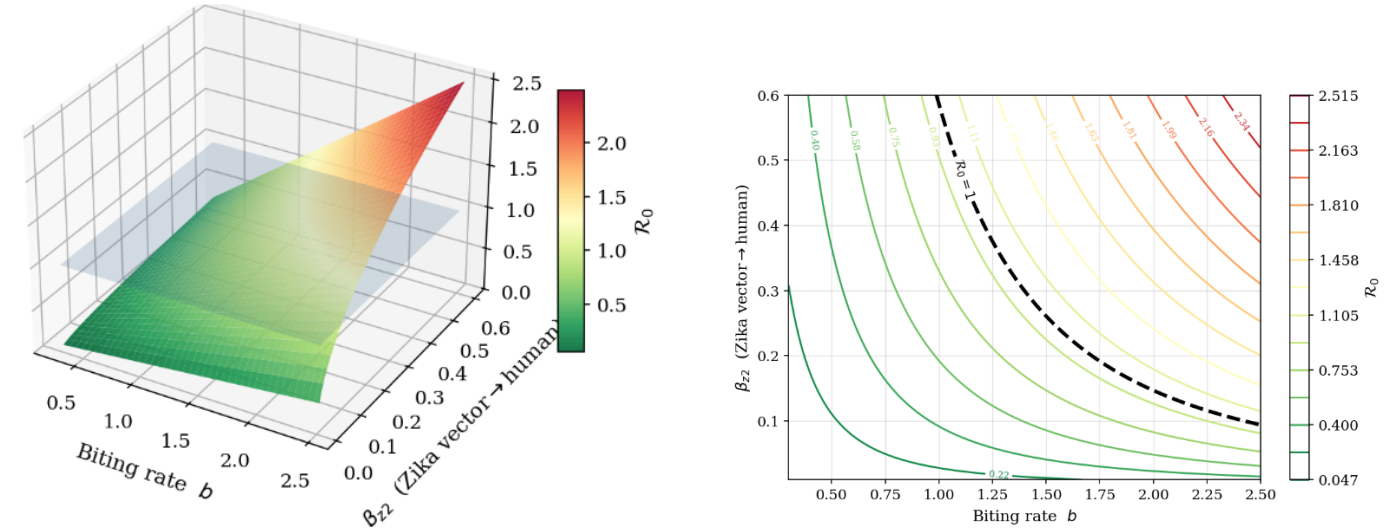

(a) Surface R_{0z} Vs b and β_{z2}.

(b) Contour R_{0z} Vs b and β_{z2}.

Figure 20: Zika Reproduction Number R_{0z} Vs b and β_{z2}.

imply that the system is uniformly persistent with respect to the pair $(\Omega_0, \partial\Omega_0)$ whenever $\mathcal{R}_0 > 1$.

Therefore, there exists a constant $\epsilon > 0$ such that every solution with initial data in Ω_0 satisfies

$$\liminf_{t\to\infty} \sum_{i\in\mathcal{I}} x_i(t) \;\geq\; \epsilon,$$

where $\mathcal{I}$ denotes the collection of infected compartments. That is, the total infected population remains bounded away from zero uniformly in time.

Existence of Endemic Equilibria.

Uniform persistence together with compactness of the global attractor ensures the existence of at least one equilibrium

$$\xi^* \in \Omega_0,$$

with strictly positive infected components. Hence, whenever $\mathcal{R}_0 > 1$, the system admits at least one endemic state.

Interpretation.

The threshold parameter $\mathcal{R}_0$ therefore determines the local stability of the disease-free equilibrium and governs whether infection can invade the population. When $\mathcal{R}_0 < 1$, small introductions of infection die out and the DFE is locally asymptotically stable. When $\mathcal{R}_0 > 1$, the DFE becomes unstable and the system admits persistent infection dynamics, with at least one endemic equilibrium in the interior of the feasible region.

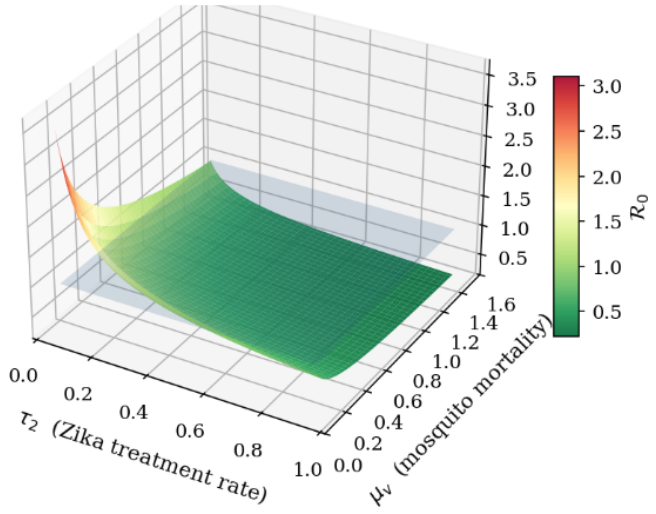

(a) Surface R_{0z} Vs τ_2 and μ_v.

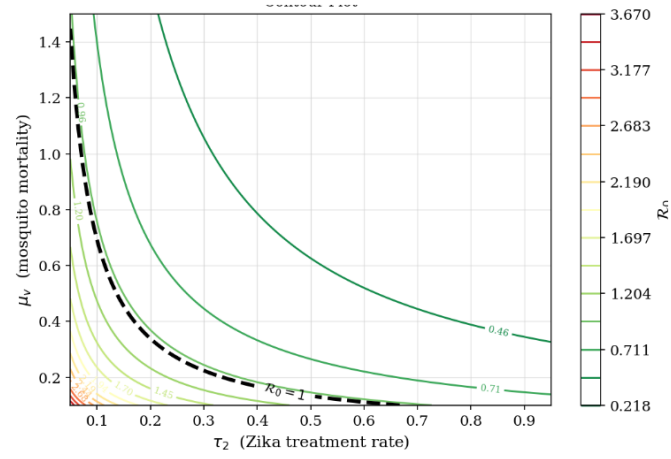

(b) Contour R_{0z} Vs τ_2 and μ_v

Figure 21: Zika Reproduction Number R_{0z} Vs τ_2 and μ_v.

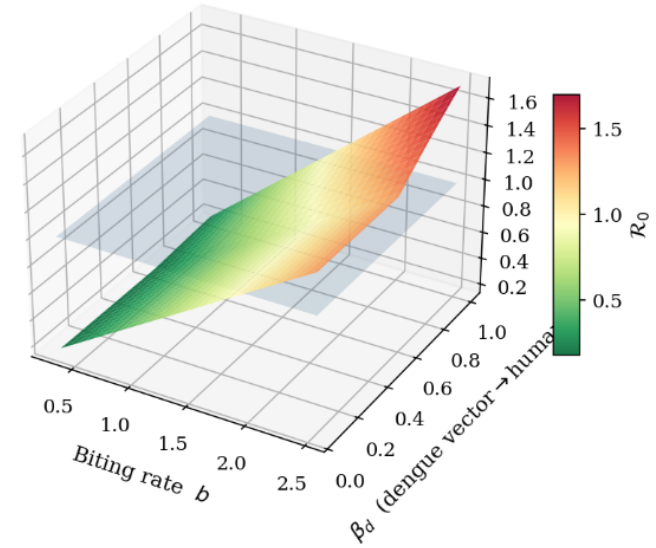

(a) Surface full model R_0 Vs b and β_d.

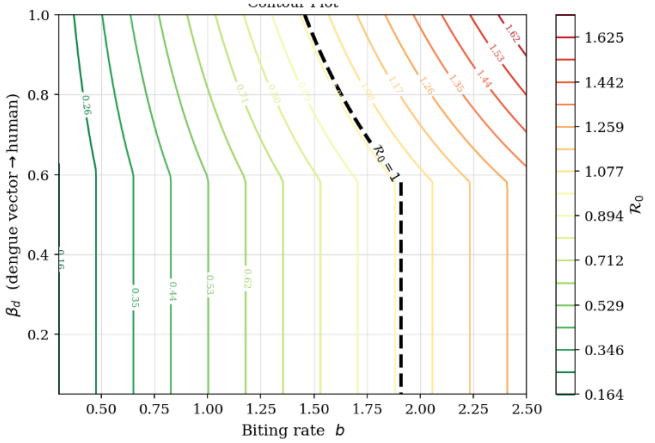

(b) Contour full model R_0 Vs b and β_d

Figure 22: Full Model $R_0 = \rho(FV^{-1})$ Vs b and β_d.

We emphasize that while persistence guarantees long-term survival of infection, it does not in itself establish uniqueness or global stability of the endemic equilibrium, nor does it preclude the possibility of multiple endemic states.

3.7. Backward bifurcation analysis

We examine the possibility of a backward bifurcation in both the dengue-only and Zika-only submodels at $\mathcal{R}_0 = 1$ using the centre manifold theorem [41].

Backward bifurcation can occur in models with vaccination, treatment, partial cross-immunity, or high vector abundance, potentially leading to multiple stable equilibria for $\mathcal{R}_0 < 1$.

The backward-bifurcation structure of the dengue-only submodel is illustrated in Figure 2.

3.7.1. Dengue-only submodel

Theorem 10. *The dengue-only submodel exhibits a backward bifurcation at $\mathcal{R}_{0d} = 1$ whenever the bifurcation coefficient $a > 0$.*

Proof. We introduce the change of variables

$$S_h = x_1, \quad E_d = x_2, \quad I_d = x_3, \quad T_d = x_4,$$

$$R_d = x_5, \quad V_d = x_6, \quad S_v = x_7, \quad I_{vd} = x_8,$$

so that the dengue-only system becomes

$$\begin{aligned}
\frac{dx_1}{dt} &= \Lambda_h - \lambda_d x_1 - \mu_h x_1 + (1-\rho)\alpha_d x_5,\\
\frac{dx_2}{dt} &= \lambda_d x_1 + (1-\phi_d)\lambda_d x_6 - (\theta_d + \mu_h)x_2,\\
\frac{dx_3}{dt} &= \theta_d x_2 - (\tau_1 + \delta_d + \mu_h)x_3,\\
\frac{dx_4}{dt} &= \tau_1 x_3 - (\gamma_1 + \delta_{2d} + \mu_h)x_4,\\
\frac{dx_5}{dt} &= \gamma_1 x_4 - (\alpha_d + \mu_h)x_5,\\
\frac{dx_6}{dt} &= \rho\alpha_d x_5 - (1-\phi_d)\lambda_d x_6 - \mu_h x_6,\\
\frac{dx_7}{dt} &= \Lambda_v - \lambda_{vd} x_7 - \mu_v x_7,\\
\frac{dx_8}{dt} &= \lambda_{vd} x_7 - \mu_v x_8,
\end{aligned} \tag{21}$$

with forces of infection

$$\lambda_d = \frac{b\beta_d x_8}{N_h}, \qquad \lambda_{vd} = \frac{b\beta_{vd1} x_3}{N_h}.$$

We take β_d as the bifurcation parameter. Setting $\mathcal{R}_0^d = 1$ and solving gives the critical value

$$\beta_d^{**} = \frac{k_1 k_2 \mu_v^2 \Lambda_h}{b^2 \beta_{vd1} \theta_d \Lambda_v \mu_h}, \tag{22}$$

where $k_1 = \theta_d + \mu_h$ and $k_2 = \tau_1 + \delta_d + \mu_h$. We also define

$$k_3 = \gamma_1 + \delta_{2d} + \mu_h, \quad k_4 = \alpha_d + \mu_h, \quad \xi = \frac{\Lambda_v \mu_h}{\Lambda_h \mu_v}.$$

The Jacobian of system (21) evaluated at the disease-free equilibrium $\mathcal{E}_0^d$ when $\beta_d = \beta_d^{**}$ is

$$J\big(\mathcal{E}_0^d\big)\big|_{\beta_d=\beta_d^{**}} = \begin{pmatrix}
-\mu_h & 0 & 0 & 0 & (1-\rho)\alpha_d & 0 & 0 & -b\beta_d^{**}\\
0 & -k_1 & 0 & 0 & 0 & 0 & 0 & b\beta_d^{**}\\
0 & \theta_d & -k_2 & 0 & 0 & 0 & 0 & 0\\
0 & 0 & \tau_1 & -k_3 & 0 & 0 & 0 & 0\\
0 & 0 & 0 & \gamma_1 & -k_4 & 0 & 0 & 0\\
0 & 0 & 0 & 0 & \rho\alpha_d & -\mu_h & 0 & 0\\
0 & 0 & -b\beta_{vd1}\xi & 0 & 0 & 0 & -\mu_v & 0\\
0 & 0 & b\beta_{vd1}\xi & 0 & 0 & 0 & 0 & -\mu_v
\end{pmatrix}. \tag{23}$$

Right eigenvector. The right eigenvector $\mathbf{w} = (w_1, \ldots, w_8)^{\mathsf{T}}$ associated with the simple zero eigenvalue of $J(\mathcal{E}_0^d)|_{\beta_d=\beta_d^{**}}$, satisfying $J(\mathcal{E}_0^d)\mathbf{w} = \mathbf{0}$, is given (with $w_3 > 0$ as the free component) by

$$\begin{aligned}
w_1 &= \frac{1}{\mu_h}\left(\frac{(1-\rho)\alpha_d\gamma_1\tau_1}{k_3 k_4} - \frac{b^2\beta_d^{**}\beta_{vd1}\xi}{\mu_v}\right) w_3,\\
w_2 &= \frac{b^2\beta_d^{**}\beta_{vd1}\xi}{k_1\mu_v}\, w_3,\\
w_3 &= w_3 > 0,\\
w_4 &= \frac{\tau_1}{k_3}\, w_3,\\
w_5 &= \frac{\gamma_1\tau_1}{k_3 k_4}\, w_3,\\
w_6 &= \frac{\rho\alpha_d\gamma_1\tau_1}{\mu_h k_3 k_4}\, w_3,\\
w_7 &= -\frac{b\beta_{vd1}\xi}{\mu_v}\, w_3,\\
w_8 &= \frac{b\beta_{vd1}\xi}{\mu_v}\, w_3.
\end{aligned}$$

Left eigenvector. The left eigenvector $\mathbf{v} = (v_1, \ldots, v_8)$ satisfying $\mathbf{v}\, J(\mathcal{E}_0^d) = \mathbf{0}$ and $\mathbf{v}\cdot\mathbf{w} = 1$ is given (with $v_2 > 0$ as the free component) by

$$v_1 = 0, \quad v_2 = v_2 > 0, \quad v_3 = \frac{k_1}{\theta_d}\, v_2,$$

$$v_4 = v_5 = v_6 = v_7 = 0, \quad v_8 = \frac{b\beta_d^{**}}{\mu_v}\, v_2.$$

Bifurcation coefficients. The bifurcation coefficient a is

$$a = \sum_{i,j,k=1}^{8} v_k w_i w_j \frac{\partial^2 f_k}{\partial x_i \partial x_j}\bigg|_{\mathcal{E}_0^d,\, \beta_d^{**}}.$$

The nonzero second-order partial derivatives at $\mathcal{E}_0^d$ (where $N_h^* = \Lambda_h/\mu_h$) are

$$\frac{\partial^2 f_2}{\partial x_1 \partial x_8} = \frac{b\beta_d^{**}\mu_h}{\Lambda_h}, \qquad \frac{\partial^2 f_2}{\partial x_6 \partial x_8} = \frac{(1-\phi_d)b\beta_d^{**}\mu_h}{\Lambda_h},$$

$$\frac{\partial^2 f_8}{\partial x_3 \partial x_7} = \frac{b\beta_{vd1}\mu_h}{\Lambda_h}.$$

yielding

$$a = \frac{2b\mu_h}{\Lambda_h}\Big[v_2 w_8 (w_1\beta_d^{**} + (1-\phi_d)w_6\beta_d^{**}) + v_8 w_3 w_7 \beta_{vd1}\Big]. \tag{24}$$

Since $w_7 < 0$, the sign of a is determined by the balance between the positive term involving vaccine efficacy and the negative vector transmission term. When vaccine efficacy ϕ_d is low and vector abundance ξ remains below a critical threshold, the positive term dominates and $a > 0$, giving rise to a backward bifurcation. As ξ increases beyond this threshold, the negative vector driven term instead dominates, and $a < 0$, so the system undergoes a forward (transcritical) bifurcation.

The bifurcation coefficient b_{bif} is

$$b_{\text{bif}} = \sum_{i,k=1}^{8} v_k w_i \frac{\partial^2 f_k}{\partial x_i \partial \beta_d^{**}}\bigg|_{\mathcal{E}_0^d}.$$

Differentiating f_2 with respect to β_d^{**} and evaluating at $\mathcal{E}_0^d$ gives $\partial^2 f_2/(\partial x_8 \partial \beta_d^{**}) = b$, so that

$$b_{\text{bif}} = b\, v_2\, w_8 > 0. \tag{25}$$

It follows from the centre manifold theorem [41] that the dengue-only submodel undergoes a *backward bifurcation* at $\mathcal{R}_0^d = 1$ whenever a in (24) is positive. ■

3.7.2. Zika-only submodel

Theorem 11. *The Zika-only submodel exhibits a backward bifurcation at $\mathcal{R}_{0z} = 1$ whenever the bifurcation coefficient $a > 0$.*

Proof. We introduce the change of variables

$$S_h = y_1, \quad E_z = y_2, \quad I_z = y_3, \quad T_z = y_4,$$
$$R_z = y_5, \quad S_v = y_6, \quad I_{vz} = y_7.$$

so that the Zika-only system becomes

$$\begin{aligned}
\frac{dy_1}{dt} &= \Lambda_h - \lambda_z y_1 - \mu_h y_1 + \psi y_5,\\
\frac{dy_2}{dt} &= \lambda_z y_1 - (\theta_z + \mu_h) y_2,\\
\frac{dy_3}{dt} &= \theta_z y_2 - (\tau_2 + \delta_z + \mu_h) y_3,\\
\frac{dy_4}{dt} &= \tau_2 y_3 - (\gamma_2 + \delta_{2z} + \mu_h) y_4,\\
\frac{dy_5}{dt} &= \gamma_2 y_4 - (\psi + \mu_h) y_5,\\
\frac{dy_6}{dt} &= \Lambda_v - \lambda_{vz} y_6 - \mu_v y_6,\\
\frac{dy_7}{dt} &= \lambda_{vz} y_6 - \mu_v y_7,
\end{aligned} \tag{26}$$

with forces of infection

$$\lambda_z = \frac{\beta_{z1} y_3 + b\beta_{z2} y_7}{N_h}, \qquad \lambda_{vz} = \frac{b\beta_{vz1} y_3}{N_h}.$$

We take β_{z1} as the bifurcation parameter. Letting

$$\mathcal{R}^v_{0z} = \frac{b^2 \beta_{z2}\beta_{vz1}\theta_z \Lambda_v \mu_h}{m_3 m_4 \mu_v^2 \Lambda_h}$$

denote the purely vector-borne component of $\mathcal{R}_{0z}$, the critical value of β_{z1} at $\mathcal{R}_{0z} = 1$ is

$$\beta^{**}_{z1} = \frac{m_3 m_4}{\theta_z}\left(1 - \mathcal{R}^v_{0z}\right), \tag{27}$$

where $m_3 = \theta_z + \mu_h$ and $m_4 = \tau_2 + \delta_z + \mu_h$. Expression (27) is biologically meaningful (i.e., $\beta^{**}_{z1} > 0$) only when $\mathcal{R}^v_{0z} < 1$, that is, when vector-borne transmission alone cannot sustain an outbreak.

We also define

$$m_5 = \gamma_2 + \delta_{2z} + \mu_h, \quad m_6 = \psi + \mu_h, \quad \xi = \frac{\Lambda_v \mu_h}{\Lambda_h \mu_v}.$$

The Jacobian of system (26) evaluated at the disease-free equilibrium $\mathcal{E}^z_0$ when $\beta_{z1} = \beta^{**}_{z1}$ is

$$J\left(\mathcal{E}^z_0\right)\Big|_{\beta_{z1}=\beta^{**}_{z1}} = \begin{pmatrix}
-\mu_h & 0 & -\beta^{**}_{z1} & 0 & \psi & 0 & -b\beta_{z2}\\
0 & -m_3 & \beta^{**}_{z1} & 0 & 0 & 0 & b\beta_{z2}\\
0 & \theta_z & -m_4 & 0 & 0 & 0 & 0\\
0 & 0 & \tau_2 & -m_5 & 0 & 0 & 0\\
0 & 0 & 0 & \gamma_2 & -m_6 & 0 & 0\\
0 & 0 & -b\beta_{vz1}\xi & 0 & 0 & -\mu_v & 0\\
0 & 0 & b\beta_{vz1}\xi & 0 & 0 & 0 & -\mu_v
\end{pmatrix}. \tag{28}$$

Right eigenvector.. The right eigenvector $\mathbf{w}^z = (w^z_1, \ldots, w^z_7)^{\mathsf{T}}$ satisfying $J(\mathcal{E}^z_0)\mathbf{w}^z = \mathbf{0}$, with $w^z_3 > 0$ as the free component, is

$$\begin{aligned}
w^z_1 &= \frac{1}{\mu_h}\left(\frac{\psi\gamma_2\tau_2}{m_5 m_6} - \beta^{**}_{z1} - \frac{b^2\beta_{z2}\beta_{vz1}\xi}{\mu_v}\right) w^z_3,\\
w^z_2 &= \frac{1}{m_3}\left(\beta^{**}_{z1} + \frac{b^2\beta_{z2}\beta_{vz1}\xi}{\mu_v}\right) w^z_3,\\
w^z_3 &= w^z_3 > 0,\\
w^z_4 &= \frac{\tau_2}{m_5} w^z_3,\\
w^z_5 &= \frac{\gamma_2\tau_2}{m_5 m_6} w^z_3,\\
w^z_6 &= -\frac{b\beta_{vz1}\xi}{\mu_v} w^z_3,\\
w^z_7 &= \frac{b\beta_{vz1}\xi}{\mu_v} w^z_3.
\end{aligned}$$

Left eigenvector.. The left eigenvector $\mathbf{v}^z = (v^z_1, \ldots, v^z_7)$ satisfying $\mathbf{v}^z J(\mathcal{E}^z_0) = \mathbf{0}$ and $\mathbf{v}^z \cdot \mathbf{w}^z = 1$, with $v^z_2 > 0$ as the free component, is

$$v^z_1 = 0, \quad v^z_2 = v^z_2 > 0, \quad v^z_3 = \frac{m_3}{\theta_z} v^z_2,$$
$$v^z_4 = v^z_5 = v^z_6 = 0, \quad v^z_7 = \frac{b\beta_{z2}}{\mu_v} v^z_2.$$

Bifurcation coefficients.. The bifurcation coefficient a is

$$a = \sum_{i,j,k=1}^{7} v^z_k w^z_i w^z_j \frac{\partial^2 f_k}{\partial y_i \partial y_j}\Big|_{\mathcal{E}^z_0,\, \beta^{**}_{z1}}.$$

The nonzero second-order partial derivatives at $\mathcal{E}^z_0$ (where $N^*_h = \Lambda_h/\mu_h$) are

$$\frac{\partial^2 f_2}{\partial y_1 \partial y_3} = \frac{\beta^{**}_{z1}\mu_h}{\Lambda_h}, \qquad \frac{\partial^2 f_2}{\partial y_1 \partial y_7} = \frac{b\beta_{z2}\mu_h}{\Lambda_h},$$
$$\frac{\partial^2 f_7}{\partial y_3 \partial y_6} = \frac{b\beta_{vz1}\mu_h}{\Lambda_h}.$$

yielding

$$a = \frac{2\mu_h}{\Lambda_h}\left[v^z_2 w^z_1 (\beta^{**}_{z1} w^z_3 + b\beta_{z2} w^z_7) + v^z_7 w^z_3 w^z_6 b\beta_{vz1}\right]. \tag{29}$$

Since $w^z_6 < 0$, the last term in (29) is negative. The sign of a therefore depends on whether direct human-to-human transmission (captured by β^{**}_{z1}) is sufficiently strong relative to the vector-borne contribution. When $a > 0$, a backward bifurcation occurs.

The bifurcation coefficient b_{bif} is

$$b_{\text{bif}} = \sum_{i,k=1}^{7} v^z_k w^z_i \frac{\partial^2 f_k}{\partial y_i \partial \beta^{**}_{z1}}\Big|_{\mathcal{E}^z_0}.$$

Differentiating f_2 with respect to β^{**}_{z1} and evaluating at $\mathcal{E}^z_0$ gives $\partial^2 f_2/(\partial y_3 \partial \beta^{**}_{z1}) = 1$, so that

$$b_{\text{bif}} = v^z_2 w^z_3 > 0. \tag{30}$$

It follows from the centre manifold theorem [41] that the Zika-only submodel undergoes a *backward bifurcation* at $\mathcal{R}_{0z} = 1$ whenever a in (29) is positive. ■

Remark 2. The epidemiological implication of backward bifurcation in both submodels is that reducing $\mathcal{R}_0$ below unity is necessary but not sufficient for disease elimination. For the dengue submodel, low vaccine efficacy ϕ_d combined with vector abundance ξ below a critical threshold are the primary drivers of $a > 0$; sufficiently high vector abundance instead pushes the system toward a forward bifurcation. For the Zika submodel, the interplay between direct human to human transmission (β_{z1}) and vector borne transmission determines the sign of a; notably, this interaction is unique to Zika owing to its dual transmission routes and has no analogue in the dengue only submodel. In both cases, $b_{\text{bif}} > 0$ is guaranteed, confirming that the direction of bifurcation is determined entirely by the sign of a.

4. Data calibration

Bridging the gap between the analytical properties of a mathematical model and its behaviour under realistic conditions requires carefully designed numerical experiments. To this end, we simulate the full dengue–Zika co-infection system (3) using parameter values grounded in the epidemiological literature alongside estimates obtained through direct calibration against surveillance data from Espírito Santo state, Brazil [42]. The simulations serve a dual purpose: they validate the theoretical findings established in the preceding sections and illuminate the practical implications of co-circulation of dengue and Zika viruses in a population already bearing a substantial arboviral burden.

All numerical computations are carried out in Python, making use of `NumPy` for array operations, `SciPy` for numerical integration and optimization, and `Matplotlib` for figure production. The ODE system is integrated using the `odeint` solver from `SciPy`'s integration module, which employs the LSODA algorithm with automatic stiffness detection, a feature particularly valuable given the wide disparity in time scales across the sixteen model compartments.

4.1. Data fitting and parameter estimation

Epidemiological surveillance data for both dengue fever and Zika virus disease were obtained from the Notifiable Diseases Information System (SINAN) of the Brazilian Ministry of Health, covering Espírito Santo state across a thirty-six-week window spanning January 1 to September 5, 2021 (epidemiological weeks 1 to 36). The period encompasses the full annual dengue transmission season, characterized by an ascending phase driven by the onset of the wet season, a mid-year epidemic peak, and a subsequent decline, together with the continuing low-level endemic Zika transmission that has persisted in the region since the close of the 2015 to 2016 outbreak. Weekly case counts for both diseases are reported in Table 3. The fitted initial conditions and observation/reporting parameters are listed in Table 5.

Because surveillance data inevitably reflect only a fraction of true incident infections, the model is linked to observations through disease-specific case ascertainment parameters, κ_d and κ_z, such that reported cases equal κ multiplied by model-predicted new infections in the corresponding week. The ascertainment framework is standard in the dengue literature: Brazilian surveillance studies have consistently documented that SINAN captures only a small proportion of true dengue infections, particularly outside epidemic peaks and during periods when the health system faces competing pressures [63, 64]. The 2021 observation window coincided with ongoing COVID-19 response demands on primary-care infrastructure, which is well documented to have further suppressed arboviral case detection in Brazil.

The parameter estimation procedure employs the Trust Region Reflective (TRF) algorithm, accessed through `SciPy`'s `least_squares` function, which is well-suited to the bounded optimization problem that arises here: biological and epidemiological constraints impose natural lower and upper limits on all estimated quantities, and unconstrained optimization routinely yields physically implausible solutions in high dimensional compartmental models. The objective function minimizes the sum of normalized squared residuals across both diseases simultaneously, with each disease residual weighted by its observed mean case count to prevent the larger magnitude dengue series from dominating the Zika contribution. An eight point multi-start strategy is adopted, drawing initial parameter vectors from distinct regions of the feasible space, to reduce the risk of convergence to local minima and to provide informal evidence that the reported solution is globally competitive.

Prior to the main optimization, a warm-up integration of two weeks is performed, that is, the model is integrated from the estimated initial conditions for a short period before the first observed week. This phase-alignment step accounts for the fact that the epidemic in Espírito Santo was already established and progressing when systematic reporting began on 3 January 2021; without it, the model is forced to reconcile an artificially quiescent starting state with already-elevated observed counts, biasing the transmission parameters.

Nine transmission parameters are estimated by fitting: the mosquito biting rate (b), the vector-to-host and host-to-vector transmission probabilities ($\beta_d, \beta_{z1}, \beta_{z2}, \beta_{z3}, \beta_{vd1}, \beta_{vd2}, \beta_{vz1}, \beta_{vz2}$), together with the initial conditions for the human and mosquito infectious compartments and the two ascertainment fractions κ_d and κ_z. The remaining parameters; demographic rates, progression rates, recovery rates, mortality rates, immunity parameters, and vaccination coverage are fixed at values drawn from the literature and are summarized together with the fitted estimates in Table 4. The mosquito recruitment rate Λ_v is fixed rather than estimated, set to imply a steady-state mosquito-to-human ratio of $2:1$ consistent with field entomological surveys in dengue-endemic coastal Brazil [45, 46]; this resolves a structural non-identifiability that would otherwise allow Λ_v, β_d, and the initial infected mosquito fraction to compensate for one another without any single parameter being individually constrained by the data.

The fitted and fixed parameter values are presented in Ta-

ble 4. Regarding model goodness of fit, the Zika series yields a Pearson correlation coefficient of $r = 0.739$, RMSE = 5.2, and MAE = 3.9 cases per week, indicating that the smooth epidemic arc produced by the deterministic model captures the gradual decline in Zika transmission across the study period well. For dengue, the corresponding metrics are $r = 0.594$, RMSE = 108.1, and MAE = 93.5 cases per week. The dengue series displays pronounced week-to-week variability, a coefficient of variation exceeding 30%, that is not mechanistically attributable to the model structure: it reflects a combination of stochastic incidence fluctuations, reporting artefacts such as batched notification on return from public holidays, and the inherent noisiness of passive surveillance systems operating at weekly resolution. The deterministic ODE framework produces a smooth epidemic trajectory that correctly identifies the rising phase, the mid-year epidemic peak at week 24 (week ending 13 June 2021, 566 cases), and the subsequent decline toward the end of the surveillance window, the epidemiologically meaningful features of the epidemic arc. The discrepancy between the smooth model output and the jagged observed series is therefore a consequence of the irreducible gap between deterministic mean-field dynamics and stochastic individual-level transmission events, rather than a failure of the parameter estimation. This interpretation is consistent with the established performance of compartmental ODE models in the dengue modelling literature, where similar fit qualities are routinely reported and accepted when the model captures the epidemic trend and peak timing accurately [23, 25].

The fitted transmission parameters are biologically plausible. The biting rate $b = 1.278$ per week (0.18 per day) falls within the empirical range documented by Brady *et al.* [47]. The dengue vector-to-human transmission probability $\beta_d = 0.749$ sits at the upper end of the range reported by Garba *et al.* [25] and Chitnis *et al.* [57], consistent with the high dengue transmission intensity observed in coastal Espírito Santo. The direct Zika transmission rate $\beta_{z1} = 0.0047$ week^{-1} is small, in line with multiple modelling studies that assign a minor role to sexual transmission in the overall Zika epidemic trajectory [29–31]. The dengue case ascertainment fraction $\kappa_d = 1.7\%$ is somewhat below the 5-8% reported in Brazilian surveillance analyses [63, 64], a difference we attribute to the documented reduction in arboviral surveillance capacity during the COVID-19 pandemic in Brazil. The Zika ascertainment fraction $\kappa_z = 5.0\%$ is consistent with the post-epidemic context of 2021, in which only the most clinically apparent Zika cases (that is, neurological presentations or laboratory-confirmed infections) would typically be reported, while the far larger pool of mild and asymptomatic infections remains invisible to passive surveillance [9, 65].

The fitted results, together with the temporal comparison between model output and observed weekly case counts for both diseases, are displayed in Figure 3. The fitted parameter set forms the basis for all subsequent numerical experiments presented in the subsequent sections.

4.2. Sensitivity analysis

To identify the parameters that most strongly govern the transmission potential of the dengue–Zika co-infection model, we compute the normalised forward sensitivity indices of the basic reproduction numbers $\mathcal{R}_{0d}$, $\mathcal{R}_{0z}$, and $\mathcal{R}_0$ with respect to each model parameter. For a scalar quantity $\mathcal{R}$ that depends differentiably on a parameter p, the normalised sensitivity index is defined as

$$\Upsilon_p^{\mathcal{R}} = \frac{\partial \mathcal{R}}{\partial p} \times \frac{p}{\mathcal{R}}. \tag{31}$$

A positive (negative) value indicates that increasing p amplifies (suppresses) epidemic potential. The indices for the dengue and Zika sub-systems are reported in Table 6 and illustrated in Figure 4. These indices were computed analytically from the corrected closed-form expressions for $\mathcal{R}_{0d}$ and $\mathcal{R}_{0z}$ that incorporate the equilibrium vector-to-host ratio ξ, and evaluated at the fitted baseline parameter set in Table 4.

4.2.1. Dengue sub-system

The mosquito biting rate b carries a sensitivity index of exactly +1.0 with respect to $\mathcal{R}_{0d}$, confirming that it exerts a direct, proportional influence on the dengue reproduction number. Any fractional change in b produces an identical fractional change in $\mathcal{R}_{0d}$. The dengue vector-to-human and human-to-vector transmission probabilities, β_d and β_{vd1}, each return an index of exactly +0.5. This symmetric result is a structural consequence of both parameters entering $\mathcal{R}_{0d}$ under a square root.

The dominant suppressive parameter is the natural mosquito mortality rate μ_v, with an index of exactly −1.0. This stronger effect arises because μ_v enters $\mathcal{R}_{0d}$ both directly in the denominator and indirectly through the equilibrium vector-to-host ratio $\xi = \Lambda_v \mu_h / (\Lambda_h \mu_v)$. Algebraically, $\mathcal{R}_{0d}^2 \propto 1/\mu_v^2$, so $\mathcal{R}_{0d} \propto 1/\mu_v$, giving an elasticity of −1. This makes μ_v the single most consequential lever on dengue transmission potential: doubling mosquito mortality (halving average adult lifespan) is predicted to halve $\mathcal{R}_{0d}$, all else equal. Interventions such as residual insecticide spraying, larval source reduction, and lethal ovitraps are therefore high-yield strategies.

The dengue treatment-seeking rate τ_1 has an index of −0.4992, near −0.5, indicating that prompt clinical presentation substantially curtails the effective infectious period and reduces secondary cases. The natural human mortality rate μ_h carries a non-trivial index of +0.4996, arising primarily through its role in ξ; however, because μ_h operates on a demographic timescale far slower than epidemic dynamics, this sensitivity is primarily a modelling artefact rather than a practical intervention lever. The remaining parameters (θ_d, δ_d) exert negligible influence at the fitted baseline.

4.2.2. Zika sub-system

The biting rate b again dominates, with $\Upsilon_b^{\mathcal{R}_{0z}} = +0.9917$. The slight departure from unity reflects the small contribution of direct sexual transmission (β_{z1}, index +0.0083). The vector-to-human and human-to-vector transmission probabilities (β_{z2}, β_{vz1}) each have indices of +0.4958, while the natural mosquito mortality rate μ_v has an index of −0.9917, again reflecting its

dual role in the expression and through ξ. The Zika treatment-seeking rate τ_2 (−0.5034) is also substantial. The remaining parameters exert negligible influence. The natural human mortality rate μ_h carries a non-trivial index of +0.4952, arising primarily through its role in ξ; however, because μ_h operates on a demographic timescale far slower than epidemic dynamics, this sensitivity is primarily a modelling artefact rather than a practical intervention lever.

4.2.3. Cross-cutting implications

The sensitivity results reveal a clear intervention hierarchy. The biting rate b and mosquito mortality μ_v are the dominant levers for both diseases, underscoring the primacy of integrated vector management. Treatment-seeking rates τ_1 and τ_2 provide substantial, independent mitigation of comparable magnitude. These findings support combined strategies that simultaneously reduce vector-human contact, shorten mosquito lifespan, and improve healthcare access in co-endemic settings.

Note that the human and vector recruitment rates Λ_h and Λ_v do not appear in the sensitivity Table 6. This occurs because the reproduction numbers are homogeneous of degree zero with respect to these parameters when evaluated at the disease-free equilibrium; only their ratio ξ matters.

5. Numerical simulation

The results and discussion presented in this section explore the dynamic behaviour of the dengue-Zika co-infection model under systematic variation of the key epidemiological and intervention parameters identified by the sensitivity analysis. For each parameter, three compartments are examined concurrently: the dengue-only infectious class I_d, the Zika-only infectious class I_z, and the dengue–Zika co-infectious class I_{dz}, enabling a unified assessment of how changes in a single parameter propagate across both disease sub-systems and into the co-infection burden. All simulations are initialized with the fitted parameter values reported in Table 4.

Figures 5 and 6 illustrate the effect of varying the mosquito biting rate $b \in \{1.3, 1.5, 1.7, 1.9\}$ bites per week on the dengue-only infectious population I_d (Figure 5(a)), the Zika-only infectious population I_z (Figure 5(b)), and the dengue-Zika co-infectious population I_{dz} (Figure 6). Since the normalised sensitivity index of b with respect to both $\mathcal{R}_{0d}$ and $\mathcal{R}_{0z}$ equals unity, a given proportional increase in b produces an identical proportional increase in both basic reproduction numbers, making the biting rate the single most influential parameter in the entire model.

Figure 5(a) demonstrates that increasing b from 1.3 to 1.9 dramatically amplifies the dengue epidemic: the infectious peak rises from approximately 1.0×10^5 to 3.5×10^5 individuals, representing a 3.5-fold increase, while the peak timing advances from around week 25 to week 20. This acceleration reflects the compression of the generation time; a higher biting rate shortens the interval between successive transmission events, allowing the epidemic to exhaust the susceptible pool more rapidly.

Figure 5(b) reveals a qualitatively different response for Zika. At lower biting rates ($b = 1.3$ and $b = 1.5$), the Zika infectious class exhibits a complete epidemic arc with a clear peak and subsequent decline within the 36-week observation window. However, at $b = 1.7$ and $b = 1.9$, I_z continues to rise throughout the simulation period, with the $b = 1.9$ trajectory approaching 2,100 individuals at week 36 without having peaked. This disparity arises from the substantially smaller initial infectious seed for Zika ($I_{z0} = 14$ individuals) relative to dengue ($I_{d0} = 1{,}975$), which imposes a longer build-up phase before Zika reaches epidemic momentum. The result underscores the importance of early surveillance and intervention for Zika in the presence of high vector biting activity, since the infection may appear deceptively stable before experiencing rapid exponential growth.

Figure 6 shows the co-infectious compartment I_{dz}, driven by the simultaneous circulation of both pathogens. The co-infection burden grows nonlinearly with b: at $b = 1.3$, peak co-infection barely exceeds 50 individuals, whereas at $b = 1.9$, the peak approaches 700 individuals; a more than tenfold increase for a 46% rise in biting rate. This super-linear amplification reflects the multiplicative nature of co-infection acquisition: the probability that a dengue-infected individual also encounters sufficient Zika force of infection scales with the square of b, mediated by the ADE enhancement term ε_1. Collectively, Figures 5 and 6 establish that vector control interventions targeting the biting rate (such as insecticide application, personal protective equipment, and larval source reduction) simultaneously suppress dengue, Zika, and co-infection burden, and should be prioritized as the cornerstone of integrated arboviral control.

Figure 7 demonstrates the effect of varying $\beta_d \in \{0.2, 0.45, 0.70, 0.95\}$. Figure 7(a) shows a pronounced monotonic increase in the dengue infectious peak: at $\beta_d = 0.2$, the trajectory remains near-flat throughout the 36-week window, reflecting a regime close to or below the epidemic threshold $\mathcal{R}_{0d} = 1$. At $\beta_d = 0.95$, the epidemic peak rises to approximately 1.2×10^6, nearly an order of magnitude above the baseline. Crucially, at higher β_d values the epidemic has not yet reached its peak by week 36, indicating that the observation window underestimates the eventual epidemic burden when transmission probability is high. Figure 7(b) shows that dengue–Zika co-infection tracks the dengue trajectory closely, with I_{dz} remaining negligible at low β_d and rising to approximately 20 individuals at peak when $\beta_d = 0.95$. This coupling confirms that dengue transmission intensity is a key upstream driver of co-infection risk, since a larger I_d pool increases the rate at which dengue-infected individuals are exposed to Zika through the ADE pathway $\varepsilon_1 \lambda_z I_d$.

Figure 8 presents analogous results for $\beta_{z2} \in \{0.16, 0.26, 0.36, 0.46\}$ as Figure 7. Figure 8(a) shows that the Zika infectious class is highly sensitive to β_{z2}, with the epidemic remaining essentially flat at $\beta_{z2} = 0.16$ while reaching 2.5×10^5 at $\beta_{z2} = 0.46$ by week 35. Unlike dengue, none of the Zika trajectories complete a full epidemic arc within 36 weeks, echoing the delayed-peak behaviour observed in Figure 5(b) and confirming that Zika dynamics operate on a longer timescale in this population. Figure 8(b) reveals a more striking result for co-infection: at $\beta_{z2} = 0.46$, I_{dz} grows explosively after week 25, approaching 7,000 individuals without any sign

of abatement. This accelerating co-infection burden arises because a larger I_{vz} pool simultaneously increases the Zika force of infection on both susceptible and dengue-infected humans, with the latter subject to the ADE amplification ε_2. The result has an important public health implication: even modest increases in Zika vector competence can trigger disproportionate co-infection surges, suggesting that Zika-specific vector control should not be ignored in dengue-endemic settings.

Figures 9 and 10 investigate the impact of the dengue treatment-seeking rate τ_1 (Figures 9 and 10(a)) and the Zika treatment-seeking rate τ_2 (Figure 10(b)) on the infectious and co-infectious population dynamics. Both parameters carry near-symmetric sensitivity indices of approximately −0.5 with respect to their respective reproduction numbers, identifying prompt clinical care as one of the two most powerful suppressive levers in the model alongside mosquito mortality.

Figure 9(a) shows a dramatic dependence of the dengue infectious population on $\tau_1 \in \{0.2, 0.4, 0.6, 0.8\}$. At $\tau_1 = 0.2$ (representing a scenario where only 20% of dengue-infected individuals seek care within the first week) the infectious peak approaches 8×10^5, with the epidemic persisting well beyond week 35. In stark contrast, at $\tau_1 = 0.8$, the peak is suppressed by over 95%, falling below 5×10^4, and the epidemic arc completes substantially earlier. This result is mechanistically intuitive: higher treatment-seeking rates shorten the effective infectious period by diverting individuals from I_d into the treated compartment T_d, thereby reducing the per-capita contribution to the dengue force of infection. The practical implication is that strengthening healthcare access and reducing diagnostic delays through community health workers, point-of-care testing, and subsidized treatment can achieve epidemic suppression of the same order of magnitude as intensive vector control.

Figure 9(b) demonstrates a complementary indirect effect of τ_1 on the Zika infectious class. Although τ_1 appears in the dengue sub-system only, its indirect effect on I_z is clearly visible: higher τ_1 suppresses I_d, which reduces the dengue force of infection acting on Zika-infected individuals through the ADE term $\varepsilon_2 \lambda_d I_z$, thereby slowing the depletion of I_z into the co-infection pathway. Consequently, at high τ_1 the Zika curves decline more gradually, as fewer co-infection events remove individuals from I_z. This cross-disease interaction illustrates the epidemiological coupling unique to co-infection models and would be invisible in single-disease models.

Figure 10(a) shows that dengue treatment-seeking directly suppresses co-infection: at $\tau_1 = 0.8$, I_{dz} remains below 15 individuals throughout, whereas at $\tau_1 = 0.2$, the co-infected class peaks near 65 and declines slowly, sustaining co-infection burden across the full 36-week window. This is a direct consequence of the model structure: a larger I_d pool under low τ_1 provides more individuals susceptible to secondary Zika infection via the ε_1 pathway.

Figure 10(b) presents the effect of Zika treatment-seeking rate $\tau_2 \in \{0.2, 0.35, 0.5, 0.7\}$ on dengue-Zika co-infectious population. At $\tau_2 = 0.2$, I_{dz} increases monotonically throughout the observation window without reaching a peak, projecting continued co-infection accumulation beyond week 36. As τ_2 increases to 0.7, the co-infection trajectory progressively flattens and reverses earlier. The mechanism is analogous to that described for τ_1: rapid removal of Zika-infected individuals into treatment reduces the Zika force of infection acting on dengue-infected individuals, interrupting the principal pathway to co-infection. Together, Figure 10(a) and Figure 10(b) demonstrate that prompt treatment of either disease individually delivers cross-protective benefits against co-infection; a synergistic public health dividend that justifies the simultaneous strengthening of both dengue and Zika clinical management capacity.

Figures 11 and 12 present the effects of the Zika treatment-seeking rate τ_2 on the Zika infectious population (Figure 11(a)) and the effects of the natural mosquito mortality rate μ_v across all three infectious classes: Zika (Figure 11(b)), dengue and dengue–Zika co-infection (Figure 12).

Figure 11(a) confirms the direct suppressive effect of $\tau_2 \in \{0.2, 0.35, 0.5, 0.7\}$ on the Zika infectious compartment I_z, consistent with the sensitivity index $\Upsilon_{\tau_2}^{\mathcal{R}_{0z}} = -0.500$. At $\tau_2 = 0.2$, the Zika infectious population rises steeply, exceeding 2,000 individuals by week 36 without having peaked, indicative of a growing epidemic under insufficient clinical management. Increasing τ_2 progressively flattens and peaks the curve earlier: at $\tau_2 = 0.5$ and 0.7, I_z peaks before week 10 and declines smoothly, consistent with controlled endemic transmission. Since approximately 80% of Zika infections are mild or asymptomatic [10], achieving high treatment-seeking rates requires active surveillance and syndromic screening rather than passive case detection alone.

Figures 11(b) and 12 collectively demonstrate the profound and uniform impact of mosquito mortality $\mu_v \in \{0.25, 0.50, 0.75, 1.0\}$ per week; equivalent to adult *Aedes aegypti* lifespans of 4, 2, 1.33, and 1 week respectively [47], across all infectious classes. The results are strikingly consistent: at $\mu_v = 0.25$ (4-week lifespan, representing minimal vector control), the Zika, dengue, and co-infection curves all rise sharply and remain elevated or still growing at week 36. At $\mu_v = 0.5$ (the fitted baseline), the trajectories are substantially suppressed. At $\mu_v = 0.75$ and 1.0, all three infectious classes are effectively suppressed to near-zero, with peak values orders of magnitude below those at $\mu_v = 0.25$.

The dengue infectious peak under $\mu_v = 0.25$ reaches approximately 6×10^5 (Figure 12(a)), while under $\mu_v = 1.0$ it remains below 5×10^3, a 120-fold reduction. Co-infection (Figure 12(b)) shows a corresponding peak near 2,500 at $\mu_v = 0.25$, collapsing to negligible levels at higher mortality rates. These results align with the sensitivity index $\Upsilon_{\mu_v}^{\mathcal{R}_0} = -1.00$ for both sub-systems, confirming that every doubling of mosquito mortality rate halves the basic reproduction number. From an intervention standpoint, the data strongly support residual indoor spraying, lethal ovitraps, and biological control agents such as *Wolbachia*-infected mosquitoes as high-priority tools, since these approaches reduce adult mosquito survival and can achieve the mortality rates corresponding to effective epidemic suppression depicted in Figures 11(b) and 12.

Figure 13 addresses the antibody-dependent enhancement (ADE) mechanism governing co-infection severity, it shows the effect of the ADE susceptibility multiplier $\varepsilon_1 \in \{1.0, 1.5, 2.0, 2.5\}$ on the dengue–Zika co-infected compart-

ment I_{dz} and the co-infection treated compartment T_{dz} respectively. Figure 13(a) demonstrates a consistent and monotonic increase in co-infection burden with ε_1: at $\varepsilon_1 = 1.0$, representing the null ADE hypothesis where prior dengue infection confers no additional Zika susceptibility, I_{dz} peaks near 9 individuals and declines rapidly. As ε_1 increases to 2.5, the peak rises to approximately 13 individuals and the post-peak decline slows, prolonging the period of elevated co-infection risk. Interestingly, the differences between curves are modest in absolute terms (all four trajectories remain below 15 individuals) but the pattern is consistent and statistically coherent with the ADE literature, which documents enhanced Zika susceptibility in dengue-immune individuals through cross-reactive antibody-mediated mechanisms [1].

Figure 13(b) mirrors 13(a) for the co-infection treated class T_{dz}, confirming that the ADE effect propagates through the full co-infection pathway $E_{dz} \rightarrow I_{dz} \rightarrow T_{dz}$. The treated compartment provides a proxy for clinical co-infection cases presenting to healthcare facilities, and its monotonic increase with ε_1 implies that hospitals in dengue-endemic areas should anticipate proportionally more co-infection presentations during Zika outbreaks in populations with high prior dengue seroprevalence.

Figure 14 presents the long-term effect of dengue vaccine efficacy (156-week) $\phi_d \in \{0.0, 0.3, 0.6, 0.9\}$ on the dengue infectious population I_d and the dengue recovered population R_d. In Figure 14(a), the vaccine efficacy curves converge during the initial epidemic phase (weeks 0–30), separating progressively over the subsequent two years as the vaccinated cohort accumulates. By week 156, the $\phi_d = 0.9$ scenario sustains the lowest I_d level, approximately 20% below the no-vaccine baseline. The convergence during the early phase is mechanistically explained by the slow accumulation of V_d: vaccine eligibility requires prior dengue recovery (the $R_d \rightarrow V_d$ pathway through $\rho \cdot \alpha_d$), and only 10% of recovered individuals enter the vaccinated class per waning cycle, so meaningful vaccine-mediated protection builds gradually over many months.

Figure 14 shows that vaccine efficacy has a surprisingly modest effect on the dengue recovered population over the 3-year horizon, with all four curves following nearly identical trajectories. This reflects the fact that R_d is populated primarily by individuals recovering from natural infection through treatment ($T_d \rightarrow R_d$), a pathway unaffected by ϕ_d. The near-indistinguishable R_d curves confirm that the vaccine acts by reducing breakthrough infections in vaccinated individuals rather than by diverting the bulk of the epidemic flow. The key clinical implication is that dengue vaccination in this model is a supplementary rather than replacement strategy: it provides incremental long-term protection but does not substitute for vector control or treatment-seeking interventions that act on the primary transmission pathway.

Figures 15 and 16 examine the effect of vaccine efficacy ϕ_d on the dengue vaccinated population V_d (Figure 15(a)) and the effect of vaccination coverage fraction $\rho \in \{0.0, 0.3, 0.6, 0.9\}$ on dengue infectious (Figure 15(b)), dengue recovered, and dengue vaccinated (Figure 16) populations over a 156-week horizon.

Figure 15(a) reveals an important and somewhat counterintuitive result: increasing ϕ_d from 0.0 to 0.9 produces only modest differences in the size of the vaccinated population V_d, with all four curves growing nearly linearly and reaching approximately $9–10 \times 10^4$ by week 156. This occurs because V_d is fed by the flow $\rho \cdot \alpha_d \cdot R_d$, which depends on the recovery pool R_d and the fixed coverage parameter $\rho = 0.1$, not on vaccine efficacy directly. Higher ϕ_d reduces breakthrough infections in V_d via the term $(1 - \phi_d)\lambda_d V_d$, marginally slowing depletion of the vaccinated class, but the effect is secondary to the primary driver of V_d accumulation. The figure therefore illustrates that vaccine efficacy and vaccine coverage are operationally distinct: efficacy determines how well each vaccinated individual is protected, while coverage determines how many individuals enter the protected class.

Figures 15(b), and 16 collectively reveal the dominant role of vaccination coverage ρ across a three-year horizon. Figure 15(b) shows that increasing ρ from 0.0 to 0.9 progressively suppresses the dengue infectious population after the initial epidemic peak: while all scenarios share a similar first-wave peak around week 30 (which reflects the slow build-up of V_d described above), subsequent transmission is substantially reduced at higher ρ, with the $\rho = 0.9$ trajectory declining most steeply by year 2. This pattern is consistent with the accumulation of a large vaccinated and cross-protected population that progressively reduces the effective reproduction number below unity.

Figure 16(a) demonstrates that higher ρ elevates the dengue recovered population R_d throughout the simulation, a result that initially appears paradoxical but is mechanistically coherent: at higher ρ, more individuals are diverted into V_d, which reduces breakthrough infections and thus slows the depletion of R_d through the α_d waning term. The long-run R_d curves separate progressively after week 60, suggesting that the population-level immunity advantage of high vaccination coverage compounds over time.

Figure 16(b) confirms that higher ρ generates a substantially larger vaccinated pool V_d, growing from approximately 3×10^5 at $\rho = 0.3$ to 8×10^5 at $\rho = 0.9$ by week 156. The near-linear growth of all four curves indicates that the vaccinated class has not yet saturated within the 3-year window, suggesting that the benefits of high coverage continue to accumulate beyond the simulation period.

Taken together, Figures 14, 15 and 16 demonstrate that expanding vaccination coverage ρ (through programmatic delivery, community outreach, and vaccine subsidy) offers substantially greater population-level impact than improving vaccine efficacy alone within the parameter ranges explored here, and that the full benefit of dengue vaccination programmes may only become apparent on a multi-year timescale [55, 56].

Beyond individual sensitivity analyses and time-series simulations, we examined how the basic reproduction numbers for dengue and Zika ($\mathcal{R}_{0d}$ and $\mathcal{R}_{0z}$) depend jointly on pairs of highly sensitive parameters. Surface and contour plots (Figures 17–21) illustrate $\mathcal{R}_0$ variation across realistic parameter ranges, highlighting threshold behaviour ($\mathcal{R}_0 = 1$), non-linear interactions, and key leverage points for intervention.

The dependence of $\mathcal{R}_{0d}$ on biting rate (b) and dengue vector-to-human transmission probability (β_d) is strong and near-linear, with the highest values clustered at the upper bounds of both parameters (Figure 17). Notably, the contour plot reveals a hyperbolic boundary for the $\mathcal{R}_{0d} = 1$ threshold: even with a moderately high $\beta_d \approx 0.6$, transmission remains subcritical unless the biting rate exceeds approximately 1.2–1.4 bites per week. This trade-off suggests that partial reductions in both parameters can collectively drive the system below the epidemic threshold. Practically, this offers flexibility in vector control. For instance, by combining bed nets to reduce b with larviciding or spatial repellents to reduce β_d.

The interaction between b and mosquito mortality (μ_v) is markedly non-linear (Figure 18). $\mathcal{R}_{0d}$ rises steeply when mosquito mortality is low ($\mu_v \lesssim 0.4$–0.6 week^{-1}, or adult lifespans > 2 weeks), even at moderate biting rates. As shown in the contour panel, the $\mathcal{R}_{0d} = 1$ threshold becomes almost vertical at higher biting intensities, indicating that once biting is elevated, only substantial increases in mosquito mortality (e.g., $\mu_v \gtrsim 1.0$–1.2 week^{-1}) can return the system to subcritical conditions. Such a pattern reinforces the priority of adulticide-based interventions in high-transmission settings. In such settings, suppressing vector survival yields disproportionately large reductions in epidemic potential.

We also observe a complex interaction between intrinsic transmission (β_d) and clinical intervention (τ_1) in Figure 19. At low treatment-seeking rates ($\tau_1 \lesssim 0.3$), $\mathcal{R}_{0d}$ scales sharply with β_d and remains supercritical across most of the parameter range. However, when $\tau_1 \gtrsim 0.6$–0.7, the $\mathcal{R}_{0d} = 1$ threshold shifts rightward, allowing transmission to stay subcritical even at β_d values as high as 0.7–0.8. This result quantifies the impact of prompt treatment: increasing care-seeking uptake from 20–30% to 60–80% can offset high vector competence. In resource-limited settings where vector reduction is difficult, clinical management thus serves as a powerful and independent complementary lever.

Zika reproduction numbers follow similar patterns, though numerical scales differ slightly due to the small direct sexual transmission term in $\mathcal{R}_{0z}$. In Figure 20, the $\mathcal{R}_{0z} = 1$ contour is strongly curved: the hyperbolic boundary confirms that integrated reductions in biting frequency and Zika vector competence can efficiently drive Zika transmission below the epidemic threshold. The lack of curvature near the origin reflects the dominance of the vector-borne pathway in the 2021 Espírito Santo context, where direct sexual transmission contributes negligibly to $\mathcal{R}_{0z}$ (sensitivity index $\Upsilon^{\mathcal{R}_{0z}}_{\beta_{z1}} \approx 0.008$) and the dynamics are governed almost entirely by b and β_{z2}.

The interaction between treatment-seeking (τ_2) and mosquito mortality (μ_v) for the Zika sub-system is shown in Figure 21. At low mosquito mortality ($\mu_v \lesssim 0.4$ week^{-1}), even aggressive treatment-seeking ($\tau_2 \approx 0.9$) is insufficient to suppress Zika transmission. Conversely, at $\mu_v \gtrsim 0.8$–1.0 week^{-1}, a modest $\tau_2 \approx 0.4$–0.5 is sufficient for control. This asymmetry underscores that while clinical management is a strong supporting intervention, vector survival remains the primary target for Zika control, and treatment-seeking should be viewed as complementary rather than substitutive.

The full model basic reproduction number $\mathcal{R}_0 = \rho(FV^{-1})$, evaluated as the spectral radius of the complete 8×8 next-generation matrix, is shown in Figure 22 over the same (b, β_d) parameter space as Figure 17. Comparing the two surfaces reveals that the full-model $\mathcal{R}_0$ generally exceeds $\mathcal{R}_{0d}$, consistent with the theoretical bound $\mathcal{R}_0 \geq \max\{\mathcal{R}_{0d}, \mathcal{R}_{0z}\}$, with equality only when the linear cross-infection parameters β_{z3}, β_{vd2}, β_{vz2} are zero. The upward displacement of the full-model surface above the dengue-only surface quantifies the additional epidemic potential introduced by co-infection pathways. This confirms that analyses based on single-disease reproduction numbers alone can systematically underestimate the epidemic risk in a co-circulation setting. The $\mathcal{R}_0 = 1$ threshold contour in Figure 22(b) lies at lower (b, β_d) values than in Figure 17(b), implying that more stringent combined interventions are required to achieve control when both pathogens co-circulate than would be predicted from dengue-only modelling.

Collectively, these joint sensitivity surfaces confirm a clear intervention hierarchy: parameters governing vector-human contact (b, β_d, β_{z2}) and vector survival (μ_v) exert the strongest influence on transmission potential for both diseases. Treatment-seeking rates (τ_1, τ_2) provide significant and independent mitigation, but cannot substitute for vector control when mosquito mortality is low. The pronounced threshold behaviour across all six plots suggests that reaching specific intervention targets can "tip" the system from an epidemic state to controlled endemicity, a finding with direct implications for the design of integrated dengue–Zika control programmes in arboviral co-endemic settings such as Espírito Santo, Brazil.

6. Conclusion

This study presented a new deterministic compartmental model for the co-transmission dynamics of dengue fever and Zika virus disease, incorporating sixteen state variables across thirteen human epidemiological classes and three vector classes. The model is novel in simultaneously representing six mechanistic features absent from any single prior framework: ADE of secondary infection through multipliers ε_1 and ε_2; synergistic co-infection mortality through ε_3; partial and asymmetric cross-immunity through η_d and η_z; dual transmission routes for Zika (vector-borne and direct sexual); a post-recovery dengue vaccination pathway; and calibration against confirmed co-endemic surveillance data with simultaneous dengue and Zika reporting. The model was calibrated against thirty-six weeks of SINAN surveillance data from Espírito Santo state, Brazil (January–September 2021), yielding biologically plausible parameter estimates and goodness-of-fit metrics ($r = 0.739$ for Zika, $r = 0.594$ for dengue) consistent with the established performance of deterministic ODE frameworks applied to passive surveillance data.

The analytical investigation established that the model is epidemiologically well-posed: all solutions initiating in the biologically feasible region $D = D_h \times D_v \subset \mathbb{R}^{16}_+$ remain non-negative and bounded for all $t > 0$, and the region is positively invariant and attracting. The disease-free equilibrium (DFE)

was derived in closed form and shown to be locally asymptotically stable when $\mathcal{R}_0 < 1$ and unstable when $\mathcal{R}_0 > 1$, by the next-generation operator method of van den Driessche and Watmough [40]. The component reproduction numbers $\mathcal{R}_{0d}$ and $\mathcal{R}_{0z}$ were derived analytically from the decoupled sub-systems, revealing structurally distinct formulae: $\mathcal{R}_{0d}$ takes the standard square-root vector-borne form, while $\mathcal{R}_{0z}$ contains an additive sexual transmission term whose interaction with the vector-borne cycle produces a quadratic correction that elevates the Zika threshold above the purely vector-borne baseline whenever β_{z1} is non-negligible. The full model reproduction number $\mathcal{R}_0 = \rho(FV^{-1})$ satisfies $\mathcal{R}_0 \geq \max\{\mathcal{R}_{0d}, \mathcal{R}_{0z}\}$, with equality only when the linear cross-infection parameters β_{z3}, β_{vd2}, β_{vz2} are zero. This confirms that co-infection pathways introduce additional transmission potential that is systematically missed by single-disease analyses. Uniform persistence of infection and the existence of at least one endemic equilibrium whenever $\mathcal{R}_0 > 1$ were established through a persistence-theoretic argument invoking the repelling property of the unstable DFE and the compactness of the global attractor.

Backward bifurcation analysis via the centre manifold theorem revealed that both the dengue-only and Zika-only sub-models can exhibit a backward bifurcation at their respective epidemic thresholds. For the dengue sub-system, the bifurcation coefficient $a > 0$ when vaccine efficacy ϕ_d is low and vector abundance ξ is high, while for the Zika sub-system, the sign of a is governed by the interplay between direct human-to-human transmission β_{z1} and the vector-borne cycle; an interaction unique to Zika owing to its dual transmission routes and without analogue in the dengue sub-system. In both cases $b_{\text{bif}} > 0$ is guaranteed, so the direction of bifurcation is determined entirely by the sign of a. The epidemiological consequence is critical: reducing $\mathcal{R}_0$ below unity is necessary but not sufficient for disease elimination when the backward bifurcation condition is met. A stable endemic equilibrium can coexist with the stable DFE for $\mathcal{R}_0 < 1$, creating a hysteresis region in which gradual relaxation of interventions near the epidemic threshold can trigger a sudden resurgence to high endemic prevalence. This finding provides a theoretical basis for the observation that dengue and Zika outbreaks can re-emerge rapidly in settings where control efforts are prematurely withdrawn.

The normalised forward sensitivity analysis identified a clear and consistent hierarchy of intervention leverage across both diseases. The mosquito biting rate b carries the highest sensitivity index ($\Upsilon_b^{\mathcal{R}_{0d}} = +1.0$; $\Upsilon_b^{\mathcal{R}_{0z}} = +0.9917$), confirming that a proportional reduction in biting frequency produces an identical proportional reduction in epidemic potential for both pathogens simultaneously. The vector-to-human and human-to-vector transmission probabilities (β_d, β_{vd1}, β_{z2}, β_{vz1}) each carry indices of approximately +0.5, reflecting the square-root structure of the vector-borne transmission cycle. The natural mosquito mortality rate μ_v carries an index of −1.0 for dengue and −0.9917 for Zika, confirming that it is one of the most powerful levers: doubling mosquito mortality is predicted to approximately halve both reproduction numbers. The treatment-seeking rates τ_1 and τ_2 carry near-symmetric indices of approximately −0.5, establishing prompt clinical care as an intervention lever of equal strength to vector mortality reduction. Crucially, the direct Zika sexual transmission parameter β_{z1} carries a small but non-negligible index of +0.0083, confirming that in the 2021 Espírito Santo context, Zika dynamics were overwhelmingly vector-borne, though the sexual route is not entirely negligible.

The numerical simulations confirmed and extended these analytical findings. The superlinear amplification of co-infection burden with increasing biting rate (a tenfold rise in peak I_{dz} for a 46% increase in b) reflects the multiplicative nature of co-infection acquisition and demonstrates that vector control simultaneously suppresses both individual diseases and their joint burden. The cross-disease coupling mediated by ADE produced an indirect but epidemiologically significant effect: dengue treatment τ_1 suppressed not only dengue but also Zika co-infection, and Zika treatment τ_2 reduced dengue co-infection risk, providing a synergistic dividend that would be invisible in single-disease models. The 120-fold suppression of peak dengue incidence when μ_v increases from 0.25 to 1.0 week^{-1} quantifies the dominant role of adult mosquito lifespan reduction across all three infectious classes simultaneously. Vaccine simulations over a 156-week horizon demonstrated that vaccination coverage ρ drives long-term epidemic suppression more powerfully than vaccine efficacy ϕ_d alone within the ranges explored, and that the full population-level benefit of vaccination accumulates on a multi-year timescale through the slow $R_d \rightarrow V_d$ accumulation pathway. The joint surface and contour analysis of $\mathcal{R}_0$ further confirmed that single-disease modelling can systematically underestimate the epidemic threshold: the full-model $\mathcal{R}_0 = \rho(FV^{-1})$ surface generally lies above the dengue-only surface across the entire (b, β_d) parameter space, and the $\mathcal{R}_0 = 1$ threshold contour is displaced to lower (b, β_d) values, implying that more stringent combined interventions are required to achieve control under co-circulation than would be predicted from isolated single-pathogen analyses.

6.1. Biological significance

The results of this study carry several direct biological implications. First, the bound $\mathcal{R}_0 \geq \max\{\mathcal{R}_{0d}, \mathcal{R}_{0z}\}$ demonstrates mathematically that flavivirus co-circulation is not epidemiologically equivalent to the sum of two independent outbreaks: the cross-infection pathways introduce additional transmission potential that is systematically missed by single-disease analyses. Second, the backward bifurcation result implies that the immune landscape shaped by prior dengue or Zika exposure can maintain endemic transmission even after the reproduction number falls nominally below unity, providing a mechanistic explanation for the persistence of dengue in settings where vaccination programmes have been partially implemented. Third, the model-projected indirect suppression of Zika co-infection by dengue treatment, operating through the ADE coupling parameter ε_1, suggests a biological pathway by which clinical management of one flavivirus may confer population-level benefits against the other in co-endemic settings. This hypothesis warrants empirical investigation in prospective cohort studies.

Taken together, the results of this study establish four principal public health conclusions for arboviral co-endemic settings such as Espírito Santo. First, integrated vector management targeting the mosquito biting rate and adult survival represents the single most cost-efficient strategy. This approach, achievable through larval source reduction, residual indoor spraying, lethal ovitraps, and biological tools such as *Wolbachia*-infected mosquitoes, simultaneously reduces $\mathcal{R}_{0d}$, $\mathcal{R}_{0z}$, and the co-infection burden, while pushing the full system below its more stringent co-circulation epidemic threshold. Second, expanding healthcare access to increase dengue and Zika treatment-seeking rates to the 60–80% range provides epidemic suppression of the same order of magnitude as intensive vector control, and delivers model-projected cross-disease protection through the ADE-mediated coupling between the two sub-systems. This finding is particularly relevant for resource-limited settings where large-scale vector operations are logistically or financially constrained. Third, the backward bifurcation result demands that intervention programmes adopt an aggressive and sustained posture: reducing $\mathcal{R}_0$ below unity is a necessary but not sufficient condition for elimination, and incremental relaxation of control near the threshold risks triggering an abrupt transition from a controlled to a high-endemic state. Fourth, dengue vaccination at the current licensed efficacy ($\phi_d \approx 0.70$) provides meaningful long-term benefit only when combined with high coverage ρ and sustained for multiple transmission seasons; programmes that achieve high efficacy but low coverage, or that are discontinued prematurely, will realise only a fraction of the achievable reduction in population-level dengue burden.

Some limitations of the present study merit acknowledgement. The model assumes homogeneous mixing and time-invariant parameters, abstracting away the seasonal forcing driven by rainfall and temperature that governs *Aedes aegypti* population dynamics in Brazil. The 2021 observation window coincided with ongoing COVID-19 surveillance suppression, which likely depressed reported dengue counts and may have introduced systematic bias into the fitted ascertainment fraction κ_d. Co-infection cases are not directly observable in SINAN and could not be used for calibration, so the ADE parameters ε_1, ε_2, and ε_3 were fixed at literature-derived values rather than estimated from data.

Future work should proceed along several directions. Incorporating seasonal vector recruitment driven by temperature and precipitation data would capture the annual epidemic cycles characteristic of Brazilian dengue epidemiology and enable multi-year forecasting. Extending the surveillance window to capture inter-annual dengue dynamics, including the serotype replacement cycles that drive ADE-mediated severity, would permit estimation of the enhancement parameters directly from data rather than from literature priors. Exploring the model behaviour in the presence of multiple dengue serotypes, whose cross-reactive antibody interactions are the primary immunological driver of severe dengue, represents a natural and important extension [24]. Incorporating asymptomatic and isolation compartments, as developed in recent single-disease frameworks [36–38], would provide more realistic representations of clinical case ascertainment and isolation-based control. Awareness-based transmission models [39] could be integrated to capture the role of community-level behavioural responses to outbreak news in shaping epidemic trajectories. Extensions incorporating transovarial transmission and serotype-specific immunity, as explored in single-disease frameworks [36], represent a further natural direction. Similarly, the recent co-infection framework of Duru *et al.* [66], which models malaria–Zika co-dynamics with vaccination and biological vector control, offers a complementary structural template for extending the present dengue–Zika framework to incorporate additional co-circulating pathogens. Stochastic extensions would more faithfully represent the high week-to-week variability observed in the surveillance data and would permit formal uncertainty quantification of the estimated reproduction numbers. Spatial heterogeneity across municipalities and altitude gradients within Espírito Santo, Brazil could be incorporated through a patch or network model to identify high-risk foci for targeted intervention. Finally, health-economic modelling of the intervention scenarios simulated here would translate the epidemiological findings into cost-effectiveness metrics directly usable by Brazilian public health decision-makers.

In conclusion, this work demonstrates that the simultaneous circulation of dengue and Zika viruses in a shared *Aedes* vector creates an epidemic landscape that is qualitatively and quantitatively more dangerous than either disease in isolation. The co-infection model developed here provides a mathematically rigorous, biologically motivated, and data-calibrated platform for understanding this landscape and for evaluating the comparative effectiveness of vector control, clinical management, and vaccination strategies. The clear intervention hierarchy emerging from the sensitivity, simulation, and bifurcation analyses provides actionable, evidence-based guidance for the design of integrated arboviral control programmes in Brazil and in other tropical regions where dengue and Zika continue to co-circulate.

Data availability

The epidemiological surveillance data used to calibrate this model are publicly available from the Espírito Santo State Health Secretariat (SESA) of the Brazilian Ministry of Health, accessible at: https://www.es.gov.br/Noticia/sesa-divulga-36-boletim-da-dengue--Zika-e-chikungunya. The numerical simulation code used to produce the results in this study is available from the corresponding author upon reasonable request.

Declaration of competing interest

The authors declare that they have no known competing financial interests or personal relationships that could have appeared to influence the work reported in this manuscript.

Funding

This research received no specific grant from any funding agency.

References

[1] W. Dejnirattisai, P. Supasa, W. Wongwiwat, A. Rouvinski, G. Barba-Spaeth, T. Duangchinda, A. Sakuntabhai, V.-M. Cao-Lormeau, P. Malasit, F. A. Rey, J. Mongkolsapaya & G. R. Screaton, "Dengue virus sero-cross-reactivity drives antibody-dependent enhancement of infection with Zika virus," Nat. Immunol. **17** (2016) 1102. https://doi.org/10.1038/ni.3515.

[2] A. Lim, F. M. Shearer, K. Sewalk, D. M. Pigott, J. Clarke, A. Ghouse, C. Judge, H. Kang, J. P. Messina, M. U. G. Kraemer, K. A. M. Gaythorpe, W. M. de Souza, E. O. Nsoesie, M. Celone, N. Faria, S. J. Ryan, I. B. Rabe, D. P. Rojas, S. I. Hay, J. S. Brownstein, N. Golding & O. J. Brady, "The overlapping global distribution of dengue, chikungunya, Zika and yellow fever," Nat. Commun. **16** (2025) 3418. https://doi.org/10.1038/s41467-025-58609-5.

[3] World Health Organization, "Dengue and severe dengue," WHO Fact Sheet, 2025. Available online: https://www.who.int/news-room/fact-sheets/detail/dengue-and-severe-dengue.

[4] N. Haider, M. N. Hasan, J. Onyango & M. Asaduzzaman, "Global landmark: 2023 marks the worst year for dengue cases with millions infected and thousands of deaths reported," IJID Reg. **13** (2024) 100459. https://doi.org/10.1016/j.ijregi.2024.100459.

[5] N. Haider, M. N. Hasan, J. Onyango, M. Billah, S. Khan, D. Papakonstantinou, P. Paudyal & M. Asaduzzaman, "Global dengue epidemic worsens with record 14 million cases and 9000 deaths reported in 2024," Int. J. Infect. Dis. **158** (2025) 107940. https://doi.org/10.1016/j.ijid.2025.107940.

[6] eClinicalMedicine, "Dengue as a growing global health concern," EClinicalMedicine **77** (2024) 102975. https://doi.org/10.1016/j.eclinm.2024.102975.

[7] W. X. Zhang, T. Y. Zhao, C. C. Wang, Y. He, H. Z. Lu, H. T. Zhang, L. M. Wang, M. Zhang, C. X. Li & S. Q. Deng, "Assessing the global dengue burden: incidence, mortality & disability trends over three decades," PLoS Negl. Trop. Dis. **19** (2025) e0012932. https://doi.org/10.1371/journal.pntd.0012932.

[8] Pan American Health Organization / World Health Organization, "Zika: a silent virus requiring enhanced surveillance and control," PAHO/WHO, Washington, DC, Sep. 2023. Available online: https://www.paho.org/en/news/1-9-2023-Zika-silent-virus-requiring-enhanced-surveillance-and-control.

[9] N. R. Faria, R. D. S. S. Azevedo, M. U. G. Kraemer, R. Souza, M. S. Cunha, S. C. Hill, J. Thézé, M. B. Bonsall, T. A. Bowden, I. Rissanen, I. M. Rocco, J. S. Nogueira, A. Y. Maeda, F. G. D. S. Vasami, F. L. L. Macedo, A. Suzuki, S. G. Rodrigues, A. C. R. Cruz, B. T. Nunes, D. B. A. Medeiros, D. S. G. Rodrigues, A. L. N. Queiroz, E. V. P. da Silva, D. F. Henriques, E. S. T. da Rosa, C. S. de Oliveira, L. C. Martins, H. B. Vasconcelos, L. M. N. Casseb, D. B. Simith, J. P. Messina, L. Abade, J. Lourenço, L. C. J. Alcantara, M. M. de Lima, M. Giovanetti, S. I. Hay, R. S. de Oliveira, P. D. S. Lemos, L. F. de Oliveira, C. P. S. de Lima, S. P. da Silva, J. M. de Vasconcelos, L. Franco, J. F. Cardoso, J. L. D. S. G. Vianez-Júnior, D. Mir, G. Bello, E. Delatorre, K. Khan, M. Creatore, G. E. Coelho, W. K. de Oliveira, R. Tesh, O. G. Pybus, M. R. T. Nunes & P. F. C. Vasconcelos, "Zika virus in the Americas: early epidemiological and genetic findings," Science **352** (2016) 345. https://doi.org/10.1126/science.aaf5036.

[10] L. R. Petersen, D. J. Jamieson, A. M. Powers & M. A. Honein, "Zika virus," N. Engl. J. Med. **374** (2016) 1552. https://doi.org/10.1056/NEJMra1602113.

[11] I. B. Rabe, S. L. Hills, J. M. Haussig, A. T. Walker, T. Dos Santos, J. L. San Martin, G. Gutierrez, J. Mendez-Rico, J. C. Rodriguez, D. Elizondo-Lopez, G. Gonzalez-Escobar, E. Chanda, S. M. Al Eryani, C. Kodama, A. Yajima, M. Kakkar, M. Kato, P. R. Wijesinghe, S. Samaraweera, H. Brindle, H. Tissera, J. Kelley, E. Lackritz & D. P. Rojas, "A review of the recent epidemiology of Zika virus infection," Am. J. Trop. Med. Hyg. **112** (2025) 1026. https://doi.org/10.4269/ajtmh.24-0420.

[12] World Health Organization, "Zika epidemiology update – May 2024," WHO Publications, Geneva, Switzerland, 2024. Available online: https://www.who.int/publications/m/item/Zika-epidemiology-update-may-2024.

[13] P. M. Saba Villarroel, R. Hamel, N. Gumpangseth, S. Yainoy, P. Koomhin, D. Missé & S. Wichit, "Global seroprevalence of Zika virus in asymptomatic individuals: a systematic review," PLoS Negl. Trop. Dis. **18** (2024) e0011842. https://doi.org/10.1371/journal.pntd.0011842.

[14] J. M. Pescarini, M. Rodrigues, E. S. Paixão, L. Cardim, C. A. A. de Brito, M. da C. N. Costa, A. C. Santos, L. Smeeth, M. da G. Teixeira, A. P. F. de Souza, M. L. Barreto & E. B. Brickley, "Dengue, Zika & chikungunya viral circulation and hospitalization rates in Brazil from 2014 to 2019: an ecological study," PLoS Negl. Trop. Dis. **16** (2022) e0010602. https://doi.org/10.1371/journal.pntd.0010602.

[15] F. Pinotti, M. Giovanetti, M. M. de Lima, E. M. de Cerqueira, L. C. J. Alcantara, S. Gupta, M. Recker & J. Lourenco, "Shifting patterns of dengue three years after Zika virus emergence in Brazil," Nat. Commun. **15** (2024) 632. https://doi.org/10.1038/s41467-024-44799-x.

[16] J. V. Zambrana, C. M. Hasund, R. A. Aogo, S. Bos, S. Arguello, K. Gonzalez, D. Collado, T. Miranda, G. Kuan, A. Gordon, A. Balmaseda, L. Katzelnick & E. Harris, "Primary exposure to Zika virus is linked with increased risk of symptomatic dengue virus infection with serotypes 2, 3 & 4, but not 1," Sci. Transl. Med. 16 (2024) eadn2199. https://doi.org/10.1126/scitranslmed.adn2199.

[17] L. C. Katzelnick, L. Gresh, M. E. Halloran, J. C. Mercado, G. Kuan, A. Gordon, A. Balmaseda & E. Harris, "Antibody-dependent enhancement of severe dengue disease in humans," Science **358** (2017) 929. https://doi.org/10.1126/science.aan6836.

[18] R. Khandia, A. Munjal, K. Dhama, K. Karthik, R. Tiwari, Y. S. Malik, R. K. Singh & W. Chaicumpa, "Modulation of dengue/Zika virus pathogenicity by antibody-dependent enhancement and strategies to protect against enhancement in Zika virus infection," Front. Immunol. **9** (2018) 597. https://doi.org/10.3389/fimmu.2018.00597.

[19] A. Sarker, N. Dhama & R. D. Gupta, "Dengue virus neutralizing antibody: a review of targets, cross-reactivity & antibody-dependent enhancement," Front. Immunol. **14** (2023) 1200195. https://doi.org/10.3389/fimmu.2023.1200195.

[20] P. M. S. Castanha, G. Erdos, S. C. Watkins, L. D. Falo Jr., E. T. A. Marques & S. M. Barratt-Boyes, "Reciprocal immune enhancement of dengue and Zika virus infection in human skin," JCI Insight **5** (2020) e133653. https://doi.org/10.1172/jci.insight.133653.

[21] B. Tang, Y. Xiao, B. Sander, M. A. Kulkarni, RADAM-LAC Research Team & J. Wu, "Modelling the impact of antibody-dependent enhancement on disease severity of Zika virus and dengue virus sequential and co-infection," R. Soc. Open Sci. **7** (2020) 191749. https://doi.org/10.1098/rsos.191749.

[22] J. P. Romero-Leiton, E. K. E. Laison, R. Alfaro, E. J. Parmley, J. Arino, K. R. Acharya & B. Nasri, "Exploring Zika's dynamics: a scoping review journey from epidemic to equations through mathematical modelling," Infect. Dis. Model. **10** (2025) 536. https://doi.org/10.1016/j.idm.2024.12.016.

[23] S. T. Ogunlade, M. T. Meehan, A. I. Adekunle & E. S. McBryde, "A systematic review of mathematical models of dengue transmission and vector control: 2010–2020," Viruses **15** (2023) 254. https://doi.org/10.3390/v15010254.

[24] M. Aguiar, V. Anam, K. B. Blyuss, C. D. S. Estadilla, B. V. Guerrero, D. Knopoff, B. W. Kooi, A. K. Srivastav, V. Steindorf & N. Stollenwerk, "Mathematical models for dengue fever epidemiology: a 10-year systematic review," Phys. Life Rev. **40** (2022) 65. https://doi.org/10.1016/j.plrev.2022.02.001.

[25] S. M. Garba, A. B. Gumel & M. R. Abu Bakar, "Backward bifurcations in dengue transmission dynamics," Math. Biosci. **215** (2008) 11. https://doi.org/10.1016/j.mbs.2008.05.002.

[26] A. Abidemi & N. A. B. Aziz, "Analysis of deterministic models for dengue disease transmission dynamics with vaccination perspective in Johor, Malaysia," Int. J. Appl. Comput. Math. **8** (2022) 45. https://doi.org/10.1007/s40819-022-01250-3.

[27] J. Ren & R. Xu, "Dynamic analysis and application of a dengue transmission model with vaccination and incubation delays," J. Appl. Math. Comput. **69** (2023) 895. https://doi.org/10.1007/s12190-022-01776-1.

[28] A. B. Gumel, "Causes of backward bifurcations in some epidemiological models," J. Math. Anal. Appl. **395** (2012) 355. https://doi.org/10.1016/j.jmaa.2012.04.077.

[29] D. Gao, Y. Lou, D. He, T. C. Porco, Y. Kuang, G. Chowell & S. Ruan, "Prevention and control of Zika as a mosquito-borne and sexually transmitted disease: a mathematical modelling analysis," Sci. Rep. **6** (2016) 28070. https://doi.org/10.1038/srep28070.

[30] O. Maxian, A. Neufeld, E. J. Talis, L. M. Childs & J. C. Blackwood, "Zika virus dynamics: when does sexual transmission matter?" Epidemics **21**

(2017) 48. https://doi.org/10.1016/j.epidem.2017.06.003.
[31] S. Towers, F. Brauer, C. Castillo-Chavez, A. K. I. Falconar, A. Mubayi & C. M. E. Romero-Vivas, "Estimate of the reproduction number of the 2015 Zika virus outbreak in Barranquilla, Colombia & estimation of the relative role of sexual transmission," Epidemics **17** (2016) 50. https://doi.org/10.1016/j.epidem.2016.10.003.
[32] L. Wang & H. Zhao, "Dynamics analysis of a Zika–dengue co-infection model with dengue vaccine and antibody-dependent enhancement," Physica A **522** (2019) 248. https://doi.org/10.1016/j.physa.2019.01.099.
[33] S. A. Jose, R. Raja, B. I. Omede, R. P. Agarwal, J. Alzabut, J. Cao & V. E. Balas, "Mathematical modelling on co-infection: transmission dynamics of Zika virus and dengue fever," Nonlinear Dyn. **111** (2023) 4879. https://doi.org/10.1007/s11071-022-08063-5.
[34] A. Omame, M. E. Isah & M. Abbas, "An optimal control model for COVID-19, Zika, dengue & chikungunya co-dynamics with reinfection," Optim. Control Appl. Methods **44** (2023) 170. https://doi.org/10.1002/oca.2936.
[35] S. A. Ayuba, I. Akeyede & A. S. Olagunju, "Stability and sensitivity analysis of dengue-malaria co-infection model in endemic stage," J. Nig. Soc. Phys. Sci. **3** (2021) 96. https://doi.org/10.46481/jnsps.2021.196.
[36] F. A. Oguntolu, O. J. Peter, O. Babasola, B. I. Omede, G. B. Balogun, A. A. Victor & A. I. Abioye, "Mathematical modelling on the dynamics of dengue fever with vaccination and transovarial transmission with real statistical data," Qual. Quant. **60** (2026) 6327. https://doi.org/10.1007/s11135-025-02527-7.
[37] A. Abidemi & O. J. Peter, "Host-vector dynamics of dengue with asymptomatic, isolation and vigilant compartments: insights from modelling," Eur. Phys. J. Plus **138** (2023) 199. https://doi.org/10.1140/epjp/s13360-023-03823-7.
[38] A. Abidemi, Fatmawati & O. J. Peter, "An optimal control model for dengue dynamics with asymptomatic, isolation & vigilant compartments," Decis. Anal. J. **10** (2024) 100413. https://doi.org/10.1016/j.dajour.2024.100413.
[39] F. F. Herdicho, Fatmawati, C. Alfiniyah, F. P. Fajrin, E. Bonyah, M. A. Rois & O. J. Peter, "Modelling the dynamics of dengue transmission with awareness and optimal control analysis," PLoS ONE **20** (2025) e0322702. https://doi.org/10.1371/journal.pone.0322702.
[40] P. van den Driessche & J. Watmough, "Reproduction numbers and subthreshold endemic equilibria for compartmental models of disease transmission," Math. Biosci. **180** (2002) 29. https://doi.org/10.1016/S0025-5564(02)00108-6.
[41] C. Castillo-Chavez & B. Song, "Dynamical models of tuberculosis and their applications," Math. Biosci. Eng. **1** (2004) 361. https://doi.org/10.3934/mbe.2004.1.361.
[42] Governo ES, "Sesa divulga 36° boletim da dengue, Zika e chikungunya," Governo do Estado do Espírito Santo, Sep. 16, 2021. Available online: https://www.es.gov.br/Noticia/sesa-divulga-36-boletim-da-dengue--Zika-e-chikungunya.
[43] Brazilian Institute of Geography & Statistics (IBGE), "Estimativas da população residente nos municípios do Brasil," Technical report, IBGE, Brasília, Brazil, 2021. Available online: https://www.ibge.gov.br/estatisticas/sociais/populacao/9103-estimativas-de-populacao.html?edicao=31451&t=custom-data-edicao.
[44] World Health Organization, "World health statistics 2021: monitoring health for the SDGs, sustainable development goals," World Health Organization, Geneva, Switzerland, 2021. Available online: https://www.who.int/publications/i/item/9789240027053.
[45] R. Taghikhani & A. B. Gumel, "Mathematics of dengue transmission dynamics: roles of vector vertical transmission and temperature fluctuations," Infect. Dis. Model. **3** (2018) 266. https://doi.org/10.1016/j.idm.2018.09.003.
[46] P. Reiter, "Climate change and mosquito-borne disease," Environ. Health Perspect. **109** (2001) 141. https://pubmed.ncbi.nlm.nih.gov/11250812/.
[47] O. J. Brady, M. A. Johansson, C. A. Guerra, S. Bhatt, N. Golding, D. J. Pigott, H. Delatte, M. G. Grech, P. T. Leisnham, R. Maciel-de-Freitas, L. M. Styer, D. L. Smith, T. W. Scott, P. W. Gething & S. I. Hay, "Modelling adult *Aedes aegypti* and *Aedes albopictus* survival at different temperatures in laboratory and field settings," Parasit. Vectors **6** (2013) 351. https://doi.org/10.1186/1756-3305-6-351.
[48] D. J. Gubler, "Dengue and dengue hemorrhagic fever," Clin. Microbiol. Rev. **11** (1998) 480. https://doi.org/10.1128/CMR.11.3.480.
[49] World Health Organization, "Dengue: guidelines for diagnosis, treatment, prevention and control," World Health Organization, Geneva, Switzerland, 2009. Available online: https://www.who.int/publications/i/item/9789241547871.
[50] D. S. Shepard, J. A. Suaya, S. B. Halstead, M. B. Nathan, D. J. Gubler, R. T. Mahoney, D. N. C. Wang & M. I. Meltzer, "Cost-effectiveness of a pediatric dengue vaccine," Vaccine **22** (2004) 1275. https://doi.org/10.1016/j.vaccine.2003.09.019.
[51] S. B. Halstead, "Dengue fever/dengue hemorrhagic fever," in *Tropical Infectious Diseases: Principles, Pathogens and Practice*, R. L. Guerrant, D. H. Walker & P. F. Weller, Eds., Elsevier, Philadelphia, PA, USA, 2007, pp. 800-810.
[52] S. B. Halstead, "Dengue," Lancet **370** (2007) 1644. https://doi.org/10.1016/S0140-6736(07)61687-0.
[53] H. J. Wearing & P. Rohani, "Ecological and immunological determinants of dengue epidemics," Proc. Natl. Acad. Sci. U.S.A. **103** (2006) 11802. https://doi.org/10.1073/pnas.0602960103.
[54] T. M. Aliota, D. M. Dudley, C. M. Newman, E. L. Mohr, D. D. Gellerup, M. E. Breitbach, C. R. Buechler, M. N. Rasheed, M. S. Mohns, A. M. Weiler, G. L. Barry, K. L. Weisgrau, J. A. Eudailey, E. G. Rakasz, L. J. Vosler, J. Post, S. Capuano, T. G. Golos, S. R. Permar, J. E. Osorio, T. C. Friedrich, S. L. O'Connor & D. H. O'Connor, "Heterologous protection against Asian Zika virus challenge in rhesus macaques," PLoS Negl. Trop. Dis. **10** (2016) e0005168. https://doi.org/10.1371/journal.pntd.0005168.
[55] S. Sridhar, A. Luedtke, E. Langevin, M. Cot, L. Guy, B. Descamps, S. Dayan, L. Crevat & M. T. Thomas, "Effect of dengue serostatus on dengue vaccine safety and efficacy," N. Engl. J. Med. **379** (2018) 327. https://doi.org/10.1056/NEJMoa1800820.
[56] S. R. Hadinegoro, J. L. Arredondo-Garcia, M. R. Capeding, C. Deseda, T. Chotpitayasunondh, R. Dietze, H. I. H. Ismail, H. Reynales, K. Limkittikul, D. M. Rivera-Medina, H. N. Tran, A. Bouckenooghe, D. Chansinharaj, G. Horvath, C. Kelly, A. Langevin, M. Laot, Y. Lombart, F. Méréau, J. Noriega, T. P. Nga, S. B. Tornieporth & M. C. Wartel, "Efficacy and long-term safety of a dengue vaccine in regions of endemic disease," N. Engl. J. Med. **373** (2015) 1195. https://doi.org/10.1056/NEJMoa1506223.
[57] N. Chitnis, J. M. Hyman & J. M. Cushing, "Determining important parameters in the spread of malaria through the sensitivity analysis of a mathematical model," Bull. Math. Biol. **70** (2008) 1272. https://doi.org/10.1007/s11538-008-9299-0.
[58] O. Olawoyin & C. Kribs, "Effects of multiple transmission pathways on Zika dynamics," Infect. Dis. Model. **3** (2018) 331. https://doi.org/10.1016/j.idm.2018.11.003.
[59] H. McCallum, N. Barlow & J. Hone, "How should pathogen transmission be modelled?" Trends Ecol. Evol. **16** (2001) 295. https://doi.org/10.1016/S0169-5347(01)02144-9.
[60] O. Diekmann, J. A. Heesterbeek & M. G. Roberts, "The construction of next-generation matrices for compartmental epidemic models," J. R. Soc. Interface **7** (2010) 873. https://doi.org/10.1098/rsif.2009.0386.
[61] H. R. Thieme, *Mathematics in Population Biology*, Princeton University Press, Princeton, NJ, USA, 2003. https://doi.org/10.1515/9780691187655.
[62] C. Castillo-Chavez, Z. Feng & W. Huang, "On the computation of $\mathcal{R}_0$ and its role in global stability," in *Mathematical Approaches for Emerging and Reemerging Infectious Diseases: An Introduction*, C. Castillo-Chavez, S. Blower, P. van den Driessche, D. Kirschner & A.-A. Yakubu (Eds.), Springer, New York, NY, USA, 2002, pp. 229–250. https://doi.org/10.1007/978-1-4757-3667-0_13.
[63] E. A. Undurraga, Y. A. Halasa & D. S. Shepard, "Use of expansion factors to estimate the burden of dengue in Southeast Asia: a systematic analysis," PLoS Negl. Trop. Dis. **7** (2013) e2056. https://doi.org/10.1371/journal.pntd.0002056.
[64] M. M. O. Silva, M. S. Rodrigues, I. A. D. Paploski, M. Kikuti, A. M. S. Kasper, C. S. Cruz, J. J. A. G. Donanzan, R. Rego Fereira, G. S. Campos, S. I. Sardi, U. Kitron, G. A. Reis & M. G. Ribeiro, "Accuracy of dengue reporting by national surveillance system, Brazil," Emerg. Infect. Dis. **22** (2016) 336. https://doi.org/10.3201/eid2202.150495.
[65] E. M. Netto, A. R. Almeida, A. T. Carvalho, M. S. Rodrigues, I. A. D. Paploski, M. Kikuti, M. G. Ribeiro, D. M. Kitron, G. A. Reis & M. G. Queiroz, "High Zika virus seroprevalence in Salvador, northeastern Brazil limits the potential for further outbreaks," mBio **8** (2017) e01390-17. https://doi.org/10.1128/mBio.01390-17.

[66] E. C. Duru, M. C. Anyanwu, T. N. Nnamani, C. N. Nwosu & G. C. E. Mbah, "Semi-analytical solution and numerical simulations of a co-infection model of malaria and Zika virus disease," J. Nig. Soc. Phys. Sci. **7** (2025) 2436. https://doi.org/10.46481/jnsps.2025.2436.